

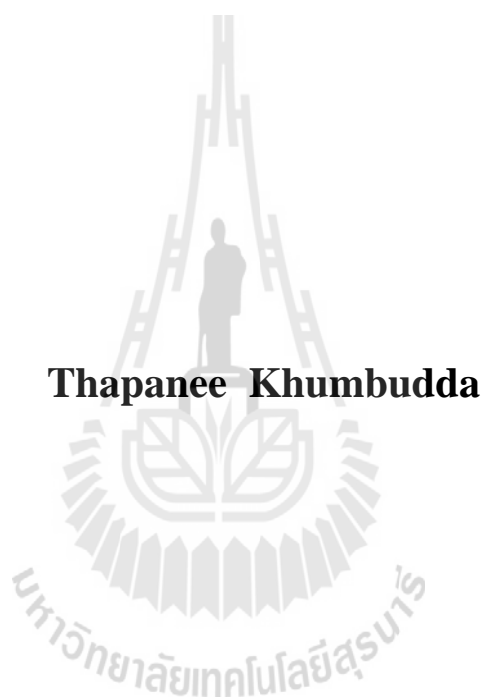
การสังเคราะห์โซเดียมซีโอไลต์ และโซเดียมซีโอไลต์เมมเบรนจากกาถิน
สำหรับการแยกน้ำออกจากสารละลายเอทานอลโดยพอเวปพอเรชัน



นางสาวฐาปนี คำบุตรดา

วิทยานิพนธ์นี้เป็นส่วนหนึ่งของการศึกษาตามหลักสูตรปริญญาวิทยาศาสตรดุษฎีบัณฑิต
สาขาวิชาเคมี
มหาวิทยาลัยเทคโนโลยีสุรนารี
ปีการศึกษา 2558

**SYNTHESIS OF SODIUM ZEOLITES AND SODIUM
ZEOLITE MEMBRANES FROM KAOLIN FOR
WATER SEPARATION FROM ETHANOL
SOLUTIONS BY PERVAPORATION**



Thapanee Khumbudda

**A Thesis Submitted in Partial Fulfillment of the Requirements for the
Degree of Doctor of Philosophy in Chemistry
Suranaree University of Technology
Academic Year 2015**

**SYNTHESIS OF SODIUM ZEOLITES AND SODIUM ZEOLITE
MEMBRANES FROM KAOLIN FOR WATER SEPARATION
FROM ETHANOL SOLUTIONS BY PERVAPORATION**

Suranaree University of Technology has approved this thesis submitted in partial fulfillment of the requirements for the Degree of Doctor of Philosophy.

Thesis Examining Committee

(Assoc. Prof. Dr. Jatuporn Wittayakun)

Chairperson

(Asst. Prof. Dr. Kunwadee Rangriwatananon)

Member (Thesis Advisor)

(Asst. Prof. Dr. Aahiruk Chaisena)

Member

(Asst. Prof. Dr. Thanaporn Manyum)

Member

(Asst. Prof. Dr. Sanchai Prayoonpokarach)

Member

(Prof. Dr. Sukit Limpijumnong)

Vice Rector for Academic Affairs
and Innovation

(Prof. Dr. Santi Maensiri)

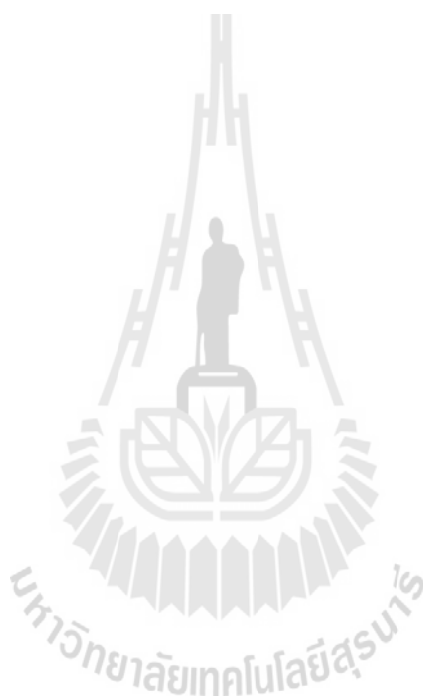
Dean of Institute of Science

ฐาปนี คำบุตรดา : การสังเคราะห์โซเดียมซีโอไลต์ และโซเดียมซีโอไลต์เมมเบรนจากเกาลิน
สำหรับการแยกน้ำออกจากสารละลายเอทานอลโดยเพอแวปพอเรชัน (SYNTHESIS OF
SODIUM ZEOLITES AND SODIUM ZEOLITE MEMBRANES FROM KAOLIN FOR
WATER SEPARATION FROM ETHANOL SOLUTIONS BY PERVAPORATION)
อาจารย์ที่ปรึกษา : ผู้ช่วยศาสตราจารย์ ดร.กุลวดี รังษิวัฒนานนท์, 140 หน้า.

จุดสนใจหลักของวิทยานิพนธ์นี้เพื่อศึกษาการดึงน้ำออกจากสารละลายเอทานอลด้วย
โซเดียมซีโอไลต์ที่ชอบน้ำชนิดต่าง ๆ (อะนาลซีม โซเดียมเจบีดับเบิลยู โซดาไลต์และแคนคริไนต์)
และโซเดียมซีโอไลต์เมมเบรน (อะนาลซีมเมมเบรน) ทั้งโซเดียมซีโอไลต์ และโซเดียมซีโอไลต์
เมมเบรนได้ถูกสังเคราะห์ขึ้นจากวัสดุในท้องถิ่น ได้แก่ ดินขาวเพื่อลดต้นทุนของการผลิต โซเดียม-
ซีโอไลต์ถูกสังเคราะห์ขึ้นด้วยวิธีไฮโดรเทอร์มอล โดยใช้ดินขาวคิบ ดินขาวที่ผ่านการกำจัด
อะลูมิเนียมและดินขาวที่ผ่านการเผา ได้เฟสบริสุทธิ์และความเป็นผลึกสูงของโซเดียมซีโอไลต์
ทุกตัวภายในระยะเวลาที่สั้นของการเกิดปฏิกิริยา 6-12 ชั่วโมง ได้ตรวจสอบความสามารถของการ
ดึงน้ำออกจากเอทานอลของซีโอไลต์เหล่านี้ อะนาลซีมแสดงความสามารถในการกำจัดน้ำได้สูงสุด
ในสารละลายเอทานอลในช่วงความเข้มข้นร้อยละ 85.0-97.0 โดยปริมาตร เนื่องจากตำแหน่งของ
กรดลิวอิสมีความแรงที่มากกว่า ดังนั้นอะนาลซีมเมมเบรนจึงถูกสังเคราะห์ขึ้นเพื่อแยกสารผสมของ
น้ำและเอทานอลด้วยกระบวนการเพอแวปพอเรชัน บนพื้นฐานความเป็นไปได้ของโมเลกุลขนาด
เล็กของน้ำสามารถผ่านเข้าไปในช่องของอะนาลซีมแต่โมเลกุลขนาดใหญ่ของเอทานอลถูกขัดขวาง

อะนาลซีมเมมเบรนที่เหมาะสมถูกสังเคราะห์บนเซรามิกรูพรุน ซึ่งถูกเตรียมด้วยส่วนผสม
ของคริสโตแบไลต์ร้อยละ 10.0 โดยมวล แคลเซียมคาร์บอเนตร้อยละ 2.5 โดยมวล ถ่านกัมมันต์
ร้อยละ 2.5 โดยมวล และดินขาวร้อยละ 85.0 โดยมวล การสังเคราะห์อะนาลซีมเมมเบรนถูกเตรียม
โดยกระบวนการแบบอินซิตู (*in situ method*) ซึ่งใช้ดินขาวคิบ ดินขาวที่ผ่านการกำจัดอะลูมิเนียม
และสารเคมี เป็นวัตถุดิบในการผลิตผลิตภัณฑ์ขนาดเล็กละเอียดของอะนาลซีมประมาณ 20-37 ไมโครเมตร และ
ความหนาของชั้นอะนาลซีมประมาณ 45-67 ไมโครเมตร ได้มาจากดินขาวคิบร่วมกับการบ่ม ดินขาว
ที่ผ่านการกำจัดอะลูมิเนียม และสารเคมี อะนาลซีมเมมเบรนเหล่านี้แสดงค่าการแยกสูงมากกว่า
10,000 สำหรับเอทานอลที่ความเข้มข้นเริ่มต้นร้อยละ 90 โดยมวล และ 95 โดยมวล และยังพบอีก
ว่าอะนาลซีมเมมเบรนจากดินขาวคิบร่วมกับการบ่ม เป็นเวลา 3 วันให้ค่าฟลักซ์ของน้ำ (0.27
กิโลกรัมต่อตารางเมตรต่อชั่วโมง) สูงกว่าอะนาลซีมเมมเบรนจากวัตถุดิบในการผลิตอื่น ๆ อย่างเช่น
อะนาลซีมเมมเบรนที่มาจากดินขาวคิบร่วมกับการบ่ม เพียง 1 วัน อะนาลซีมเมมเบรนที่มาจากดิน-
ขาวที่ผ่านการกำจัดอะลูมิเนียม และอะนาลซีมเมมเบรนจากสารเคมีที่มีค่าฟลักซ์ของน้ำเท่ากับ 0.25
กิโลกรัมต่อตารางเมตรต่อชั่วโมง 0.22 กิโลกรัมต่อตารางเมตรต่อชั่วโมงและ 0.19 กิโลกรัมต่อ

ตารางเมตรต่อชั่วโมงตามลำดับ อาจเนื่องมาจากความหนาของชั้นอะนาไลซิสที่ได้จากดินขาวดิบ
ร่วมกับการบ่ม 3 วัน มีค่าน้อยกว่าจากแหล่งอื่น ๆ



สาขาวิชาเคมี

ปีการศึกษา 2558

ลายมือชื่อนักศึกษา _____

ลายมือชื่ออาจารย์ที่ปรึกษา _____

THAPANEE KHUMBUDDA : SYNTHESIS OF SODIUM ZEOLITES
AND SODIUM ZEOLITE MEMBRANES FROM KAOLIN FOR WATER
SEPARATION FROM ETHANOL SOLUTIONS BY PERVAPORATION.
THESIS ADVISOR : ASST. PROF. KUNWADEE
RANGSRIWATANANON, Ph.D. 140 PP.

RAW KAOLIN/DEALUMINATED KAOLIN/METAKAOLIN/JBW/ ANA/SOD/
CAN/DEHYDRATION/ANA MEMBRANE/POROUS CERAMIC SUPPORT/
PORE FORMER/MULLITE/PERVAPORATION

The main focus of this thesis was to study the dehydration of ethanol solution by various types of hydrophilic sodium zeolites (ANA, JBW, SOD and CAN) and sodium zeolite membranes (ANA membranes). Both of sodium zeolites and sodium zeolite membranes were synthesized from local material as kaolin for reducing the costs. Sodium zeolites were synthesized by hydrothermal method using raw kaolin, dealuminated kaolin and calcined kaolin. The pure phase and high crystallinity of all sodium zeolites were observed within a short reaction period of 6-12 hours. The capability of ethanol dehydration of these sodium zeolites were investigated. ANA showed the highest dehydration of ethanol solutions within the concentration range of 85.0-97.0%v/v due to its stronger Lewis acid site. Consequently, ANA membrane was synthesized for separation of water/ethanol mixture by pervaporation based on a possibility for small water molecule able to pass through channel of ANA but the bigger molecule of ethanol was prevented.

A suitable ANA membrane was synthesized on the porous ceramic support which was prepared with the ingredients of 10.0 wt% of cristobalite, 2.5 wt% of

CaCO_3 , 2.5 wt% of activated carbon and 85 wt% of kaolin. The syntheses of ANA membranes were carried out by in situ synthesis method using raw kaolin, dealuminated kaolin and chemicals as starting material sources. The small crystals of ANA about 20-37 μm and ANA layer thickness about 45-67 μm were obtained by using raw kaolin with aging, dealuminated kaolin and chemicals. All these ANA membranes showed a high separation factor as $>10,000$ for ethanol feed concentration of 90.0 wt% and 95.0 wt%. The ANA membrane from raw kaolin aged for 3 days presented the total water flux ($0.27 \text{ kg/m}^2\text{h}$) higher than that of ANA membranes from the other starting material sources such as the total water flux of ANA membrane from raw kaolin aged for 1 day, dealuminated kaolin and chemicals was $0.25 \text{ kg/m}^2\text{h}$, $0.22 \text{ kg/m}^2\text{h}$ and $0.19 \text{ kg/m}^2\text{h}$, respectively. This may be due to the thickness of ANA layer from raw kaolin aged for 3 days was less than the others.

School of Chemistry

Academic Year 2015

Student's Signature_____

Advisor's Signature_____

ACKNOWLEDGEMENTS

The success of my thesis work comes from the help of many people. I would like to express my gratitude to all those. First, I would like to thank my advisor, Assistant Professor Dr. Kunwadee Rangriwatananon, for the encouragement in the Ph.D. program. She taught me different ways to solve problems. She has provided valuable review, comments, and suggestions during the finalization of the document. I also wish to thank all my thesis committee members Assistant Professor Dr. Aphiruk Chaisena, Assistant Professor Dr. Thanaporn Manyum and Assistant Professor Dr. Sanchai Prayoonpokarach for their valuable, suggestion and criticism.

My thanks go to the Chairperson of School of Chemistry, Associate Professor Dr. Jatuporn Wittayakun for serving as the chairperson of the committee and all lecturers at the School of Chemistry for their suggestions and encouragement. I would like to thanks all the staffs at the Center of Scientific and Technological Equipment for their service and helpful suggestions. I wish to thank Zeolite's group, Material Chemistry Research Unit and all my friends at the Suranaree University of Technology for their kindness and help, all of the staff at the Center for Scientific and Technological Equipment for their assistance and suggestion for the use of XRF, XRD, FT-IR, GC, TPD, DTA/TGA and SEM.

Last but not least, I would like to thank my family for their understanding, encouragement and support during the whole period of my education.

Thapanee Khumbudda

CONTENTS

	Page
ABSTRACT IN THAI	I
ABSTRACT IN ENGLISH.....	III
ACKNOWLEDGEMENTS	V
CONTENTS	VI
LIST OF TABLES	XI
LIST OF FIGURES.....	XII
LIST OF ABBREVIATIONS	XX
CHAPTER	
I INTRODUCTION	1
1.1 Research objectives	1
1.2 Scope and limitations of the study	3
II LITERATURE REVIEW	4
2.1 Fundamental zeolite structure	4
2.1.1 Structure of analcime.....	5
2.1.2 Structure of Na-J(BW).....	5
2.1.3 Structure of cancrinite	6
2.1.4 Structure of sodalite.....	7
2.2 Clay mineral	7
2.2.1 Kaolinite for zeolitization.....	9
2.2.2 Nucleation and growth process of the zeolite synthesis	11

CONTENTS (Continued)

	Page
2.3 The adsorption of water from ethanol with zeolite	13
2.4 Synthesis of zeolites	16
2.4.1 Synthesis of ANA	17
2.4.2 Synthesis of SOD, CAN and JBW	19
2.5 Porous ceramic supports.....	21
2.6 Related researches	23
2.6.1 Preparation of zeolitic membrane for separation of water/ethanol mixture	27
2.7 The separation of water/ethanol mixture by pervaporation.....	29
2.8 References	36
III HIGH TEMPERATURE SYNTHESIS OF JBW, ANA, SOD AND CAN FROM RAW AND MODIFIED KAOLIN FOR ETHANOL DEHYDRATION	44
3.1 Abstract	44
3.2 Introduction	44
3.3 Experiment	46
3.3.1 Materials	46
3.3.2 Synthesis of sodium zeolites	47
3.3.2.1 Synthesis of ANA and CAN.....	47
3.3.2.2 Synthesis of JBW and SOD.....	47
3.3.3 Characterization of starting materials and sodium zeolites	48

CONTENTS (Continued)

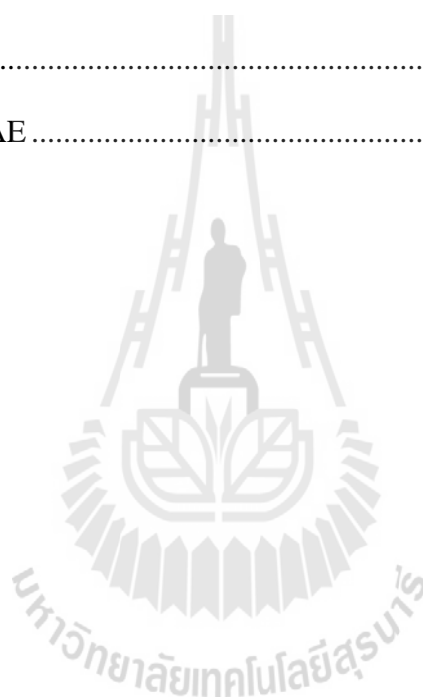
	Page
3.3.4 Dehydration of ethanol solution	49
3.4 Results and discussion.....	49
3.4.1 Analysis of starting material.....	49
3.4.2 Syntheses of sodium zeolites	54
3.4.2.1 Synthesis of ANA and JBW	56
3.4.2.2 Synthesis of CAN and SOD	61
3.4.3 Acidity analysis by NH ₃ -TPD	66
3.4.4 Thermal analysis.....	68
3.4.5 Dehydration in ethanol solution	70
3.5 Conclusions	71
3.6 References	72
IV FACILE HYDROTHERMAL SYNTHESIS OF ZEOLITIC ANA MEMBRANE FROM RAW KAOLIN, DEALUMINATED KAOLIN AND CHEMICAL SOURCE	78
4.1 Abstract	78
4.2 Introduction	79
4.3 Experiment	81
4.3.1 Materials	81
4.3.2 Preparation of porous ceramic support.....	82
4.3.2.1 Preparation of cristobalite.....	82
4.3.2.2 Preparation of porous ceramic disc.....	82

CONTENTS (Continued)

	Page
4.3.3 ANA membranes synthesis	84
4.3.3.1 ANA membrane from porous ceramic supports.....	84
4.3.3.2 The ANA membrane were synthesized by using RK, DK24 and chemical as starting material	85
4.3.4 Characterization.....	86
4.4 Results and discussion.....	86
4.4.1 Characteristic of porous ceramic support	86
4.4.2 Characteristics of ANA membrane.....	96
4.4.2.1 ANA membrane from RK source.....	96
4.4.2.2 ANA membrane from DK24 source.....	106
4.4.2.3 ANA membrane from chemical source.....	111
4.5 Conclusions	113
4.6 References	113
V THE PERVAPORATION FOR SEPARTION WATER/ETHANOL MIXTURE THROUGH ZEOLITIC ANA MEMBRANES.....	119
5.1 Abstract	119
5.2 Introduction	120
5.3 Experiment	121
5.3.1 Materials	121
5.3.2 Pervaporation tests.....	121
5.4 Results and discussion.....	123

CONTENTS (Continued)

	Page
5.5 Conclusions	129
5.6 References	129
VI CONCLUSIONS	131
APPENDIX	134
CURRICULUM VITAE	140



LIST OF TABLES

Table	Page
2.1	Average percentage of carbon fixation in animal parts (mean \pm S.D.)..... 35
3.1	Chemical compositions (in wt%) of the starting materials determined by XRF 50
3.2	FT-IR peak assignment for functionality of RK 54
3.3	Relative crystallinity of sodium zeolites synthesized from different starting materials under various reaction periods..... 54
3.4	Total amount of adsorbed NH_3 related to Na^+ and ratio of Si/Al of sodium zeolites 68
4.1	The compositions of the the ingredients (wt%) for preparation of porous ceramic discs 83
4.2	The average pore size and percentage of porosity of porous ceramic supports 95
5.1	Pervaporation performance of ANA membranes..... 124
5.2	Pervaporation performance of zeolite membranes on ceramic support 128
6.1	Summarized the related researches on hydrothermal synthesis of sodium zeolites from different silica and alumina sources with different reaction periods 65

LIST OF FIGURES

Figure	Page
2.1 Representation of $[\text{SiO}_4]^{4-}$ or $[\text{AlO}_4]^{5-}$ tetrahedral	4
2.2 The structure of ANA (a) distorted 8-ring viewed along $[110]$ (b) framework viewed along $[001]$	5
2.3 The structure of JBW (a) 8-ring viewed along $[001]$ (b) framework viewed along $[100]$	6
2.4 The structure of CAN (a) 12-ring viewed along $[001]$ (b) framework viewed along $[001]$	6
2.5 The sodalite or β -cage (a) framework of SOD viewed along $[100]$ (b).....	7
2.6 Single octahedron (a) and the sheet structure of octahedral Units (b).....	8
2.7 Single silica tetrahedron (a) and the sheet structure of silica tetrahedrons arranged in a hexagonal network (b)	8
2.8 Structure of the kaolinite layer	9
2.9 Illustration of the proposed sequence for the formation of zeotypes	12
2.10 The snapshots of water-ethanol mixture molecules in DON zeolites for 0.5 water mole fraction of bulk phase (the row of water molecules at the bottom of the figure is the configuration of water located in the small channel)	14
2.11 Possible adsorbate structure of water on alkali ZSM5.....	15

LIST OF FIGURES (Continued)

Figure	Page
2.12 Schematic adsorbate structure of water on alkali-metal ZSM5 at the pressure indicated.....	16
2.13 Schematic illustration of formation process of zeolite NaA membrane: (a) seeded support tube and (b-d) membranes after 1, 2, and 3 hours, respectively, of the synthesis.....	25
2.14 Schematic representation for the formation of NaA zeolite membranes prepared by primary and secondary crystallization	28
2.15 Schematic representation of (a) pervaporation across a membrane and (b) the separation properties of water/ethanol mixture	30
2.16 Repeating unit of zeolite H-SOD	30
2.17 Schematic representations of (a) non-zeolite pores in the intercrystalline boundaries of a zeolite membrane layer and (b) the intracrystalline and intercrystalline pathways for mass transfer in the zeolite layer	31
3.1 XRD patterns of RK (a), DK5 (b), DK24 (c) and MK (d).....	50
3.2 FT-IR skeletal spectra (B) and OH stretching vibration spectra (A) of RK (a), DK5 (b), DK24 (c) and MK (d)	53
3.3 XRD patterns of ANA from different starting materials; DK24 with different reaction periods such as 6 h (a), 12 h (b), 24 h (c) and 48 h (d); MK (e) and RK (f) with reaction period of 48 h	56
3.4 The simulated XRD powder pattern of ANA	57
3.5 The simulated XRD powder pattern of JBW	57

LIST OF FIGURES (Continued)

Figure	Page
3.6 SEM image of ANA from DK24 with reaction period of 24 h.....	58
3.7 XRD patterns of ANA zeolite and SiO ₂ from DK4.5 (a), DK5 (b), DK5.5 (c) and DK6 (d) with reaction period 6 h and from DK6 with reaction period 48 h (e)	59
3.8 SEM image of ANA from DK5.5 with reaction period 6 h.....	59
3.9 XRD patterns of JBW zeolite (a) with different reaction period such as 6 h (a), 12 h (b), 24 h (c) and 48 h (d)	60
3.10 SEM image of JBW from RK with reaction period 24 h.....	61
3.11 XRD patterns (A) of CAN from different starting materials; DK24 with different reaction periods such as 6 h (a), 12 h (b), 24 h (c) and 48 h (d); MK (e) and RK (f) with reaction period of 48 h	62
3.12 The simulated XRD powder pattern of CAN.....	62
3.13 SEM image of CAN from DK5.5 with reaction period 12 h	63
3.14 XRD patterns of CAN from DK5 with reaction period of 12 h (a) and from DK5.5 with different reaction periods such as 6 h (b), 12 h (c) and 24 h (d).....	64
3.15 XRD patterns of product in synthesis SOD zeolite at reaction period of 6 h (a), 12 h (b) and 24 h (c)	65
3.16 The simulated XRD powder pattern of SOD	65

LIST OF FIGURES (Continued)

Figure	Page
3.17 SEM image of SOD with reaction period of 12 h (a) and the mixed phase of SOD and CAN with reaction period of 24 h (b).....	66
3.18 NH ₃ -TPD patterns of ANA, JBW, CAN and SOD	67
3.19 TGA/DTG curve of ANA, CAN, JBW and SOD	69
3.20 Adsorption of water from various ethanol concentrations.....	71
4.1 The main stages of the preparation for the porous ceramic discs	83
4.2 XRD patterns of (a) amorphous silica and (b) cristobalite from rice husk	87
4.3 XRD patterns of (a) raw kaolin, (b) calcined kaolin and (c) 10 cristobalite	87
4.4 SEM micrograph of calcined kaolin disc: (a, b) top view, (c) cross section view.....	88
4.5 XRD patterns of porous ceramic support (a) 2.5A (b) 5A and (c) 10A.....	89
4.6 Top view and cross sectional SEM micrograph of porous ceramic support for 2.5A ((a1) and (a2)), 5A ((b1) and (b2)) and 10A ((c1) and (c2))	90
4.7 XRD patterns of porous ceramic plate (a) 2.5Ca (b) 5Ca and (c) 10Ca	91
4.8 Top view and cross sectional SEM photographs of porous ceramic support for 2.5Ca ((a1) and (a2)), 5Ca ((b1) and (b2)) and 10Ca ((c1) and (c2))	92
4.9 TGA and DTA curve of CaCO ₃	93

LIST OF FIGURES (Continued)

Figure	Page
4.10	Top view (a) and cross sectional (b) SEM photographs of the 2.5ACa..... 94
4.11	XRD patterns of 2.5ACa 94
4.12	Percentage of porosity of porous ceramic supports from activated carbon and CaCO ₃ as pore formers 95
4.13	XRD patterns of ANA membrane on (a) 2.5A, (b) 2.5Ca, (c) 2.5ACa, (d) 5A and (e) 5Ca for 24 hour 96
4.14	Surface and cross-sectional SEM micrographs of the ANA membrane on 2.5A ((a1) and (a2)) and 2.5Ca ((b1) and (b2)) for 24 hours 97
4.15	Surface and cross-sectional SEM micrographs of the ANA membrane on 2.5ACa ((a1) and (a2)), 5A ((b1) and (b2)) and 5Ca ((c1) and (c2)) for 24 hours 98
4.16	Cross sectional SEM micrograph of the ANA membrane on 2.5AC for 24 hours and the results of element line analysis for aluminium (A) and silicon (B) 99
4.17	Cross-sectional SEM micrographs of 2.5ACa; before (a) and after (b) synthesized ANA membrane..... 100
4.18	Surface and cross-sectional SEM micrographs of the ANA membrane on 2.5ACa at hydrothermal time of 18 hours ((a1) and (a2)) and 24 hours ((b1) and (b2)) 101
4.19	The diagram of crystallization of ANA layer on 2.5ACa from RK..... 102

LIST OF FIGURES (Continued)

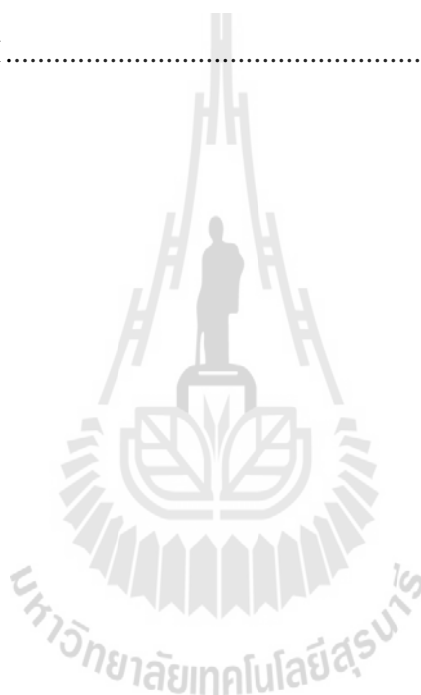
Figure	Page
4.20	Surface and cross-sectional SEM micrographs of the ANA membrane on 2.5ACa with reaction time of 18 hours using precursor aged 1 day ((a1) and (a2)), 2 days ((b1) and (b2)) and 3 days ((c1) and (c2)).....
	104
4.21	XRD patterns of the ANA membrane on 2.5ACa with reaction time of 18 hours using precursor aged (a) 1 day, (b) 2 days and (c) 3 days
	105
4.22	Surface SEM micrograph of the ANA membrane on 2.5 ACa for (a) 12, (b) 18 and (c) 24 hours
	107
4.23	Cross-sectional SEM micrograph of the ANA membrane on (a-1,2) 2.5ACa for 18 hours and (b-1,2) 24 hours
	108
4.24	XRD patterns of ANA membrane on 2.5ACa for (a) 12, (b) 18 and (c) 24 hours.....
	108
4.25	The diagram of crystallization of zeolites from DK24 with and without the support of 2.5ACa
	109
4.26	Surface and cross-sectional SEM micrograph of the ANA membrane on 2.5ACa for aging 1 day ((a1) and (a2)) and aging 2 days ((b1) and (b2))....
	110
4.27	XRD patterns of ANA membrane on 2.5ACa prepared by aging (a) 1 day and (b) 2 days
	111
4.28	Surface and cross-sectional SEM micrograph of the ANA membrane on 2.5ACa with (a) 18 hours and (b1) and (b2) 24 hours
	112
4.29	XRD patterns of the ANA membrane on 2.5ACa with (a) 18 hours and (b) 24 hours
	112

LIST OF FIGURES (Continued)

Figure	Page
5.1	Scheme of a laboratory-made set-up for the pervaporation experiment..... 121
5.2	Surface SEM micrograph of ANA membrane from 2.5ACa with 10%NaOH..... 124
5.3	Effect of temperature on pervaporation performance of ANA membrane synthesized from raw kaolin with aging 1 day and using the feed of 90 wt% ethanol solution..... 127
5.4	Diagram of carbon input, carbon fixation and carbon emission from pukung duck production..... 130
A1	GC chromatograms of standard solutions of (a) 85%v/v, (b) 90%v/v, 95%v/v and (d) 97%v/v of ethanol solutions..... 135
A2	GC chromatograms of 97%v/v ethanol solution after adsorption by ANA 136
A3	(a) Surface SEM micrograph and (b) XRD pattern of ANA membrane from kaolin sintered with 7.5%w/v NaOH 136
A4	SEM micrograph ((a)-(b)) and XRD patterns (c) of ANA membrane from 10% cristobalite sintered with 7.5%w/v NaOH 137
A5	Surface SEM micrograph and XRD patterns of ANA membrane on 2.5A ((a) and (b)), 2.5Ca ((c) and (d)) and 2.5ACa ((e) 138

LIST OF FIGURES (Continued)

Figure		Page
A6	Surface SEM micrograph and XRD patterns of ANA membrane on 2.5A ((a) and (b)), 2.5Ca ((c) and (d)), 2.5ACa ((e) and (f)) and cross-section of ANA membrane on 2.5ACa (e1) with 10% w/v NaOH.....	139



LIST OF ABBREVIATIONS

SOD	=	Sodalite
ANA	=	Analcime
JBW	=	Na-J(BW)
CAN	=	Cancrinite
XRD	=	X-ray Diffractometer
FT-IR	=	Fourier Transforms Infrared Spectrophotometer
XRF	=	X-ray Fluorescence Spectrometer
GC	=	Gas Chromatography
TPD	=	Temperature Programmed Desorption
SEM	=	Scanning Electron Microscope
DTA	=	Differential Thermal Analysis
TGA	=	Thermogravimetric Analysis
%T	=	Percent Transmittance
RK	=	Raw Kaolin
DK	=	Dealuminated Kaolin
MK	=	Metakaolin

CHAPTER I

INTRODUCTION

Bio-ethanol is one of the main alternative fuels to the fossil fuel. Bio-ethanol is produced by fermentation of biomasses such as starch and cellulose derived from various crops and bagasses. Biomass is considered as a carbon neutral and clean energy resource because it is produced by carbon fixation. The CO₂ emitted by the fossil fuel is the major cause of climate change on earth. Thus, utilization of bio-ethanol will decrease negative impacts on environment caused by increase in CO₂ compared with the fossil fuel.

High purity of bio-ethanol or anhydrous ethanol is required for various applications. But it could not be produced by a simple distillation process because of azeotropic point of ethanol-water system. The performance of molecular sieve such as zeolites or zeolite membranes is alternative well because saving energy and environment friendly. Especially, zeolite membranes have been considering because of their uniform nanoporesize, molecular sieving properties, high thermal resistance, chemical inertness and high mechanical strength.

Traditionally, zeolites were synthesized from sodium aluminosilicate gels with alkaline solution. However, the use of local source of silica and alumina to compensate chemical sources are motivated recent research effort towards synthesizing. Many types of zeolites were developed based on kaolin in previous years. But in the case of zeolite membrane, the syntheses from kaolin have been less

studied. Kaolin is a clay mineral consisted in the mineral kaolinite and it is locally available in Thailand. Furthermore, kaolin can be transformed to mullite by calcination at high temperature for preparing a ceramic support.

Therefore, the aim of this thesis focused on how to prepare an appropriate sodium zeolite membranes for separating water from ethanol solution. The thesis was divided into 3 parts. The first part (chapter III) was on the study of how to synthesize sodium zeolites using raw kaolin and modified kaolin and the capability of these synthesized sodium zeolites in dehydration of ethanol solution. The second part (chapter IV) demonstrated to how to prepare porous ceramic supports from raw kaolin and synthesize the best sodium zeolite membrane for water separation by using the conditions studied in the first part. The last part (chapter V) mentioned on the performance of these synthesized sodium zeolite membranes obtained from the study in the second part in separation water/ethanol mixture by pervaporation.

1.1 Research objectives

1.1.1 To study the use of kaolin for the synthesis of pure phases of sodium zeolites (ANA, JBW, SOD and CAN).

1.1.2 To synthesize and characterize sodium zeolites (ANA, JBW, SOD and CAN).

1.1.3 To study the ability of sodium zeolites in dehydration of ethanol solution.

1.1.4 To study the use of raw kaolin for the preparation of the porous ceramic supports.

1.1.5 To synthesize ANA membranes from raw kaolin, dealuminated kaolin and chemical source.

1.1.6 To characterize the properties of the ANA membrane.

1.1.7 To compare the results of using of different starting materials for synthesizing ANA membranes.

1.1.8 To study the performance of ANA membrane in separation of the water/ethanol mixtures by pervaporation.

1.2 Scope and limitations of the study

1.2.1 The hydrothermal syntheses of pure phases of sodium zeolites (analcime, Na-J(BW), cancrinite and sodalite) from kaolin and modified kaolin with various concentrations of NaOH solution and reaction times were carried out.

1.2.2 The starting material and the synthesized products were characterized by XRF, XRD, SEM, FT-IR and NH₃-TPD and TGA-DTG techniques.

1.2.3 The water adsorption was studied in ethanol solutions in the concentration range of 85-97% v/v.g

1.2.4 The porous ceramic supports were prepared by raw kaolin and using activated carbon and CaCO₃ as pore formers.

1.2.5 The analcime membranes were synthesized from starting material sources including raw kaolin, dealuminated kaolin and chemical.

1.2.6 The water separation from ethanol solutions with analcime membranes by a laboratory-made set-up for the pervaporation was studied.

CHAPTER II

LITERATURE REVIEW

2.1 Fundamental zeolite structures

Zeolites are naturally occurring crystalline aluminosilicate minerals. Zeolites have framework (three-dimensional) structures constructed by joining together $[\text{SiO}_4]^{4-}$ and $[\text{AlO}_4]^{5-}$ coordination polyhedra. By definition are assembled together such that the oxygen at each tetrahedral corner is shared with that in an identical tetrahedron (Si or Al), as shown in Figure 2.1. This corner (or vertex) sharing creates infinite lattices comprised of identical building blocks (unit cells) in a manner common to all crystalline materials (Dyer, 1988).



Figure 2.1 Representation of $[\text{SiO}_4]^{4-}$ or $[\text{AlO}_4]^{5-}$ tetrahedral (Dyer, 1988).

The structure formula of a zeolite is best expressed for the crystallographic unit cell as: $\text{M}_{x/n}[(\text{AlO}_2)_x (\text{SiO}_2)_y] \cdot w\text{H}_2\text{O}$ where n is the cation valence, M is the cation of valence n , w is the number of water molecules and the ratio y/x usually has values of 1-5 depending upon the structure. The sum $(x + y)$ is the total number of tetrahedral

in the unit cell. The portion in the bracket represents the framework composition (Breck, 1974).

2.1.1 Structure of analcime

Analcime (ANA) has a unit cell of $\text{Na}_{16}[\text{Al}_{16}\text{Si}_{32}\text{O}_{96}] \cdot 10\text{H}_2\text{O}$. The connection of chains leads to a topological cubic symmetry leaving irregular zeolite channels in the $[110]$ direction. The cubic unit cell is composed of 4-, 6- and 8-membered oxygen rings that form three non-intersecting channels (Figure 2.2). The aperture of the 8-ring pore opening is $1.6 \times 4.2 \text{ \AA}$.

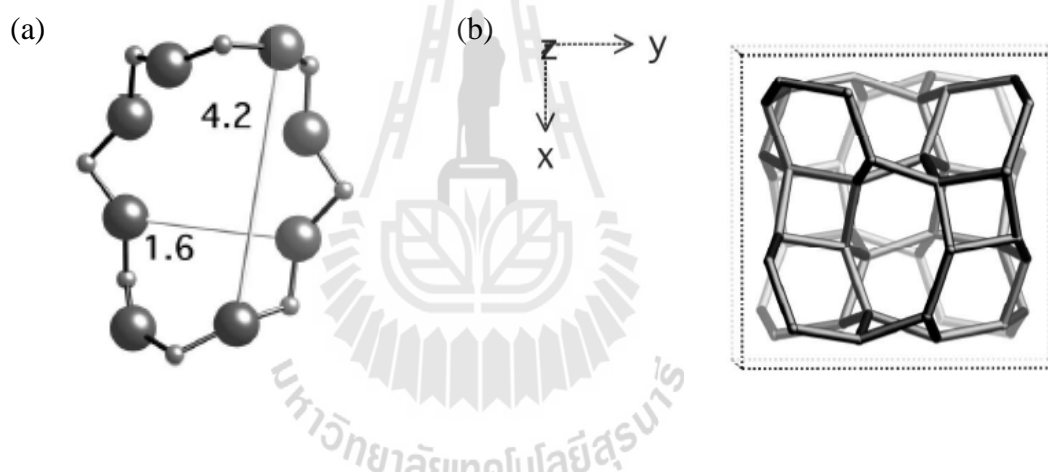


Figure 2.2 The structure of ANA (a) distorted 8-ring viewed along $[110]$ (b) framework viewed along $[001]$ (Baerlocher et al., 2001).

2.1.2 Structure of Na-J(BW)

The composition of Na-J(BW) (JBW) is $\text{Na}_3[\text{Al}_3\text{Si}_3\text{O}_{12}] \cdot \text{H}_2\text{O}$. The framework has 8-, 6- and 4- ring channels along the direction (Figure 2.3). The structure is orthorhombic. The aperture of the 8-ring pore opening is $3.7 \times 4.8 \text{ \AA}$.

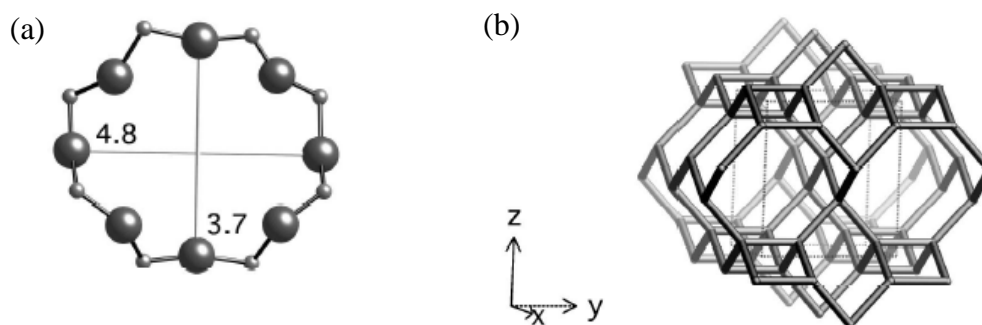


Figure 2.3 The structure of JBW (a) 8-ring viewed along [001] (b) framework viewed along [100] (Baerlocher et al., 2001).

2.1.3 Structure of cancrinite

The composition of cancrinite (CAN) is $\text{Na}_6[\text{Al}_6\text{Si}_6\text{O}_{24}] \cdot 8\text{H}_2\text{O}$. The framework of cancrinite (CAN) is featured by can cages. Can cages form the can column along c axis through the sharing of 6-ring (Figure 2.4). Six such columns are connected through sharing of 4-ring along the c axis, creating the 12-ring channel with aperture of $5.9 \times 5.9 \text{ \AA}$.

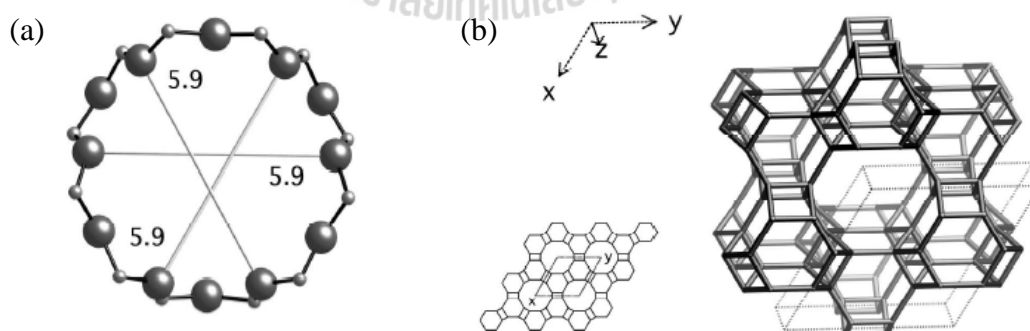


Figure 2.4 The structure of CAN (a) 12-ring viewed along [001] (b) framework viewed along [001] (Baerlocher et al., 2001).

2.1.4 Structure of sodalite

The composition of sodalite (SOD) is $\text{Na}_6[\text{Al}_6\text{Si}_6\text{O}_{24}] \cdot 8\text{H}_2\text{O}$. The SOD framework type is a body-centered cubic arrangement of β or sodalite cages joint through single 4- and 6-ring (Figure 2.5). It has only 6-ring pore openings (2.6 Å).

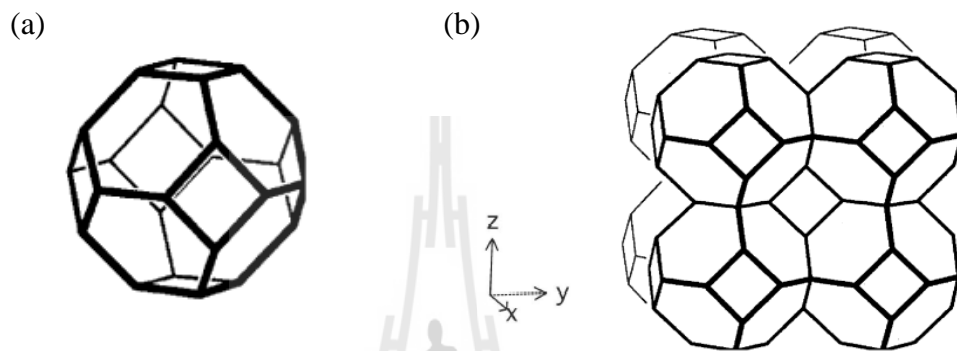


Figure 2.5 The sodalite or β -cage (a) framework of SOD viewed along [100] (b) (Baerlocher et al., 2001).

2.2 Clay minerals

The atomic structures of the common clay minerals have two structure units. One unit consists of two sheets of closely packed oxygens or hydroxyls in which aluminum, iron, or magnesium atoms are occupied in octahedral coordination (see in Figure 2.6). The second unit is built of silica tetrahedron. In tetrahedron a silicon atom is equidistant from four oxygens, or hydroxyls if needed to balance the structure, arranged in the form of a tetrahedron with a silicon atom at the center. The silica tetrahedral groups are arranged to form a hexagonal network (see in Figure 2.7) (Grim, 1968).

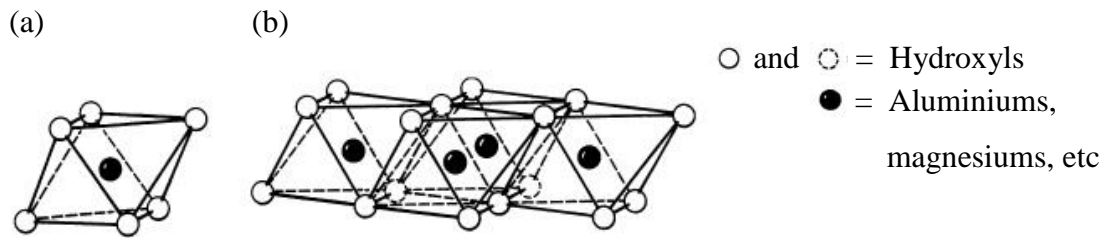


Figure 2.6 Single octahedron (a) and the sheet structure of octahedral units (b) (Grim, 1968).

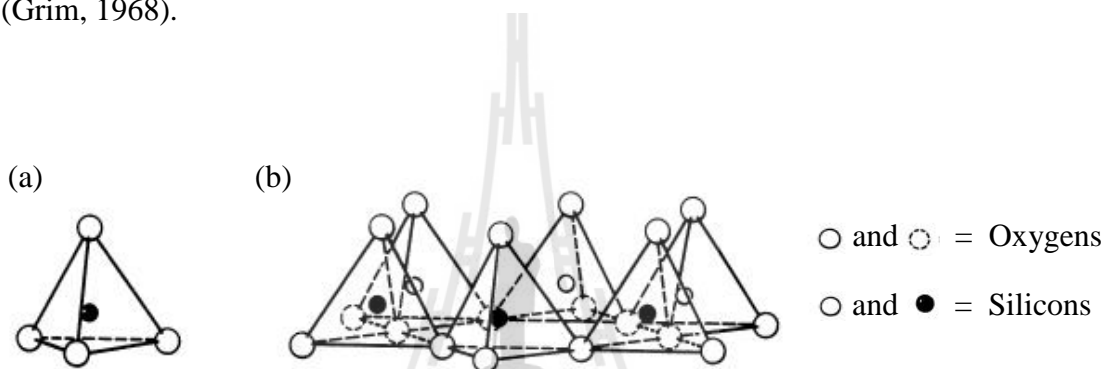


Figure 2.7 Single silica tetrahedron (a) and the sheet structure of silica tetrahedrons arranged in a hexagonal network (b) (Grim, 1968).

The crystal structure of all phyllosilicates is based on two types of layer 1:1 layers in which one tetrahedral sheet is bonded to one octahedral sheet and 2:1 layers in which one octahedral sheet is sandwiched between two tetrahedral sheet (Meunier, 2005).

Kaolinite is single-layer structure. Kaolin is a clay mineral consisted in the mineral kaolinite. The kaolin includes the clay minerals nacrite, dickite, kaolinite and halloysite (Worrall, 1986). The chemical formula of kaolinite is $(\text{OH})_4\text{Si}_2\text{Al}_2\text{O}_5$ and the theoretical composition expressed in oxides is SiO_2 , 46.54%; Al_2O_3 , 39.50%; and H_2O , 13.96%. The structure is composed of a single silica tetrahedral sheet and a

single alumina octahedral sheet combined in a unit so that the tips of the silica tetrahedrons and one of the layers of the octahedral sheet form a common layer (see in Figure 2.8). All the tips of the silica tetrahedrons point in the same direction and toward the center of the unit made by the silica and octahedral sheets.

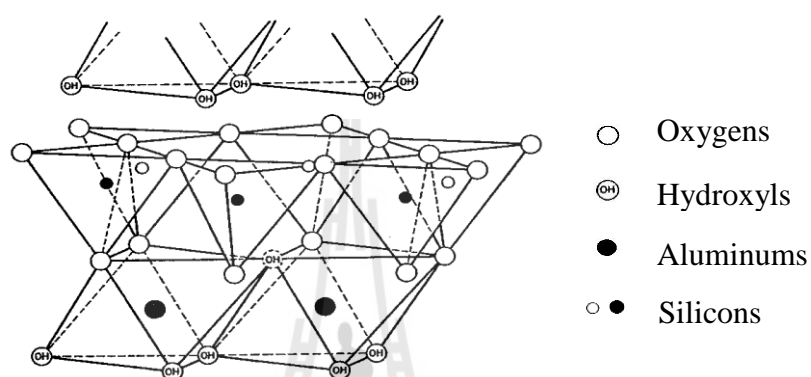
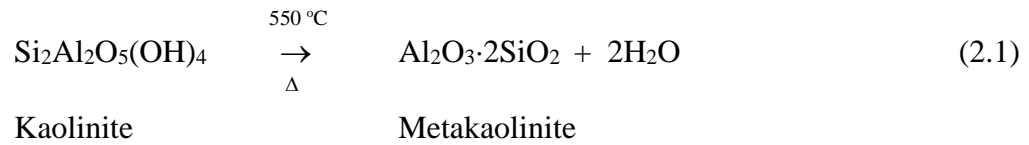


Figure 2.8 Structure of the kaolinite layer (Grim, 1968).

2.2.1 Kaolinite for zeolitization

Kaolinite is non-expanding and as a result of its high molecular stability, isomorphous substitution is limited or non-existent (Brigatti et al., 2013). Kaolinites were used as the source of alumina and silica in the zeolite synthesis were performed by calcination between 700 °C and 1000 °C to produce metakaolin by dehydroxylation process (Bosch et al., 1983; Costa et al., 1988; Chandrasekhar and Pramada, 2001). Recently, many authors used raw kaolin with and without calcinations as starting material in synthesis of zeolite (Rios et al., 2011; Hegazy et al., 2010; Liu et al., 2007; Zhao et al., 2004). The reaction (2.1) involved in metakaolinization process is:



The reaction transforms four hydroxyl groups into two water molecules, which then leaves two oxygen anions in the material, as shown in the following reaction: $4(\text{OH}^-) \rightarrow 2\text{H}_2\text{O} + 2\text{O}^{2-}$. The metakaolin then undergoes hydrothermal treatment in NaOH to produce zeolite. The general conversion reaction of reactants, such as polymeric silica and alumina, to a microporous zeolite crystalline framework, is shown as below:



According to Chang and Bell (1991), this process is a reversible mechanism, as the first reaction (2.2) is the breaking and making of T–O–T, where T can be Al or Si. Meanwhile, the latter reaction (2.3) is the condensation reaction that forms the basic framework structure of silicate and aluminosilicate units by means of electrostatic and van der Waals interaction. This reaction is catalyzed by hydroxyl ions.

The mineral phase transformation of kaolin after contraction the alkaline solutions indicates that there are two major processes involved in the reactions by the following reactions (Zhao et al., 2004);



Reaction (2.4) describes the dissolution of kaolin releasing Si and Al and reaction (2.5) describe the precipitation of zeolites.

2.2.2 Nucleation and growth process of the zeolite synthesis

The process of synthesis can be described by two main stages: (1) the dissolution of aluminosilicate compounds releasing Si and Al and (2) the zeolite crystallization. Zeolites are typically crystallized from amorphous aluminosilicate precursors in aqueous solution in the presence of alkali metals. A simple scheme of the crystallization of an amorphous aluminosilicate hydrogel to SOD and CAN is given in Figure 2.9 (Reyes et al., 2013).

(a) The dissolution of the starting materials occurred and produced an amorphous gel by the presence of small oligomers. A dissolution process promotes the formation of the nutrients (ionic species) which then are transported to the nucleation sites, indicating that the ionic species are not static, because they necessarily need to move (transportation) to the nucleation sites.

(b) A nucleation process produced an equilibrated gel. During nucleation, hydrogel composition and structure are significantly affected by thermodynamic and kinetic parameters.

(c) A polymerization of SiO_4 tetrahedra proceeds, which is represented by TO_4 primary tetrahedral building units have been joined revealing how they link together to form larger structures. A polymerization is the process that forms the

zeolite precursors, which contains tetrahedral of Si and Al randomly distributed along the polymeric chains that are cross-linked so as to provide cavities large enough to accommodate the charge balancing alkali ions.

(d) During crystal growth the TO_4 units were linked, with the formation of 4-ring and 6-ring, composed by 4 and 6 tetrahedral atoms, respectively, to create a large structure (secondary building unit) like the SOD β -cage.

(e) The crystallization of zeolite LTA occurred by linking the same secondary building units together.

(f) A phase transformation occurred as represented by the sequence of reaction: zeolite LTA \rightarrow SOD \rightarrow CAN.

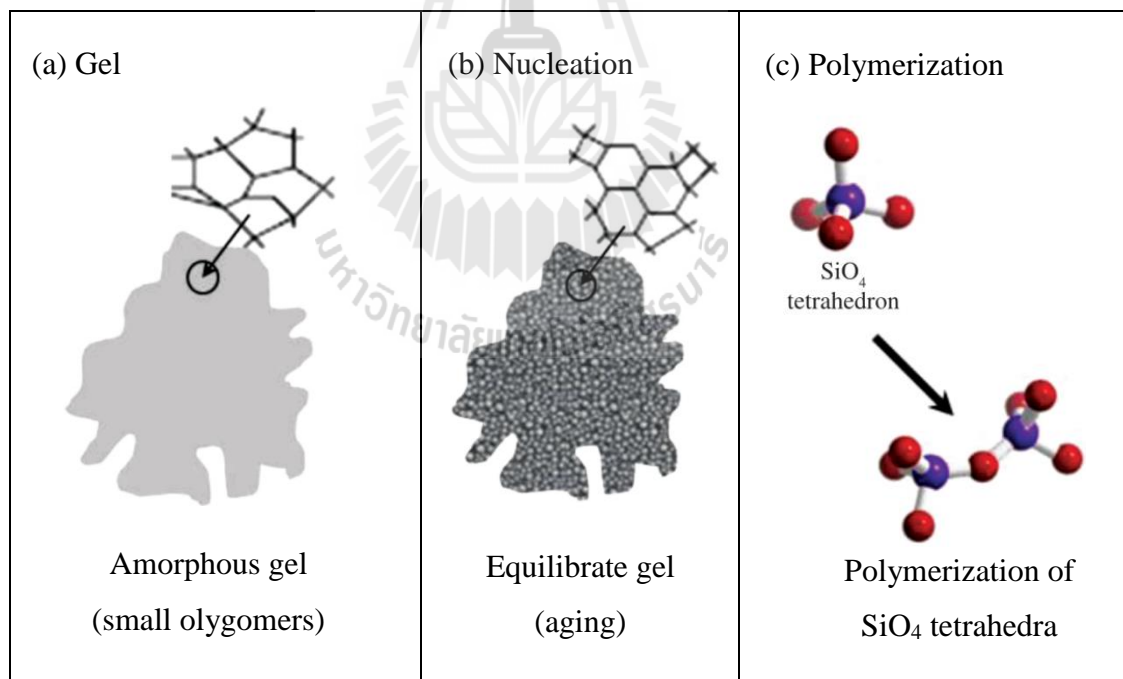


Figure 2.9 Illustration of the proposed sequence for the formation of zeotypes (Reyes et al., 2013).

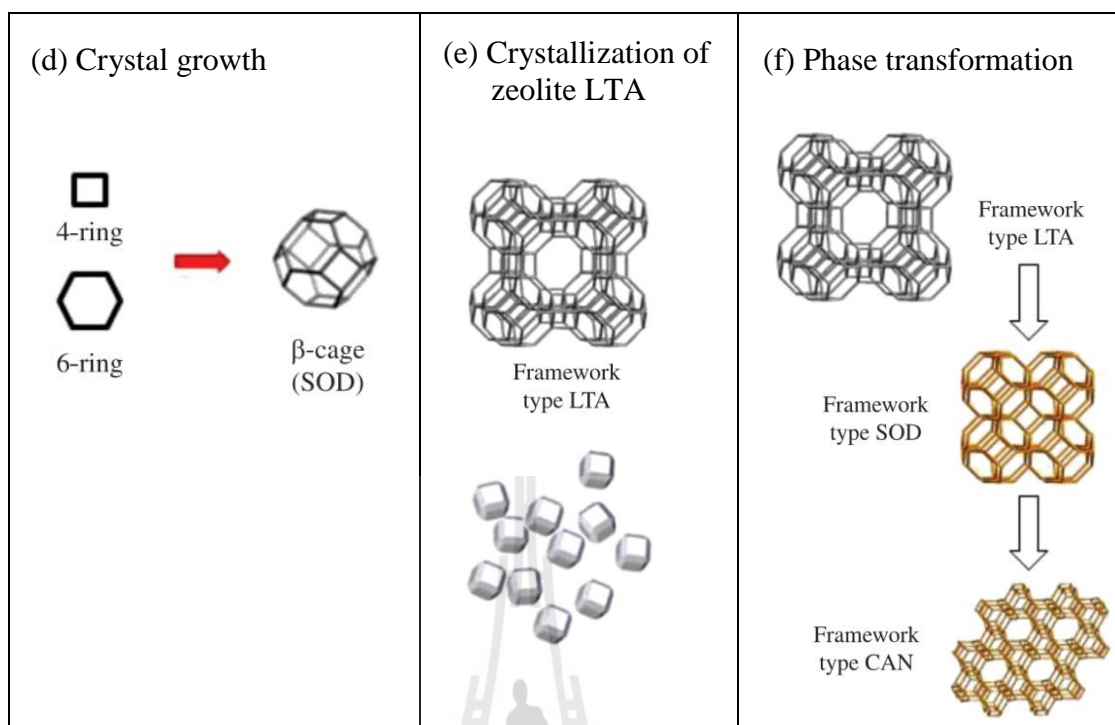


Figure 2.9 Illustration of the proposed sequence for the formation of zeotypes (Reyes et al., 2013) (Continued).

2.3 The adsorption of water from ethanol with zeolite

Hydrophilic zeolite is microporous material having small pore size and low Si/Al mol ratio. Adsorption sites for water molecules are the accessible spaces in the vicinity of cations in the micropores. Monovalent cation species, such as a sodium cation or a potassium cation showed a strong affinity to water in ethanol (Yamamoto et al., 2012). The critical diameter is 4.4 Å for an ethanol molecule and 2.6 Å for water molecule. The prevention of water or ethanol molecule from entering the narrow pores of the zeolite structure can be explained in terms of a steric hindrance. For example, zeolite 3A and 5A show comparable properties for the sorption of water, but they differ profoundly in their sorption of ethanol, which was negligible small in

zeolite 3A compared to zeolite 5A, in spite of the much larger enthalpy of sorption of ethanol in zeolite 3A (Lalik et al., 2006).

On the other hand, the snapshots of ethanol-water mixture molecules in pure silica zeolite such as DON zeolite were showed in Figure 2.10 (Lu et al., 2007). The orientation adsorption of either component, namely each adsorbed molecule located randomly, it does not prefer any special site. The water molecule could enter the smaller pores and cage of zeolites but ethanol is excluded by those small pore and cage (Figure 2.10). So the adsorption and separation performance of zeolite is not only determined by pore size but also by framework of zeolite, which determines the number of small pore and cage (Lu et al., 2007).

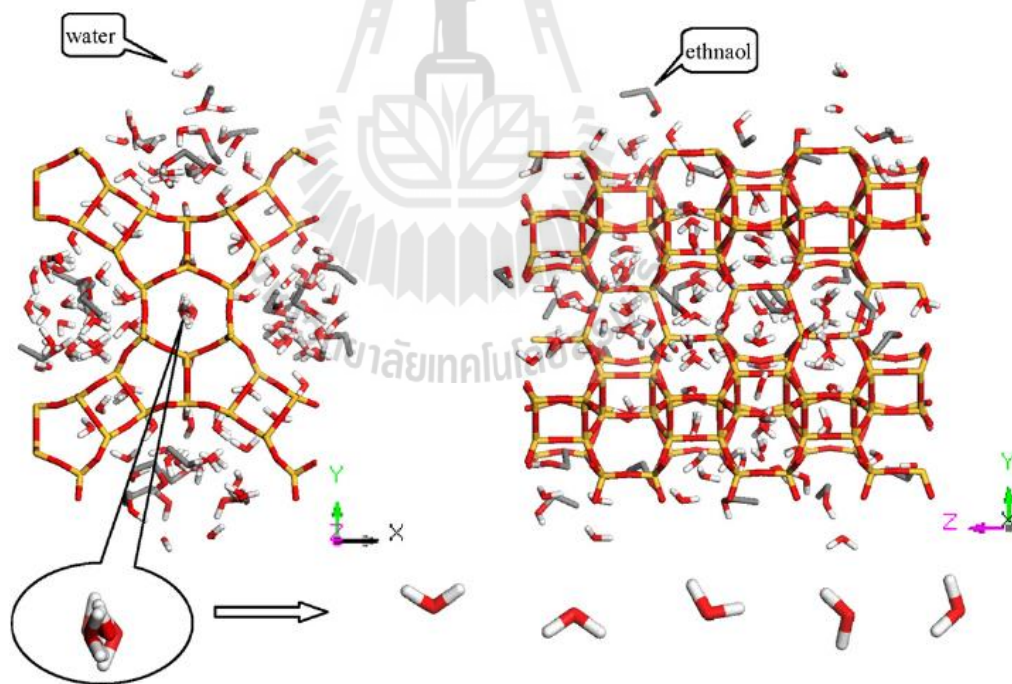


Figure 2.10 The snapshots of water-ethanol mixture molecules in DON zeolites for 0.5 water mole fraction of bulk phase (the row of water molecules at the bottom of the figure is the configuration of water located in the small channel) (Lu et al., 2007).

Figure 2.11 compiles three different adsorbate structures of water adsorbed on alkali-metal zeolites. The most likely adsorbate form is structure A while structure B shows at least for low equilibrium pressures. Water molecules adsorbed on Na^+ cations in pressure range (10^{-5} -1 mbar) were presented in Figure 2.12. At water equilibration pressures of up to 10^{-3} mbar, several water molecules are adsorbed on each alkali-metal cation without exhibiting lateral interactions (see in Figure 2.12, structure A). At equilibration at 10^{-2} to 1 mbar of water, water molecules were adsorbed on the first water layer around the alkali-metal cations (Figure 2.12, structure B and C).

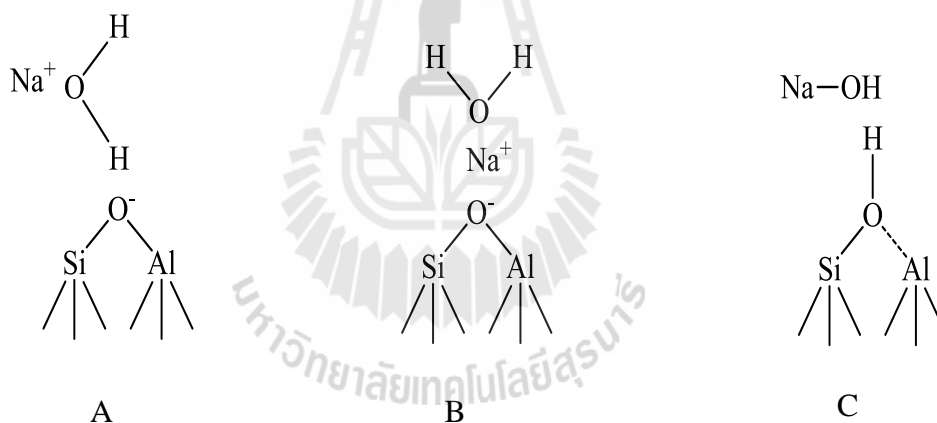


Figure 2.11 Possible adsorbate structures of water on alkali ZSM5 (Jentys et al., 1989).

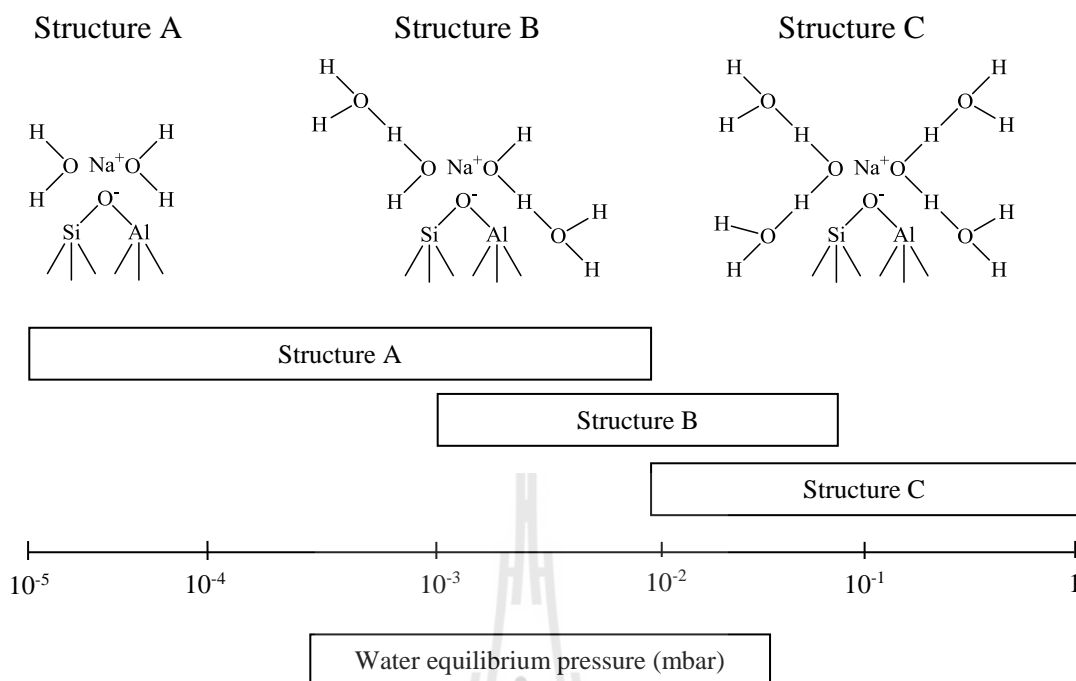


Figure 2.12 Schematic adsorbate structures of water on alkali-metal ZSM5 at the pressure indicated (Jentys et al., 1989).

2.4 Synthesis of zeolites

Zeolite synthesis is usually performed under the basic Na₂O-Al₂O₃-SiO₂-H₂O system. Increasing the ratio of OH⁻/Si leads to higher solubility of silicon and aluminum sources which will alter the polymerization state and their distribution. Higher alkalinity can decrease the polymerization degree of the silicate anions and speed up the polymerization of the polysilicate and aluminate anions. Thus, increasing alkalinity will shorten the induction period and nucleation time and speed up the crystallization of zeolites. The Si/Al ratio in the parent mixture plays an important role in determining the structure and composition of the final product. In general, zeolites with low Si/Al ratios can be crystallized from a parent mixture with low Si/Al

ratio and strong alkalinity, whereas high-silica zeolites can be crystallized from a gel with high Si/Al ratio and weak alkalinity. Hydrophilic zeolites with low Si/Al ratio and small pore size such as ANA, JBW, SOD and CAN have been interested in this research.

2.4.1 Synthesis of ANA

ANA can be synthesized by hydrothermal process and the Si/Al ratio of synthetic analcime is varied between 1.5 and 3 (Balgord and Roy, 1971). Yokomori and Idaka (1998) synthesized ANA with tetraethylorthosilicate and aluminium isopropoxide including tetramethylammonium bromide (TMABr) acted as a structure directing agent. The formal molar composition of the mixture was $13\text{SiO}_2:\text{Al}_2\text{O}_3:4\text{Na}_2\text{O}:138\text{NaCl}:3\text{TMA}_2\text{O}:3480\text{H}_2\text{O}$. The mixture was aged at 80 °C about 3 h and then heated under autogeneous pressure at 200 °C for 141 h. The crystals have an icosahedron shape with the size of about 200 μm .

Yang et al. (1997) used glycerol aluminosilicate gel and sodium aluminate in hydrothermal synthesis at 150 °C. A gel had a composition of $10.0\text{Na}_2\text{O}:1.00\text{Al}_2\text{O}_3:3.9\text{SiO}_2:100.0\text{glycerol}$. The effects of varying Si/Al ratio and NaOH content in the synthesis mixtures were investigated. It was found that when increasing the Si/Al ratio, the yields appeared in the increasing sequence of sodalite \rightarrow mixed phase of omega + analcime \rightarrow ferrierite \rightarrow offertite \rightarrow analcime. When increasing the NaOH content at constant Si/Al ratio of 6.95 the yields were occurred in the increasing sequence of amorphous \rightarrow omega \rightarrow analcime \rightarrow analcime and sodalite.

Tatlier et al. (2007) synthesized ANA with colloidal silica, sodium aluminate and sodium hydroxide by microwave and conventional heating. The clear

solution composition was presented $80\text{Na}_2\text{O}:\text{Al}_2\text{O}_3:160\text{SiO}_2:3200\text{H}_2\text{O}$. ANA with 100% crystallinity could be obtained after 2 h at $180\text{ }^\circ\text{C}$ in the presence of microwave while 65.2% with conventional heating. The crystal size was about $20\text{ }\mu\text{m}$. Montagna et al. (2011) used fumed silica and aluminium oxide hydroxide (AlOOH) at the temperature of $115\text{ }^\circ\text{C}$. The nanocrystal size of ANA (25-50 nm) was obtained. Park et al. (2012) synthesized hydrothermally with sodium silicate, sodium aluminate and sodium hydroxide. The synthesis mixture comprised of $8.0\text{Na}_2\text{O}:1.0\text{Al}_2\text{O}_3:11.5\text{SiO}_2:900\text{H}_2\text{O}$. The obtained crystal was spherical with the size of $25 \pm 4.2\text{ }\mu\text{m}$ at $150\text{ }^\circ\text{C}$ and reaction time of 2 days.

Other materials such as natural oligoclase crystals (Słaby and Kozłowski, 2002) and perlite (volcanic glass) (Dyer et al., 2004) were used for synthesis of ANA. Perlite was proved to be a successful source material for the synthesis of ANA by reacting with sodium hydroxide at $140\text{ }^\circ\text{C}$ for 24 h. Hegazy et al. (2010) used kaolin and sodium silicate as silica and alumina source for the synthesis of ANA with reaction time of 24 h at $200\text{ }^\circ\text{C}$. Well crystalline spherical particles of analcime were obtained with the size of $10\text{ }\mu\text{m}$. Atta et al. (2012) used the reaction mixture of metakaolin as alumina source, silica from rice husk ash (RHA) and sodium hydroxide for the synthesis of ANA. The mixture ($1.3\text{Na}_2\text{O}:\text{Al}_2\text{O}_3:7\text{SiO}_2:132\text{H}_2\text{O}$) was aged for 72 h with reaction time of 24 h at $180\text{ }^\circ\text{C}$. Analcime formed was found to have trapezohedral morphology with the size ranging from 15 to $25\text{ }\mu\text{m}$.

Chaisena and Rangriwatananon (2005) used modified diatomite prepared by treatment of the natural raw diatomite with heat and acid. Modified diatomite was reacted with $\text{Al}(\text{OH})_3$ and NaOH by conventional hydrothermal synthesis. The optimum condition was 10% v/v NaOH , solid/liquid ratio (S/L) = 1/10

at 140 °C for 132 h. The analcime has icosahedral shape with a diameter of approximately 100 µm. In addition, Ghobarkar and Schäfer (1999) investigated the crystal symmetry of the analcimes formed by varying the temperature in a characteristic way that the change of crystal morphology by temperature can be seen. Starting from 160 °C only orthorhombic crystals appeared. At medium temperature (230-270 °C) the symmetry changed to tetragonal and became cubic in a temperature interval between 300 and 450 °C. At 500 °C and above the tectosilicate Na-leucite was formed instead of analcime. The syntheses were performed by hydrothermal treatment of artificial glasses with $\text{Na}_{16}(\text{Al}_{16}\text{Si}_3\text{2O}_{96})\cdot 16\text{H}_2\text{O}$ for 6 weeks. The crystal sizes were varied between 500 nm and 100 µm.

2.4.2 Synthesis of SOD, CAN and JBW

Kaolin was widely used in the synthesis of CAN, SOD and JBW. Zhao et al. (2004) observed that kaolin reacted with waste solutions which were high in NaOH, NaNO_3 and NaAlO_2 . The reactions were performed at 50 °C and 80 °C for up to 2 months, resulting in the transformation of kaolin into cancrinite and sodalite. With increasing NaOH concentration and reaction temperature and decreasing NaAlO_2 concentration, the rate of transformation was increased. Lin et al. (2004) investigated the hydrothermal transformation of metakaolin in alkaline medium at 200 °C. The samples were synthesized by mixing 5 g kaolinite, 13.95 g NaOH and 30 g deionized H_2O . JBW zeolite was obtained from the transformation of zeolite A for 4 days with molar ratio of $\text{Na}_2\text{O}/\text{Al}_2\text{O}_3 = 1.45$. The high crystallinity of CAN was obtained by transformation of SOD with the molar ratio of $\text{Na}_2\text{O}/\text{Al}_2\text{O}_3 = 1.92$ for 8 days. Okubo et al. (2001) reported the transformation of SOD into CAN with similar structure and identical aluminosilicate layers of six-membered ring. CAN has

a hexagonal framework which contains small ϵ -cages made of six-membered rings while SOD has cubic framework containing only β -cages (sodalite cages) made up of 6-membered rings.

Rios et al. (2011) reported the use of triethanolamine (TEA) as a structure-directing agent with molar composition, $\text{Na}_2\text{O}:\text{Al}_2\text{O}_3:2\text{SiO}_2:0.5\text{TEA}:863\text{H}_2\text{O}$. The hydrothermal synthesis at 200 °C, resulted in phase transformation of SOD and CAN into JBW, as shown by the co-crystallization of SOD and CAN with shorter reaction times (around 6 h), followed by the transformation into JBW with longer reaction times (24-48 h). Healey et al. (2000) achieved in synthesizing pure phase of JBW from meta-kaolin under hydrothermal conditions at 225 °C for 2 days. The molar composition was $6\text{Na}_2\text{O}:3\text{K}_2\text{O}:4.12\text{Al}_2\text{O}_3:8.24\text{SiO}_2:202.8\text{H}_2\text{O}$. In addition, fly ashes were used for the synthesis of cancrinite-type zeolite at 140 °C for 72 h. The composition of synthesis was 6 g fly ashes, 7.2 g NaOH and 60 ml deionized water. The pore size was in the range from 20 Å to 200 Å (Qiu and Zheng, 2009). Furthermore, Chaisena and Rangsriwatananon (2005) used modified diatomite synthesized cancrinite and hydroxysodalite with 20% v/v NaOH (S/L = 1/10) at 180 °C after 72 h and 30% v/v NaOH (S/L = 1/30) at 100 °C for 96 h. The cancrinite appeared in fractal shape comprised of extended bar with lengths of approximately 30 μm . The prismatic particle shape of the hydroxysodalite having diameter of approximately 5 μm was obtained. Zeolite X was also used as starting material for the hydrothermal synthesis of CAN at 80 °C for 27 h (Linares et al., 2005).

Usually, the impurities of kaolinite are K_2O , CaO , MgO , etc, among which K_2O has an especial effect in the phase transition of kaolinite. The addition of MgO to kaolinite caused mullite formation via spinel or $\gamma-Al_2O_3$ phase and that of CaO caused mullite formation directly from metakaolinite (Bulens and Delmon, 1977). Yamuna et al., 2002 showed the mullite formation in kaolinite by comparing the influence of certain carbonate mineralizers such as $CaCO_3$, Na_2CO_3 and K_2CO_3 . It was found that Na_2CO_3 and K_2CO_3 gave rise to acicular mullite crystals, while $CaCO_3$ give rise to needle-shaped mullite crystals. Moreover, $CaCO_3$ and Na_2CO_3 gave rise to multiphase systems (mullite and cristobalite). When K_2CO_3 was incorporated in the samples, it gave pure phase mullite by calcination at $1,350\text{ }^\circ\text{C}$. Because $CaCO_3$ and Na_2CO_3 melt at a lower temperature and the chances of amorphous SiO_2 dissolving in them are greater compared to K_2CO_3 and the possibility of converting SiO_2 to cristobalite is greater. In addition, an apparent porosity of kaolinite- $CaCO_3$ was the maximum but bulk density was the minimum.

The porosity of ceramic membranes gains attention in the scientific community for their outstanding merits such as low cost, species diversity and novel additional properties. Also, the development of novel porous mineral-based ceramics is an important to a critical new technological revolution. Sun et al. (2009) and Wang and Lin (2012) used of rough porous alumina support to prepare ZSM-5 zeolite membrane whose the surface of rough porous alumina support was polished with SiC paper before being coated. It was found that ZSM-5 zeolite membrane showed continuous surface displaying densely packed crystals with free of crack and pinholes was observed from SEM image.

The most common one for preparation of porous mullite support is by using agents as pore former. Bai (2010) produced porous mullite ceramics from calcined carbonaceous kaolin and α -Al₂O₃ powder using graphite as pore former. Open porosity was 36.4% and pore size was in a narrower range of 0.3-5 μ m. Esharghawi et al. (2009) used Al and Mg metallic powders to produce a porous mullite ceramics from kaolin. The porosity was increased from 30 to 58%. The addition of calcite into kaolin has been applied to control or help in forming pores with suitable distribution and sizes. The calcinations of kaolin-calcite mixture resulted in anorthite (CaO·Al₂O₃·2SiO₂) phase transition without the undesirable cristobalite phase (Harabi et al., 2014).

Furthermore, another technique to produce porous mullite support is through the removal of cristobalite produced from calcined bodies of sintered kaolin by leaching with strong alkali solutions (Abbasi et al., 2010; Kazemimoghadam and Mohammadi, 2011). The porosity of the support before leaching was 24.3% while after treatment it was increased to 49%. Free silica removal was carried out with 20 wt% of NaOH solution at temperature 80 °C for 5 h.

2.6 Preparation of zeolitic membrane for separation of water/ethanol mixture

Zeolitic membranes for water separation from ethanol solution are most often prepared by hydrothermal synthesis with gel method. Hydrothermal synthesis involves crystallization of a zeolite layer onto a porous support from a gel including amorphous silica, alumina, a structure directing organic template and alkaline solution. Supports are generally alumina, stainless steel tube and mullite. The porous

support and a gel are placed in an autoclave. The different conditions of synthesis include temperature, time and gel compositions (Bowen et al., 2004). The support is immersed in a synthesis mixture containing the zeolite precursors and is kept at a certain temperature for a specific duration of time. The zeolite is produced through the formation of nuclei on the support surface followed by their consecutive growth into crystals, which under suitable conditions can grow to form a continuous and uniform film (Khajavi et al., 2007).

So far, a number of synthetic strategies have been applied to zeolite membrane synthesis, such as in situ or direct (without seeding) hydrothermal synthesis (Zah et al., 2006), secondary (seeded) growth method (Li et al., 2013), vapor phase transport (Nishiyama et al., 1996) and microwave heating (Julbe et al., 2003; Xu et al., 2004), etc. The widely-used synthesis strategies are in-situ hydrothermal synthesis, secondary growth method and microwave heating. Each of these methods has certain drawbacks, which leads to the formation of good or poor membrane. In the secondary growth method, the seed particles act as nuclei for the growth of zeolite crystals. The seed layers such as the properties like crystal size of seed particles, thickness, density and continuity are important toward the separation performance of the prepared zeolite membranes (Basak et al., 2014). The orientation of the crystal seeds on the support cannot be easily controlled and it has to be assured that a homogeneous layer of seeds with narrow size distribution is applied on the support, and rather thick membranes are formed leading to low fluxes (Khajavi et al., 2007). The formation of zeolite NaA membrane prepared by growth method might proceed as illustrated in Figure 2.13 (Okamoto et al., 2001).

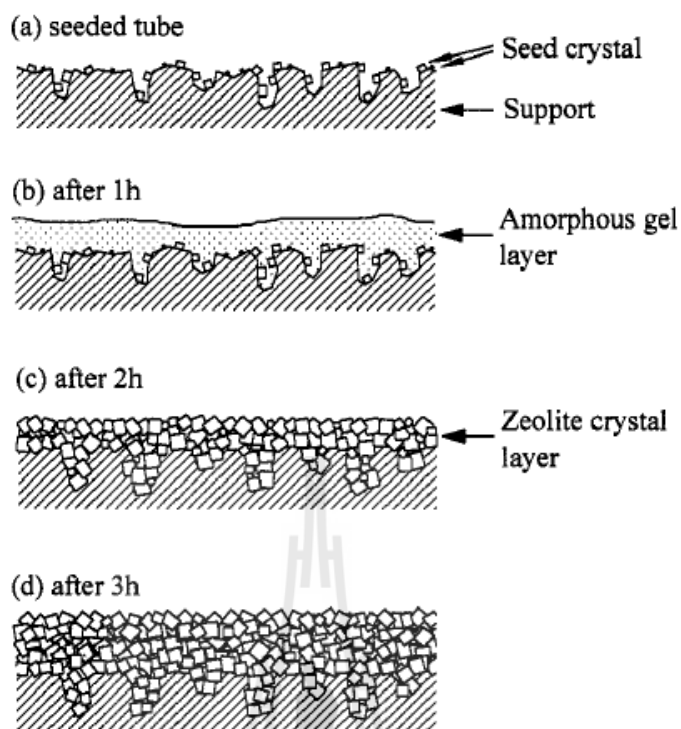


Figure 2.13 Schematic illustration of formation process of zeolite NaA membrane: (a) seeded support tube and (b-d) membranes after 1, 2, and 3 h, respectively, of the synthesis (Okamoto et al., 2001).

The use of microwaves poses inhomogeneous heating of the sol and support material. Since the penetration depth of microwaves is limited to only a few centimeters by a temperature gradient develops in the synthesis solution. The presence of this temperature gradient may explain the formation of excessive amounts of loose powder during microwave assisted membrane synthesis (Khajavi et al., 2007). While of in-situ synthesis, a simultaneous and abundant heterogeneous nucleation is the prerequisite for the formation of good quality zeolite membrane (Li et al., 2006).

In application for the separation of water/ethanol mixture many types of hydrophilic zeolite membranes were synthesized. Firstly NaA zeolite membrane,

Morigami et al. (2001) synthesized NaA zeolite on porous tubular support (mullite + Al₂O₃ + cristobalite) by secondary growth method. A gel consisting of sodium silicate, aluminum hydroxide, sodium hydroxide and DI water was prepared. The XRD patterns of the membrane showed strong peaks corresponding to NaA zeolite and weak ones to the support after crystallization for 3.5 h. Scanning electron microscope (SEM) showed complete coverage of zeolite NaA crystals with 2-4 μm in size. A cross section of these membranes with the thickness of 10 μm was observed. Okamoto et al. (2001) prepared tubular zeolite NaA membrane by using a gel and porous α-alumina support tube with shorter reaction time of 3 h at 100 °C. XRD pattern of the membrane after 3 h clearly displayed the characteristic peak of zeolite A and weak substrate peaks. The intensity of zeolite NaA peak became much weaker for the membrane after 6 h of reaction time. A dense inter-grown zeolite crystal layer of about 30 μm in thickness was formed on the outer surface.

Mohammadi and Pak (2003) used natural material as kaolin for the synthesis of zeolite A membrane by electrophoresis. The mixture slurry (kaolin + DI water + tripolyphosphate) was poured into the space between anode and cathode and the electric field was applied to the slurry. Kaolin particles due to their charges moved toward the anode and deposited on tubular modules. Kaolin on module was calcined (700 °C) to produce metakaolin. A tubular model was placed with sodium hydroxide solution in an autoclave. The maximum of zeolite A size at the surface was 1.65 μm and membrane thickness was about 500 μm. The thickness of the synthesized membrane could be increased by increasing the sodium hydroxide diffusion deeper in the module, transforming metakaolin into zeolite A. The preparation from this method showed low separation factor.

Next, Pina et al. (2004) studied the method of synthesis of NaA zeolite membrane by using a semi-continuous system. The fresh gel was periodically fed to the synthesis vessel with controlling of temperature at 90 °C. Compared this method with traditional batch methods, the procedure developed in this method provided a better control of the synthesis and crystallization condition. Kunnakorn et al., 2011 studied the synthesis of NaA zeolite membrane on an alumina support via microwaving and autoclaving. The microwave method employed shorter reaction time (30 min) at 90 °C whereas the convention method required the reaction time of 20 h at 60 °C. From SEM images, it was clearly seen that smaller zeolite crystals formed by the microwave technique was well inter-grown influencing a better performance for the separation.

In addition, porous metal were also interesting for synthesized zeolite membrane. Zhang and Liu (2011) synthesized NaA membranes for the first time on a thin porous metal substrate sheet of only 50 µm in thickness and followed by secondary hydrothermal growth. A high quality NaA zeolite membrane directly on the porous metal substrate of thickness ≤ 2 µm was obtained. A stable zeolite membrane layer of both high water flux and high selectivity was obtained by controlling the membrane thickness to less than 3 µm and to a certain degree of the zeolite growth into the substrate pore. However, ceramic supports have been continuously studied. Basak et al. (2014) prepared NaA membranes on porous α -alumina support tubes by primary (*in-situ*) and secondary (*ex-situ*) crystallization process. Poly (ethyleneimine) was used as a buffer layer for proper attachment of the NaA seed crystals onto support surface for secondary crystallization process. The membrane prepared by primary crystallization process showed better quality in terms of maximum surface coverage,

interlocked crystal arrangement and rendering better separation factor for ethanol/water mixture. The as-prepared NaA film (membrane) formed by primary and secondary crystallization on to the inner surface of the tube were showed in Figure 2.14.

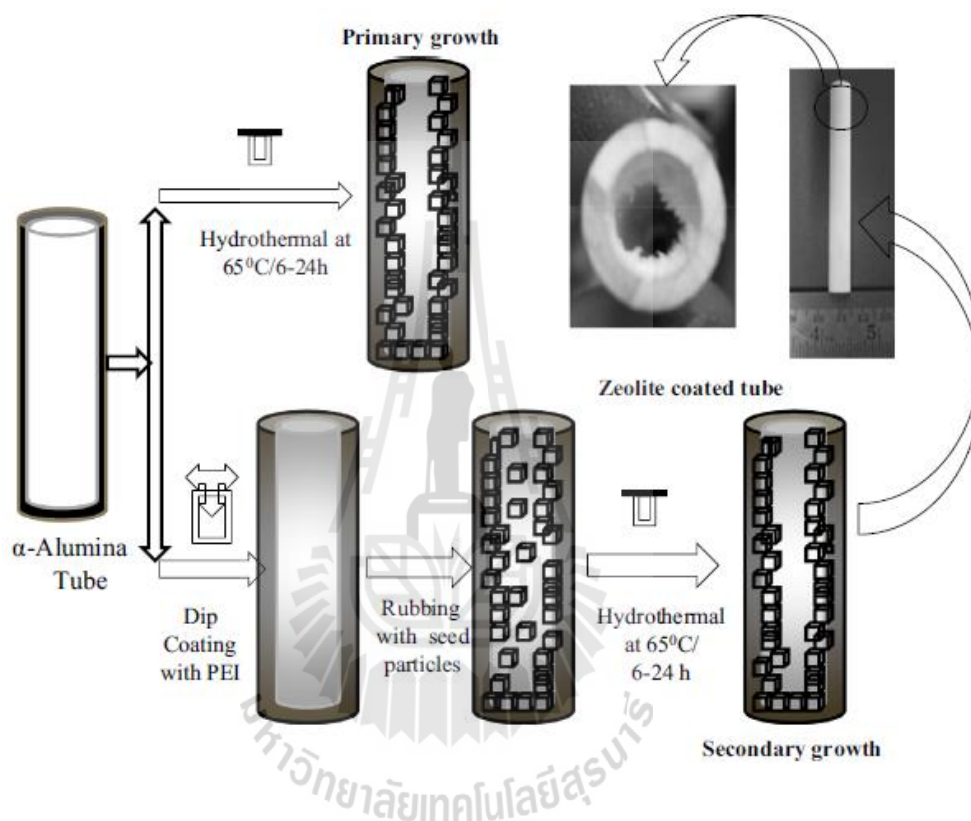


Figure 2.14 Schematic representation for the formation of NaA zeolite membranes prepared by primary and secondary crystallization (Basak et al., 2014).

Zhang et al. (2002) prepared a mordenite membrane by synthesizing mordenite on α -Al₂O₃ tube by in situ hydrothermal synthesis with tetraethylammonium bromide as template agent. By the application of aging process of the parent solution, the size of mordenite crystals could be remarkably reduced from 20-30 (without aging) to 4-5 μ m. Navajas et al. (2002) synthesized a mordenite

membrane by seeded hydrothermal synthesis followed by conventional synthesis (secondary hydrothermal synthesis). The XRD patterns showed that mordenite was only zeolite material present in the membrane.

However, the findings of other zeolite via economic way have been regarded. According by Kazemimoghadam and Mohammadi (2011) synthesized hydroxysodalite (H-SOD) from metakaolin and chemical on porous mullite tubular support by secondary crystallization method. Which support was prepared from sintering of kaolin then removed free silica. Thin layer of H-SOD were produced with impurity phase of mullite. The synthesis of H-SOD from both starting material produced high separation factor. Therefore, zeolite membrane preparation from cheap raw natural materials is of economic importance and hence it is necessary to production of zeolites by economical ways.

2.7 The separation of water/ethanol mixture by pervaporation

Pervaporation is the most commonly used membrane process for separations. The meaning of pervaporation is a contraction of the terms permeation and evaporation because vapor exits the membrane on the permeate side while the feed is a liquid as shown in Figure 2.15(a) (Bowen et al., 2004). The separation properties of membrane for dehydration of solvent by pervaporation included 3 steps: (i) adsorption of the components onto the membrane, (ii) diffusion of the components across the membrane and (iii) desorption of the components into the vapor phase at the permeate side (Pina et al., 2004). The pervaporation model of hydrophilic zeolite membrane for water/ethanol is presented in Figure 2.15(b).

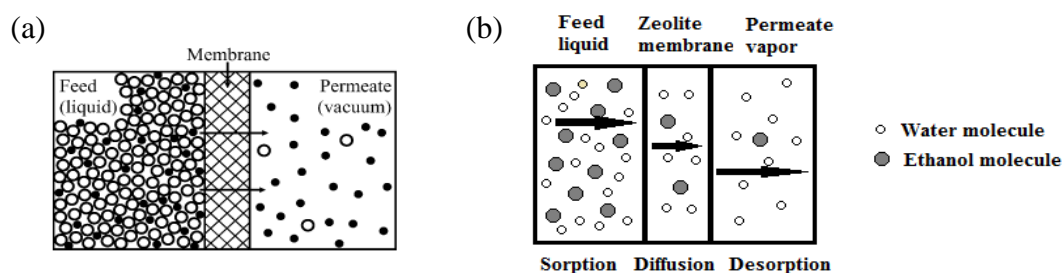


Figure 2.15 Schematic representation of (a) pervaporation across a membrane (Bowen et al., 2004) and (b) the separation properties of water/ethanol mixture (Pina et al., 2004).

The physico-chemical properties of the membranes have a great potential to separation via pervaporation. Kazemimoghadam and Mohammadi (2001) proposed that position of sodium ions in unit cells is important since these ions acted as the sites for water sorption and transport through the membrane. In H-SOD unit cell, eight sodium ions are located inside an α -cage and four ions are located in β -cages. The transport of water species through the hydroxysodalite (H-SOD) (Figure 2.16) zeolite membrane matrix comprised of three steps;

- (i) Strong adsorption of the species into α -cage from feed side.
- (ii) Surface diffusion of the species from cage to cage.
- (iii) Vaporization of the species to permeate side.

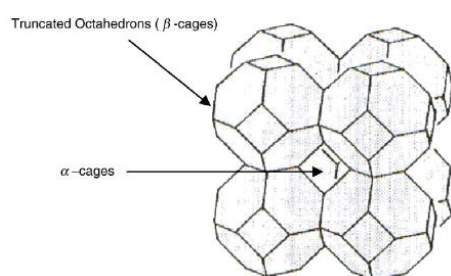


Figure 2.16 Repeating unit of zeolite H-SOD (Kazemimoghadam and Mohammadi, 2001).

Preferred molecules were adsorbed and diffused on polycrystalline zeolite membrane, not only zeolite pore but also contain transport pathways in intercrystalline regions or nonzeolitic pore (Figure 2.17(a)) (Bowen et al., 2004). The model of adsorption-diffusion by mass transfer through a composite zeolite membrane by pervaporation such as zeolite NaA membrane was represented in Figure 2.17(b) (Pera-Titus et al., 2006). The ground of polycrystalline nature of the zeolite layer is viewed as an assembly of zeolite grains that might include two different kinds of pores (Nomura et al., 2001). First kind of pore is intracrystalline or zeolite pores and second kind of pore is intercrystalline or non-zeolite pores. The former consists of subnanometric pores (mean pore size < 1 nm) defined by the zeolitic crystalline lattice, while the latter might be regarded as grain boundaries in the borderline defined between two adjacent zeolite single crystals. Both pores might involve different pathways for mass transfer owing to their different structures. Okamoto et al. (2001) proposed that water passed through the membrane by capillary condensation through both zeolitic and non-zeolitic pores.

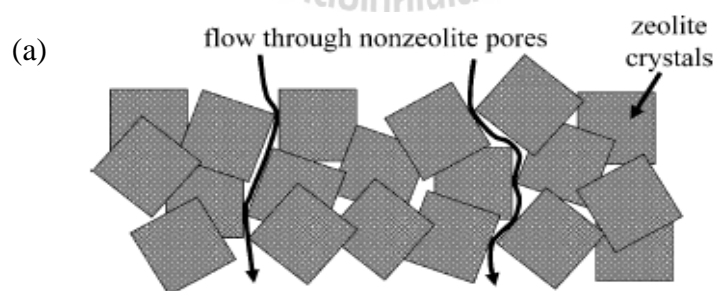


Figure 2.17 Schematic representations of (a) non-zeolite pores in the intercrystalline boundaries of a zeolite membrane layer (Bowen et al., 2004) and (b) the intracrystalline and intercrystalline pathways for mass transfer in the zeolite layer (Pera-Titus et al., 2006).

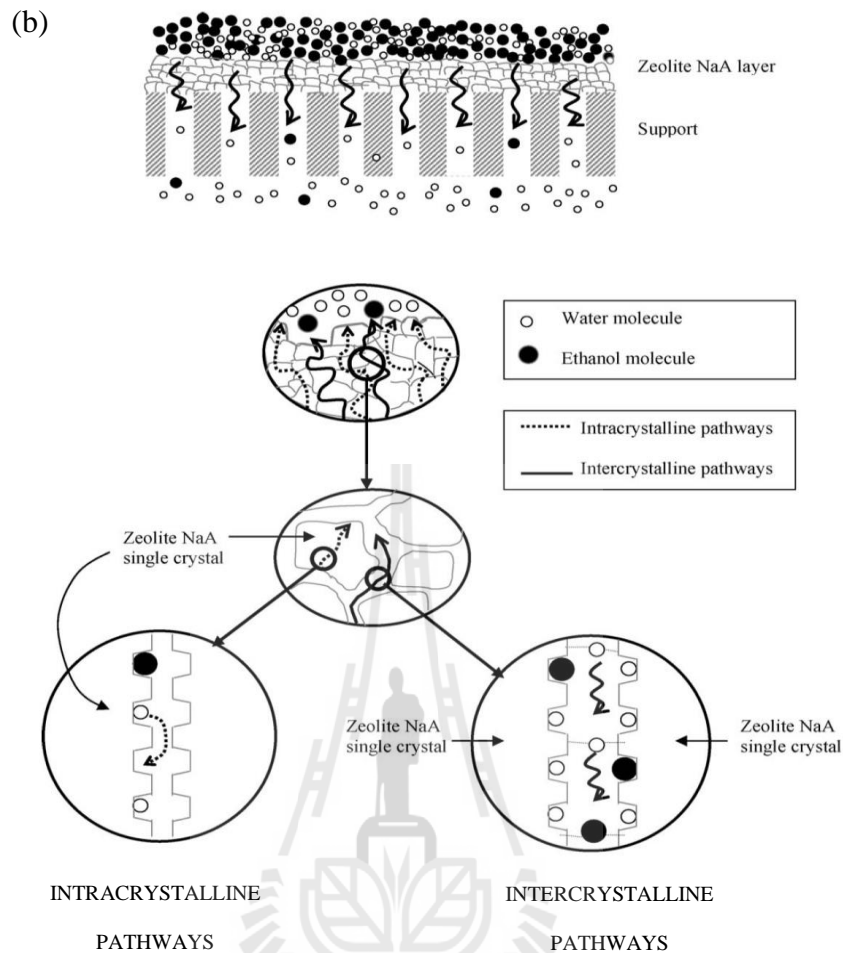


Figure 2.17 Schematic representations of (a) non-zeolite pores in the intercrystalline boundaries of a zeolite membrane layer (Bowen et al., 2004) and (b) the intracrystalline and intercrystalline pathways for mass transfer in the zeolite layer (Pera-Titus et al., 2006) (Continued).

In the case of separation of water from ethanol, many types of hydrophilic zeolites were preferred. Tanaka et al. (2001) compared zeolite A, X, Y and T membranes for ethanol dehydration. The studies indicated that zeolite A membrane showed pervaporation performance more than zeolite T, X and Y membrane, respectively. In the case of zeolite T membranes are not only offered desirable

separation properties for the dehydration of alcohols but are also stable in acetic acid. The Si/Al ratios of A, X, Y and T zeolite are 1, 1.3, 1.9 and 3.6, respectively. Kondo and Kita (2010) synthesized zeolite NaA and T-type membrane on mullite the surface of porous cylindrical mullite tubes. The pervaporation performances of zeolite NaA membranes were higher than T-type membranes. Zeolite NaA and T-type membrane showed separation factor of 10,000 and 2,100 while a total water flux of 1.69 kg/(m²h) and 1.33 kg/(m²h), respectively. The zeolite crystal layer is 10 μm for NaA and 20 μm for T-type membrane. Morigami et al. (2001) compared pervaporation performance of NaA, NaX, NaY and sodalite membrane. NaA membrane showed separation factor higher than NaX, NaY and sodalite membrane with 10,000, 360, 130 and 2, respectively. Hydroxysodalite membranes were studied by Kazemimoghadam and Mohammadi (2011). The synthesized hydroxysodalite (H-SOD) from both metakaolin and chemical on porous mullite tubular support showed the separation factor as high as 10,000 for ethanol feed concentration of 90%. The water flux was 0.32 kg/(m²h) and 0.959 kg/(m²h) for chemical source and kaolin source as starting materials, respectively.

Zeolite NaA membrane has been continuously studied because the suitable pore size is around 0.4 nm which the kinetic diameters of water and ethanol are around 0.3 and 0.42 nm, respectively (Kunnakorn et al., 2011). Mohammadi and Pak, (2003) synthesized zeolite A membrane from kaolin. The maximum size of zeolite A at the surface was 1.65 μm and membrane thickness was about 500 μm. The separation factor was 25.14. It showed low separation factor. Zeolite NaA membrane prepared by Okamoto et al. (2001) could produce 10,000 and 16,000 of separation factor while 2.15 kg/(m²h) and 1.10 kg/(m²h) of water flux of 90 wt% and 95 wt%

ethanol solution feed, respectively. A dense intergrown zeolite crystal layer of about 30 μm in thickness was formed on the outer surface. Kunnakorn et al. (2011) also presented separation factor of 10,000 and water flux of 2.82 $\text{kg}/(\text{m}^2\text{h})$. The thickness of the membrane obtained is around 7-9 μm . While Pina et al. (2004) presented the separation factor and water fluxed of 3,600 and 3.8 $\text{kg}/(\text{m}^2\text{h})$, respectively. The well-intergrown NaA layer with a thickness around 10 μm and small crystal size about 5-10 μm were obtained. Basak et al. (2014) presented NaA zeolite thickness about 20 μm . The separation factor and water flux were 42 and 0.989 $\text{kg}/(\text{m}^2\text{h})$, respectively. In addition, Zhang and Liu (2011) synthesized NaA membranes on a thin porous metal substrate sheet. A high quality NaA zeolite membrane directly on the porous metal substrate of thickness $< 2 \mu\text{m}$ was obtained. The separation factor and water flux was high as 10,000 and 4 $\text{kg}/(\text{m}^2\text{h})$, respectively.

Zhang et al. (2002) prepared a mordenite membrane by synthesizing mordenite on $\alpha\text{-Al}_2\text{O}_3$ tube. The small crystal mordenite membrane of 4-5 μm had higher performance than big crystal mordenite membrane of 20-30 μm . The separation factor and total water flux are 5,500 and 1.55 $\text{kg}/(\text{m}^2\text{h})$, respectively. While, Navajas et al. (2002) synthesized a mordenite membrane on alumina tubular supports. The membrane showed separation factor of 150 and water flux of 0.2 $\text{kg}/(\text{m}^2\text{h})$.

The pervaporation performance in ethanol dehydration of the zeolite membranes is summarized in Table 2.1.

Table 2.1 Separation of water from ethanol using various zeolite membranes.

EtOH:H₂O (mass ratio)	Membrane support	Separation layer	Separation factor	Flux (kg m⁻² h⁻¹)	Temperature (°C)	Ref.
90:10	α-Alumina	Zeolite A	10,000	2.15	75	[1]
90:10		Zeolite X	360	0.89	75	[1]
90:10		Zeolite Y	130	1.59	75	[1]
90:10		Zeolite T	830	0.81	75	[1]
90:10	Mullite, Al ₂ O ₃ , cristoalite	Zeolite NaA	10,000	2.15	75	[2]
90:10		Zeolite NaX	360	0.89	75	[2]
90:10		Zeolite NaY	130	1.59	75	[2]
90:10		Sodalite	2	0.08	75	[2]
90:10	α-Alumina	Zeolite A	10,000	2.15	75	[3]
95:5		Zeolite A	16,000	1.10	75	[3]
90:10	Metal	Zeolite A	>10,000	4	75	[4]
90:10	Alumina	Zeolite A	>10,000	2.82	70	[5]
90:10	α-Alumina	Zeolite A	42	0.989	75	[6]
-	α-Alumina	Mordenite	5,500	1.55	70	[7]
-	Metakaolin	Zeolite A	25.14	-	-	[8]
90:10	Mullite	Hydroxy-sodalite	>10,000	0.959	30	[9]

[1] Tanaka et al., 2000; [2] Morigami et al., 2001; [3] Okamoto et al., 2001; [4] Zhang and Liu, 2011; [5] Kunnakorn et al., 2011; [6] Basak et al., 2014; [7] Zhang et al., 2002; [8] Mohammadi and Pak, 2003; [9] Kazamimoghadam and Mohammadi, 2011.

2.8 References

- Abbasi, M., Mirfendereski, M., Nikbakht, M., Golshenas, M. and Mohammadi, T. (2010). Performance study of mullite and mullite–alumina ceramic MF membranes for oily wastewaters treatment. **Desalination**. 259: 169-178.
- Atta, A. Y., Jibril, B. Y., Aderemi, B. O. and Adefila, S. S. (2012). Preparation of analcime from local kaolin and rice husk ash. **Applied Clay Science**. 49: 8-13.
- Baerlocher, C., Meier, W. M. and Olson, D. H. (2001). Atlas of zeolite framework types. **Structure Commission of the International Zeolite Association**.
- Bai, J. (2010). Fabrication and properties of porous mullite ceramics from calcined carbonaceous kaolin and α -Al₂O₃. **Ceramics International**. 36: 673-678.
- Balgord, W. D. and Roy, R. (1971). Molecular sieve zeolites-1 advances in chemistry. **American Chemical Society**, Washington DC. P. 140.
- Basak, S., Kundu, D. and Naskar, M. K. (2014). Low temperature synthesis of NaA zeolite membranes: The effect of primary and secondary crystallizations. **Ceramics International**. 40: 12923-12930.
- Bosch, P., Ortiz, L. and Schifter, I. (1983). Synthesis of faujasite type zeolites from calcined kaolins. **Industrial & Engineering Chemistry Product Research and Development**. 22: 401-406.
- Bowen, T. C., Noble, R. D. and Falconer, J. L. (2004). Fundamentals and applications of pervaporation through zeolite membranes. **Journal of Membrane Science**. 245: 1-33.
- Breck, D. W. (1974). **Zeolite molecular sieve: structure chemistry and use**. John Wiley and Sons. New York.

- Brigatti, M. F., Galan, E. and Theng, B. K. (2013). Structure and mineralogy of clay minerals. **Handbook of Clay Science. Developments in Clay Science Elsevier**. 21-81.
- Chandrasekhar, S. and Pramada, P. N. (2001). Sintering behaviour of calcium exchanged low silica zeolites synthesized from kaolin. **Ceramics International**. 27: 105-114.
- Chang, C. D. and Bell, A. T. (1991). Studies on the mechanism of ZSM-5 formation. **Catalysis Letters**. 8: 305-316.
- Chaisena, A. and Rangriwatananon, K. (2005). Synthesis of sodium zeolites from natural and modified diatomite. **Materials Letters**. 59: 1474-1479.
- Chen, Y. F., Wang, M. C. and Hon, M. H. (2004). Phase transformation and growth of mullite in kaolin ceramics. **Journal of the European Ceramic Society**. 24: 2389-2397.
- Costa, E., De Lucas, A., Uguina, M. A. and Ruíz, J. C. (1988). Synthesis of 4A zeolite from calcined kaolins for use in detergents. **Industrial & Engineering Chemistry Research**. 27: 1291-1296.
- Dong, Y., Hampshire, S., Zhou, J.-e., Ji, Z., Wang, J. and Meng, G. (2011). Sintering and characterization of flyash-based mullite with MgO addition. **Journal of the European Ceramic Society**. 31: 687-695.
- Dyer, A. (1988). **An Introduction of Zeolite Molecular Seives**. John Wiley & Sons. Chichester. UK.
- Dyer, A., Tangkawanit, S. and Rangriwatananon, K. (2004). Exchange diffusion of Cu^{2+} , Ni^{2+} , Pb^{2+} and Zn^{2+} into analcime synthesized from perlite. **Microporous and Mesoporous Materials**. 75: 273-279.

- Esharghawi, A., Penot, C. and Nardou, F. (2009). Contribution to porous mullite synthesis from clays by adding Al and Mg powders. **Journal of the European Ceramic Society**. 29: 31-38.
- Grim, R. E. (1968). **Clay Mineralogy, Structure of Clay Mineral**. New York: Mcgraw-Hill. 57-66.
- Ghobarker, H. and Schäfer, O. (1999). Effect of temperature on hydrothermal synthesis of analcime and vesicite. **Materials Science and Engineering**. B60: 163-167.
- Harabi, A., Zenikheri, F., Boudaira, B., Bouzerara, F., Guechi, A. and Foughali, L. (2014). A new and economic approach to fabricate resistant porous membrane supports using kaolin and CaCO_3 . **Journal of the European Ceramic Society**. 34: 1329-1340.
- Healey, A. M. Johnson, G. M. and Weller, M. T. (2000). The synthesis and characterisation of JBW-type zeolites. Part A: Sodium/potassium aluminosilicate, $\text{Na}_2\text{K}[\text{Al}_3\text{Si}_3\text{O}_{12}]\cdot 0.5\text{H}_2\text{O}$. **Microporous and Mesoporous Materials**. 37: 153-163.
- Hegazy, E. Z., El Maksod, I. H. A. and El Enin, R. M. M. A. (2010). Preparation and characterization of Ti and V modified analcime from local kaolin. **Applied Clay Science**. 49: 149-155.
- Jentys, A., Warecka, G., Derewinski, M. and Lercher, J. A. (1989). Adsorption of water on ZSM5 zeolites. **The Journal of Physical Chemistry**. 93: 4837-4843.
- Julbe, A., Motuzas, J., Cazevielle, F., Volle, G. and Guizard, C. (2003). Synthesis of sodalite/ $\alpha\text{Al}_2\text{O}_3$ composite membranes by microwave heating. **Separation and Purification Technology**. 32: 139-149.

- Kazemimoghadam, M. and Mohammadi, T. (2011). Preparation of nano pore hydroxysodalite zeolite membranes using of kaolin clay and chemical sources. **Desalination**. 278: 438-442.
- Khajavi, S., Kapteijn, F. and Jansen, J. C. (2007). Synthesis of thin defect-free hydroxy sodalite membranes: New candidate for activated water permeation. **Journal of Membrane Science**. 299: 63-72.
- Kondo, M. and Kita, H. (2010). Permeation mechanism through zeolite NaA and T-type membranes for practical dehydration of organic solvents. **Journal of Membrane Science**. 361: 223-231.
- Kunnakorn, D., Rirksomboon, T., Aungkavattana, P., Kuanchertchoo, N., Atong, D., Hemra, K., Kulprathipanja, S. and Wongkasemjit, S. (2011). Optimization of synthesis time for high performance of NaA zeolite membranes synthesized via autoclave for water-ethanol separation. **Desalination**. 280: 259-265.
- Lalik, E., Mirek, R., Rakoczy, J. and Groszek, A. (2006). Microcalorimetric study of sorption of water and ethanol in zeolites 3A and 5A. **Catalysis Today**. 114: 242-247.
- Li, Y., Chen, H., Liu, J. and Yang, W. (2006). Microwave synthesis of LTA zeolite membranes without seeding. **Journal of Membrane Science**. 277: 230-239.
- Li, H., Wang, J., Xu, J., Meng, X., Xu, B., Yang, J., Li, S., Lu, J., Zhang, Y., He, X. and Yin, D. (2013). Synthesis of zeolite NaA membranes with high performance and high reproducibility on coarse macroporous supports. **Journal of Membrane Science**. 444: 513-522.
- Lin, D. C., Xu, X. W., Zuo, F. and Long, Y. C. (2004). Crystallization of JBW, CAN, SOD and ABW type zeolite from transformation of meta-kaolin. **Microporous and Mesoporous Materials**. 70: 63-70.

- Linares, C. F., Sánchez, S., Navarro, C. U., Rodríguez, K. and Goldwasser, M. R. (2005). Study of cancrinite-type zeolites as possible antacid agents. **Microporous and Mesoporous Materials**. 77: 215-221.
- Liu, Q., Navrotsky, A., Jove-Colon, C. F. and Bonhomme, F. (2007). Energetics of cancrinite: Effect of salt inclusion. **Microporous and Mesoporous Materials**. 98: 227-233.
- Mohammadi, T. and Pak, A. (2003). Effect of calcination temperature of kaolin as a support for zeolite membranes. **Separation and Purification Technology**. 30: 241-249.
- Montagna, G., Arletti, R., Vezzalini, G. and Renzo, F. D. (2011). Borosilicate and aluminosilicate pollucite nanocrystals for the storage of radionuclides. **Powder Technology**. 208: 491-495.
- Morigami, Y., Kondo, M., Abe, J., Kita, H. and Okamoto, K. (2001). The first large-scale pervaporation plant using tubular-type module with zeolite NaA membrane. **Separation and Purification Technology**. 25: 251-260.
- Navajas, A., Mallada, R., Téllez, C., Coronas, J., Menéndez, M. and Santamaría, J. (2002). Preparation of mordenite membranes for pervaporation of water-ethanol mixtures. **Desalination**. 148: 25-29.
- Okamoto, K.-i., Kita, H., Horii, K. and Kondo, K. T. (2001). Zeolite NaA membrane: preparation, single-gas permeation, and pervaporation and vapor permeation of water/organic liquid mixtures. **Industrial & Engineering Chemistry Research**. 40: 163-175.
- Okubo, T., Wakihara, T., Plévert, J., Nair, S., Tsapatsis, M., Ogawa, Y., Komiyama, H., Yoshimura, M. and Davis, M. E. (2001). Heteroepitaxial growth of a zeolite. **Angewandte Chemie International Edition**. 40: 1069-1071.

- Park, S. H., Chung, C. B. and Seo, G. (2012). Preparation of small analcime particles with narrow size distributions from acid-treated larger analcime particles. **Microporous and Mesoporous Materials**. 155: 201-207.
- Pera-Titus, M., Llorens, J., Cunill, F., Mallada, R. and Santamaría, J. (2005). Preparation of zeolite NaA membranes on the inner side of tubular supports by means of a controlled seeding technique. **Catalysis Today**. 104: 281-287.
- Pina, M. P., Arruebo, M., Felipe, M., Fleta, F., Bernal, M. P., Coronas, J., Menéndez, M. and Santamaría, J. (2004). A semi-continuous method for the synthesis of NaA zeolite membranes on tubular supports. **Journal of Membrane Science**. 244: 141-150.
- Qiu, W. and Zheng, Y. (2009). Removal of lead, copper, nickel, and zinc from water by a cancrinite-type zeolite synthesized from fly ash. **Chemical Engineering Journal**. 145: 483-488.
- Reyes, C. A. R., Williams, C. and Alarcón, O. M. C. (2013). Nucleation and growth process of sodalite and cancrinite from kaolinite-rich clay under low-temperature hydrothermal conditions. **Materials Research**. 16(2): 424-438.
- Ríos, C. A., Williams, C. D. and Fullen, M. A. (2009). Nucleation and growth history of zeolite LTA synthesized from kaolinite by two different methods. **Applied Clay Science**. 42: 446-454.
- Słaby, E. and Kozłowski, A. (2002). Reconstruction of crystallisation temperature of artificially grown H-analcimes by means of the IR and fluid inclusion studies. **Acta Geologica Polonica**. 52: 385-394.
- Sun, W., Wang, X., Yang, J., Lu, J., Han, H., Zhang, Y. and Wang, J. (2009). Pervaporation separation of acetic acid–water mixtures through Sn-substituted ZSM-5 zeolite membranes. **Journal of Membrane Science**. 335: 83-88.

- Talou, M. H., Villar, M. A., Camerucci, M. A. and Moreno, R. (2011). Rheology of aqueous mullite-starch suspensions. **Journal of the European Ceramic Society**. 31: 1563-1571.
- Tanaka, K., Yoshikawa, R., Ying, C., Kita, H. and Okamoto, K. (2001). Application of zeolite membranes to esterification reactions. **Catalysis Today**. 67: 121-125.
- Tatlier, M., Cigizoglu, K. B., Tokay, B. and Erdem-Şenatalar, A. (2007). Microwave vs. conventional synthesis of analcime from clear solutions. **Journal of Crystal Growth**. 306: 146-151.
- Wang, H. and Lin, Y. S. (2012). Synthesis and modification of ZSM-5/silicalite bilayer membrane with improved hydrogen separation performance. **Journal of Membrane Science**. 396: 128-137.
- Worrall, W. E. (1986). **Clays and ceramic raw materials**: Springer Science & Business Media.
- Xu, X., Bao, Y., Song, C., Yang, W., Liu, J. and Lin, L. (2004). Microwave-assisted hydrothermal synthesis of hydroxy-sodalite zeolite membrane. **Microporous and Mesoporous Materials**. 75: 173-181.
- Yamamoto, T., Kim, Y. H., Kim, B. C. and Endo, A., Thongprachan, N., and Ohmori, T. (2012). Adsorption characteristics of zeolites for dehydration of ethanol: Evaluation of diffusivity of water in porous structure. **Chemical Engineering Journal**. 181-182: 443-448.
- Yang, S., Vlessidis, A. G. and Evmiridis, N. P. (1997). Synthesis of zeolites in the system $\text{Na}_2\text{O}-\text{SiO}_2-\text{Al}_2\text{O}_3-\text{H}_2\text{O}$ -glycerol. **Microporous Materials**. 9: 273-289.

- Yokomori, Y. and Idaka, S. (1998). The crystal structure of analcime. **Microporous and Mesoporous Materials**. 21: 365-370.
- Yu, P. C., Tsai, Y. W., Yen, F. S., Yang, W. P. and Huang, C. L. (2015). Thermal characteristic difference between α -Al₂O₃ and cristobalite powders during mullite synthesis induced by size reduction. **Journal of the European Ceramic Society**. 35: 673-680.
- Zah, J., Krieg, H. M. and Breytenbach, J. C. (2006). Layer development and growth history of polycrystalline zeolite A membranes synthesised from a clear solution. **Microporous and Mesoporous Materials**. 93: 141-150.
- Zhang, J. and Liu, W. (2011). Thin porous metal sheet-supported NaA zeolite membrane for water/ethanol separation. **Journal of Membrane Science**. 371: 197-210.
- Zhang, Y., Xu, Z. and Chen, Q. (2002). Synthesis of small crystal polycrystalline mordenite membrane. **Journal of Membrane Science**. 210: 361-368.
- Zhao, H., Deng, Y., Harsh, J. B., Flury, M. and Boyle, J. S. (2004). Alteration of kaolinite to cancrinite and sodalite by simulated Hanford tank waste and its impact on cesium retention. **Clays and Clay Minerals**. 52: 1-13.

CHAPTER III

HIGH TEMPERATURE SYNTHESIS OF JBW, ANA, SOD AND CAN FROM RAW AND MODIFIED KAOLIN FOR ETHANOL DEHYDRATION

3.1 Abstract

Hydrophilic sodium zeolites (ANA, JBW, CAN and SOD) were successfully synthesized by the hydrothermal method using raw kaolin, calcined kaolin and dealuminated kaolin at 200 °C with 2.5 M and 5.0 M NaOH solutions. The starting materials and the synthesized products were characterized by XRF, XRD, SEM and FT-IR, NH₃-TPD and TGA/DTG techniques. The pure phase of all sodium zeolites with a crystallinity higher than 80% were observed within the reaction period of 6-12 h. The study of ethanol dehydration with different water contents (85.0-97.0% v/v of ethanol solution) found that ANA shows a stronger affinity to water than other zeolites. ANA can dehydrate the concentrated ethanol from 97.0% v/v to 99.9% v/v. This highest capability of ANA for dehydration might be from its stronger Lewis acid sites.

3.2 Introduction

It is prevalent that high purity of bio-ethanol is required for various applications. Also, elimination of water from fermented solvent is an essential step to

produce bioethanol for commercial uses, because the fermented solvent contains 7-14 wt% ethanol including byproducts in its water (Wang et al., 2013; Yingling et al., 2013). Thus, distillation is used as the first step to increase the concentrations of ethanol and remove its byproducts. After this distillation process, concentrations of ethanol can reach to 95 wt% only through the azeotropic point of ethanol-water system (Haelssig et al., 2012; Sato et al., 2008). However, the alternative to increase ethanol concentration of 95 wt% to 100 wt% is through the use of a molecular sieve.

Although both a molecular sieve and bio-based were used as the adsorbent for dehydration in ethanol, the molecular sieve is much more efficient (Wang et al., 2010; Al-Asheh et al., 2004). Typically, only small molecules not the large ones could pass through pores in molecular sieves, suggesting that the molecular sieves are useful to separate water and ethanol. Nevertheless, zeolite molecular sieve seem to be winning over as the selective sorbents such as zeolite NaA, mordenite and faujasite-type zeolite (X and Y) (Lalik et al., 2006; Lu et al., 2007; Muenpoowank and Rangriwatnanon, 2012; Yamamoto et al., 2012). Especially, type A zeolite are most used in the application of ethanol-water azeotrope separation which was developed to membrane due to its suitable pore size and low Si/Al ratio (Cho et al., 2010; Liu et al., 2011; Zhang and Liu, 2011). Generally, zeolites can be synthesized from chemical reagents of sodium silicate and aluminate (Tatlier et al., 2007; Yang et al., 1997) and raw materials such as kaolin (Zhao et al., 2004), diatomite (Chaisena and Rangriwatananon, 2005), perlite (Dyer et al., 2004) and fly ash (Qiu and Zheng, 2009).

However, many researchers have been trying to find a better adsorbent and a more effective way to consume less energy to reduce the cost for industrial

applications. As a result, available local materials such as clay and rock are chosen for their economic advantages. Particularly, kaolin, a kind of clay which is common with its locally available resources in Thailand has been used to synthesize sodium zeolites (Atta et al., 2012; Hegazy et al., 2010; Lin et al., 2004; Liu et al., 2007; Ríos et al., 2009) such as zeolite A, sodalite (SOD), cancrinite (CAN), Na-J(BW) (JBW) and analcime (ANA) zeolites. These sodium zeolites are hydrophilic zeolites with different pore structures.

Specifically, this present work focuses on the hydrothermal synthesis of these sodium zeolites (SOD, CAN, JBW and ANA) using local kaolin as a silica and alumina source for employing a shorter reaction period compared to other related research (Atta et al., 2012; Healey et al., 2000; Hegazy et al., 2010; Lin et al., 2004). In addition, the water adsorption was investigated in order to find out the performance efficiency of these synthesized zeolites for the dehydration of ethanol solution.

3.3 Experiment

3.3.1 Materials

Raw kaolin (RK) from Narathiwat province (Thailand) was used as starting material for synthesis of sodium zeolites. It was sieved with 63 μm mesh before it was treated in the next steps, i.e., calcination and dealumination. In the calcination, RK was calcined at 900 $^{\circ}\text{C}$ for 5 h to transform kaolin into amorphous phase of metakaolin (MK). The dealumination was performed by refluxing RK with 6.0 M H_2SO_4 (Merck) for 4.5, 5.0, 5.5, 6.0 and 24.0 h at 100 ± 3 $^{\circ}\text{C}$, denoted as DK4.5, DK5, DK5.5, DK6 and DK24, respectively. Next, the obtained solid samples were washed with deionized water (DI) until pH of filtrate was 7, later dried at 110 $^{\circ}\text{C}$.

Finally, RW, MK and DK were used as silica and alumina source for synthesizing ANA, JBW, CAN and SOD.

3.3.2 Synthesis of sodium zeolites

3.3.2.1 Synthesis of ANA and CAN

ANA and CAN were synthesized with DK as a silica source and $\text{Al}(\text{OH})_3$ (Carlo Erba) as an alumina source. The chemical compositions of reactants were similar to the ones in the synthesis of ANA and CAN from diatomite (Chaisena and Rangriwatananon, 2005). In the synthesis process of both zeolites, 1.0 g of DK24 and 0.235 g of $\text{Al}(\text{OH})_3$ were added to 2.5 M NaOH for synthesizing ANA and 5.0 M NaOH for CAN, whose molar compositions were $\text{Al}_2\text{O}_3 \cdot 8.6\text{SiO}_2 \cdot 8.0\text{Na}_2\text{O} \cdot 307.7\text{H}_2\text{O}$ for ANA and $8.6\text{SiO}_2 \cdot 46.5\text{Na}_2\text{O} \cdot 818.5\text{H}_2\text{O}$ for CAN. After the mixture was stirred for 1 h and transferred into a stainless steel autoclave and crystallized in an oven at 200 °C for 6, 12, 24 and 48 h, the product was left to cool to room temperature. Then the obtained solid phase was washed with DI water until pH 7 and dried at 110 °C. In addition, ANA and CAN were synthesized without $\text{Al}(\text{OH})_3$ adding by using DK4.5, DK5, DK5.5 and DK6 under the same conditions as mentioned above.

3.3.2.2 Synthesis of JBW and SOD

While raw kaolin and 2.5 M NaOH with the molar composition of $\text{Al}_2\text{O}_3 \cdot 2.3\text{SiO}_2 \cdot 3.6\text{Na}_2\text{O} \cdot 140.4\text{H}_2\text{O}$ were used for the synthesis of JBW, metakaolin and 5.0 M NaOH with the molar composition of $\text{Al}_2\text{O}_3 \cdot 2.3\text{SiO}_2 \cdot 17.7\text{Na}_2\text{O} \cdot 310.2\text{H}_2\text{O}$ was also utilized for the synthesis of SOD. This similar synthesis condition of ANA and CAN was also applied for JBW and SOD.

3.3.3 Characterization of starting materials and sodium zeolites

Chemical compositions of the starting materials and the synthesized sodium zeolites were determined by XRF (Horiba model XGT-5200) and identified qualitatively by X-ray diffraction technique carried on with a Bruker D5005, Ni filter, $\lambda = 1.54$, operated at 40 kV with 40 mA with Cu-K α radiation source. Percentage of crystallinity was calculated from the equation as below.

$$\% \text{ crystallinity} = \frac{\text{Integrated area from the major refraction peaks of zeolite}}{\text{Integrated area of a reference zeolite}} \times 100$$

IR spectra were recorded in the region of 4000-400 cm^{-1} by Tensor 27-Hyperion/Bruker using KBr pellet technique. Thermal analysis was performed on a model SDT 2960 at 5 $^{\circ}\text{C}/\text{min}$ up to 400 $^{\circ}\text{C}$, in air. The morphologies of the zeolites were observed on JEOL model JSM-6010LV. Acidity strength was determined by ammonia temperature programmed desorption (NH_3 -TPD) with a Bel Japan model BelcatB. The NH_3 -TPD spectra were measured using a conventional flow-through reactor connected to a thermal conductivity detector (TCD). The TCD responses were calibrated by a dose containing known amounts of ammonia. Data were collected and processed by a computer. About 200 mg of sample was activated inside the TPD reactor at 500 $^{\circ}\text{C}$ for 2 h, followed by adsorption of ammonia at 100 $^{\circ}\text{C}$. A fraction of the physically adsorbed ammonia was carried out by purging the sample with high purity helium (99.999%). The reactor temperature was ramped up at a rate of 10 $^{\circ}\text{C} \text{ min}^{-1}$ from 100-500 $^{\circ}\text{C}$ by helium flow passing through the reactor. The desorbed NH_3 was detected by TCD. The number of acid sites was calculated from the peak area compared to a reference material (ZSM-5) with a known number of acid sites analyzed with the same condition.

3.3.4 Dehydration of ethanol solution

In the adsorption study ethanol solutions were prepared with anhydrous ethanol (>99.8 wt%, Merck) with the concentration range of 85.0-97.0% v/v. Sodium zeolites (0.2500 ± 0.0002 g) were mixed with 25.00 mL of ethanol solution. The mixture was shaken at 30 °C and allowed to reach equilibrium. Afterwards, a filtrate was analyzed by gas chromatography using Hewlett Packard model HP-6890 using a capillary column of HP-INNOWax Polyethylene Glycol (30 m \times 0.32 mm) and FID detector. The injector temperature was maintained at 250 °C while triplicate 0.1 μ L of sample was injected. Helium was used as a carrier gas with a constant flow rate of 4 mL/min. The FID detector gas flow rates were set to 40.0 mL/min for hydrogen and 300 mL/min for air. The concentration of dehydrated ethanol solution was calculated from calibration curve.

3.4 Results and discussion

3.4.1 Analysis of starting material

Figure 3.1 shows the XRD patterns of RK, DK5, DK24 and MK. RK represented impurity phase of mica and quartz, while RK showed a main refraction peak at $2\theta = 12.33^\circ$ which corresponds to a basal spacing of 7.17 Å. The peak of α -quartz (Si_3O_6) (Atta et al., 2012) at the 2θ angle = 26.7° could be noticeably observed after dealumination and calcination. In the calcination, the structure of RK was transformed distinctly into amorphous phase of MK while in the dealumination of RK with H_2SO_4 , the characteristic peak of RK disappeared within the reaction time 24 h. When the reaction time was varied between 4.5, 5.0, 5.5 and 6.0 h, the molar ratios of $\text{SiO}_2/\text{Al}_2\text{O}_3$ were increased to 7.3, 9.0, 10.3 and 13.5, respectively (see Table

3.1). This indicated that aluminium-oxygen bond of kaolin was broken with H_2SO_4 reaction and Al was leached.

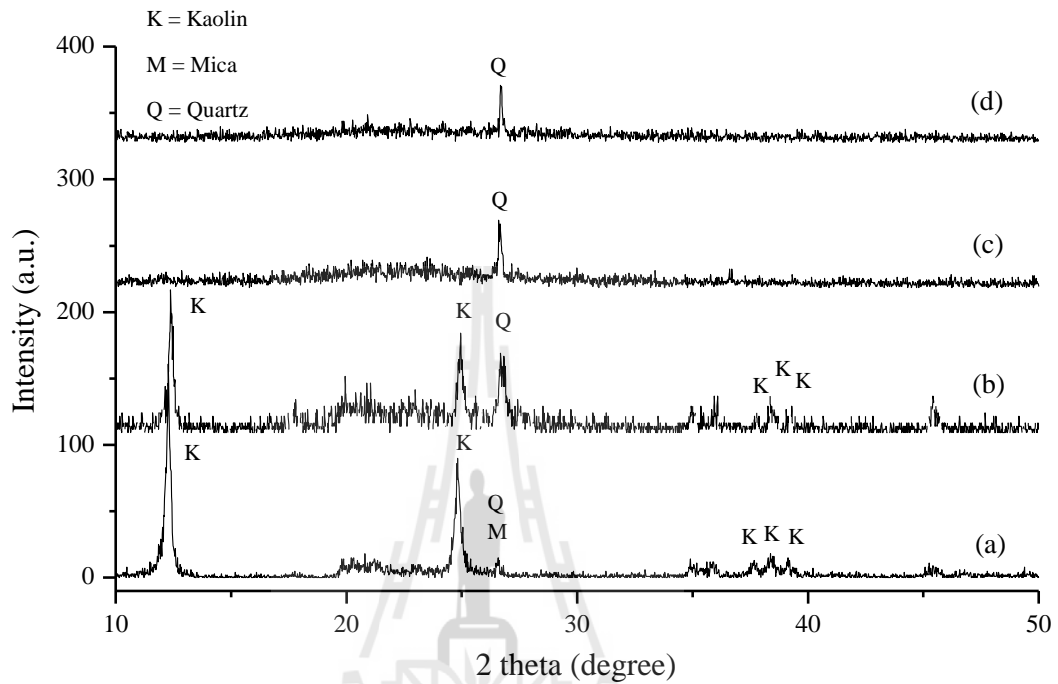


Figure 3.1 XRD patterns of RK (a), DK5 (b), DK24 (c) and MK (d).

Table 3.1 Chemical compositions (in wt%) of the starting materials determined by XRF.

Chemical composition	RK	MK	DK (h)				
			4.5	5.0	5.5	6.0	24
SiO ₂	46.9	47.1	73.9	76.8	78.4	81.1	88.9
Al ₂ O ₃	35.2	35.5	17.2	14.4	13.0	10.2	1.3
Fe ₂ O ₃	4.1	4.0	1.0	0.8	0.8	1.0	1.1
Na ₂ O	4.9	5.0	3.5	3.8	3.4	3.3	3.4
K ₂ O	4.9	4.6	3.2	2.9	3.1	3.3	4.1

Table 3.1 Chemical compositions (in wt%) of the starting materials determined by XRF (Continued).

Chemical composition	RK	MK	DK (h)				
			4.5	5.0	5.5	6.0	24
MgO	3.1	3.0	0.9	1.0	1.1	0.8	1.0
CaO	0.3	0.3	0.1	0.1	0.1	0.1	0.1
MnO ₂	0.3	0.2	0.1	0.1	0.1	0.1	0.1
TiO ₂	0.1	0.1	0.1	0.1	0.1	0.1	0.1
Molar ratio of SiO ₂ /Al ₂ O ₃	2.3	2.3	7.3	9.0	10.3	13.5	118.3

The raw kaolin and modified kaolin samples were also confirmed by FT-IR analyses and their corresponding peak assignments in the region of 4000-3000 cm⁻¹ and 1400-400 cm⁻¹ were shown in Figure 3.2 and Table 3.2. Obviously, kaolinite with mostly Al in the octahedral positions shows four peaks in the O-H stretching region (Figure 3.2(A)) (Ali Memon et al., 2013; Madejová, 2003). The strongest peak at 3696 cm⁻¹ is related to the symmetric stretching vibration. Two weak peaks at 3670 and 3653 cm⁻¹ are assigned to out-of-plane stretching vibrations (Panda et al., 2010; Madejová, 2003; Farmer, 2000). The peak at 3620 cm⁻¹ is due to inner hydroxyl groups lying between the tetrahedral and octahedral sheet (Ali Memon et al., 2013; Madejová, 2003). The intensity of these peaks was decreased progressively with increasing the reaction time of acid treatment. This result indicates that protons penetrate into the clay mineral layers and attack to the structural hydroxyl groups which lead to the dehydroxylation and a successive leaching of the Al ions from the octahedral layer (Panda et al., 2010). Aluminium ions react with sulphate ion to form

a complex of $\text{Al}_2(\text{SO}_4)_3$. The reaction between kaolin and sulphuric acid is described by the chemical equation (3.1) (Makó et al., 2006 and Ali Memon et al., 2013).



The calcination of RK at 900 °C into MK explain disappearance of hydroxyl groups. Again, the vibration of T-O-T (T=Si or Al) in the range of 1400-400 cm^{-1} was also recorded and shown in Figure 3.2(B). The FT-IR spectra of RK illustrate three peaks at 1114, 1032 and 1009 cm^{-1} assigned to three different Si-O-Si in-plane stretching mode (Castellano et al., 2010). The peak at 1114 cm^{-1} is attributed to Si-O-Si symmetrical stretching in tetrahedral (Heah et al., 2012), which shifts to lower frequencies at 1104 cm^{-1} after dealumination with reaction time of 5 hours. The peaks at 1114, 1032 and 1009 cm^{-1} disappeared and a broad band at 1103 cm^{-1} appeared with reaction time of 24 h. The peaks related to Al such as two peaks at 938 (shoulder) and 913 cm^{-1} are attributed to Al-O-H bending vibration of inner and surface OH groups, respectively. The peaks at 754 cm^{-1} and 695 cm^{-1} are assigned to vibrations of symmetric Si-O-Al stretching frequency is at 538 cm^{-1} (Ali Memon et al., 2013; Castellano et al., 2010; Makó et al., 2006). These band intensities are decreased more or less up to the time of the reflux. The FT-IR spectrum of MK showed a broad band at 798 cm^{-1} assigned to Al-O bonds in Al_2O_3 and vibration band at 1088 cm^{-1} assigned to the stretching Si-O bonds in SiO_2 (Alkan et al., 2005) indicating that calcination of kaolin resulted in the loss of crystallinity.

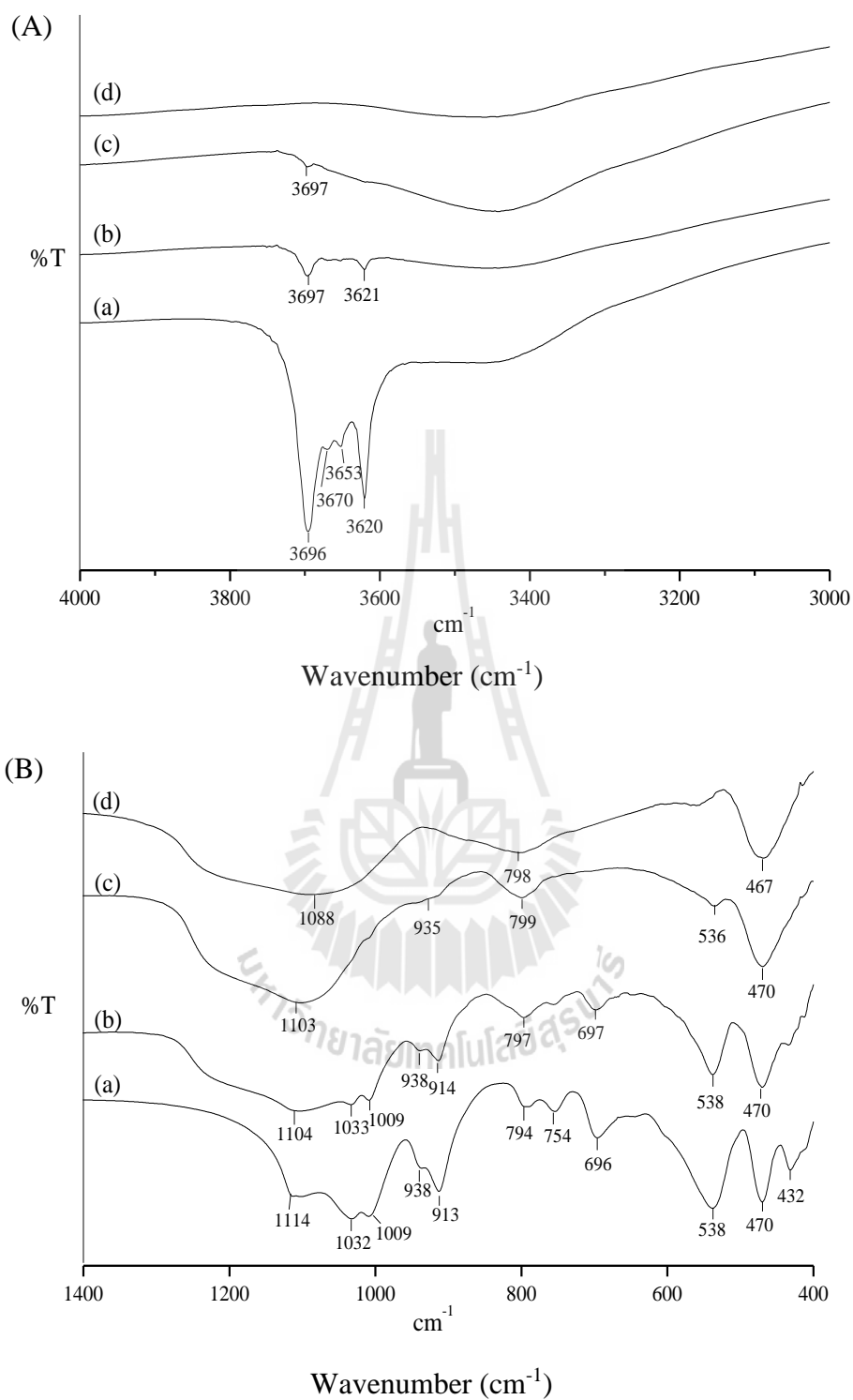


Figure 3.2 FT-IR skeletal spectra (B) and OH stretching vibration spectra (A) of RK (a), DK5 (b), DK24 (c) and MK (d).

Table 3.2 FT-IR peak assignment for functionality of RK.

Peak (cm ⁻¹)	Assignment
3696, 3670, 3653, 3620	Al-O-H stretching (structural hydroxyl groups, octahedral)
1114, 1032, 1009	Si-O-Si in plane stretching
1114	O-Si-O symmetrical stretching in tetrahedral
938, 913	Al-OH bending, bending of -OH groups on surface and inside of material, respectively
754, 696	Stretching vibrations of symmetric Si-O and Al-O
538, 470, 431	Octahedra involving Al ³⁺ ions
538	Si-O-Al stretching
470	Si-O-Si bending

3.4.2 Syntheses of sodium zeolites

The conditions of the syntheses of sodium zeolites and the percentage of crystallinity were summarized in Table 3.3.

Table 3.3 Relative crystallinity of sodium zeolites synthesized from different starting materials under various reaction periods.

No.	Molar composition in reactant	Reaction period (h)	Products	Relative crystallinity (%)
DK24 + Al(OH)₃				
1	Al ₂ O ₃ · 8.6SiO ₂ · 8.0Na ₂ O · 307.7H ₂ O	6	ANA	89.5
2	Al ₂ O ₃ · 8.6SiO ₂ · 8.0Na ₂ O · 307.7H ₂ O	12	ANA	98.5
3	Al ₂ O ₃ · 8.6SiO ₂ · 8.0Na ₂ O · 307.7H ₂ O	24	ANA	100*
4	Al ₂ O ₃ · 8.6SiO ₂ · 8.0Na ₂ O · 307.7H ₂ O	48	ANA	98.7

Table 3.3 Relative crystallinity of sodium zeolites synthesized from different starting materials under various reaction periods (Continued).

No.	Molar composition in reactant	Reaction period (h)	Products	Relative crystallinity (%)
DK4.5, DK5, DK5.5 and DK6				
5	$\text{Al}_2\text{O}_3 \cdot 7.3\text{SiO}_2 \cdot 8.0\text{Na}_2\text{O} \cdot 307.7\text{H}_2\text{O}$	6	ANA + SiO_2	-
6	$\text{Al}_2\text{O}_3 \cdot 9.0\text{SiO}_2 \cdot 8.0\text{Na}_2\text{O} \cdot 307.7\text{H}_2\text{O}$	6	ANA + SiO_2	-
7	$\text{Al}_2\text{O}_3 \cdot 10.3\text{SiO}_2 \cdot 8.0\text{Na}_2\text{O} \cdot 307.7\text{H}_2\text{O}$	6	ANA + SiO_2	-
8	$\text{Al}_2\text{O}_3 \cdot 10.3\text{SiO}_2 \cdot 8.0\text{Na}_2\text{O} \cdot 307.7\text{H}_2\text{O}$	48	ANA + SiO_2	-
9	$\text{Al}_2\text{O}_3 \cdot 13.5\text{SiO}_2 \cdot 8.0\text{Na}_2\text{O} \cdot 307.7\text{H}_2\text{O}$	6	ANA + SiO_2	-
DK24 + Al(OH)₃				
10	$\text{Al}_2\text{O}_3 \cdot 8.6\text{SiO}_2 \cdot 46.5\text{Na}_2\text{O} \cdot 818.5\text{H}_2\text{O}$	6	CAN	84.1
11	$\text{Al}_2\text{O}_3 \cdot 8.6\text{SiO}_2 \cdot 46.5\text{Na}_2\text{O} \cdot 818.5\text{H}_2\text{O}$	12	CAN	97.6
12	$\text{Al}_2\text{O}_3 \cdot 8.6\text{SiO}_2 \cdot 46.5\text{Na}_2\text{O} \cdot 818.5\text{H}_2\text{O}$	24	CAN	93.8
13	$\text{Al}_2\text{O}_3 \cdot 8.6\text{SiO}_2 \cdot 46.5\text{Na}_2\text{O} \cdot 818.5\text{H}_2\text{O}$	48	CAN	87.0
DK5 and DK5.5				
14	$\text{Al}_2\text{O}_3 \cdot 9.0\text{SiO}_2 \cdot 46.5\text{Na}_2\text{O} \cdot 818.5\text{H}_2\text{O}$	12	CAN	97.1
15	$\text{Al}_2\text{O}_3 \cdot 10.3\text{SiO}_2 \cdot 46.5\text{Na}_2\text{O} \cdot 818.5\text{H}_2\text{O}$	48	CAN	85.4
16	$\text{Al}_2\text{O}_3 \cdot 10.3\text{SiO}_2 \cdot 46.5\text{Na}_2\text{O} \cdot 818.5\text{H}_2\text{O}$	24	CAN	95.1
17	$\text{Al}_2\text{O}_3 \cdot 10.3\text{SiO}_2 \cdot 46.5\text{Na}_2\text{O} \cdot 818.5\text{H}_2\text{O}$	12	CAN	100*
RK				
18	$\text{Al}_2\text{O}_3 \cdot 2.3\text{SiO}_2 \cdot 3.6\text{Na}_2\text{O} \cdot 140.4\text{H}_2\text{O}$	6	JBW	77.7
19	$\text{Al}_2\text{O}_3 \cdot 2.3\text{SiO}_2 \cdot 3.6\text{Na}_2\text{O} \cdot 140.4\text{H}_2\text{O}$	12	JBW	80.6
20	$\text{Al}_2\text{O}_3 \cdot 2.3\text{SiO}_2 \cdot 3.6\text{Na}_2\text{O} \cdot 140.4\text{H}_2\text{O}$	24	JBW	100*
21	$\text{Al}_2\text{O}_3 \cdot 2.3\text{SiO}_2 \cdot 3.6\text{Na}_2\text{O} \cdot 140.4\text{H}_2\text{O}$	48	JBW	80.7
MK				
22	$\text{Al}_2\text{O}_3 \cdot 2.3\text{SiO}_2 \cdot 17.7\text{Na}_2\text{O} \cdot 310.2\text{H}_2\text{O}$	6	SOD	98.5
23	$\text{Al}_2\text{O}_3 \cdot 2.3\text{SiO}_2 \cdot 17.7\text{Na}_2\text{O} \cdot 310.2\text{H}_2\text{O}$	12	SOD	100*
24	$\text{Al}_2\text{O}_3 \cdot 2.3\text{SiO}_2 \cdot 17.7\text{Na}_2\text{O} \cdot 310.2\text{H}_2\text{O}$	24	SOD + CAN	-
25	$\text{Al}_2\text{O}_3 \cdot 2.3\text{SiO}_2 \cdot 17.7\text{Na}_2\text{O} \cdot 310.2\text{H}_2\text{O}$	48	SOD + CAN	-

*Sodium zeolite synthesized with this condition was selected as a reference zeolite.

3.4.2.1 Synthesis of ANA and JBW

Figure 3.3 shows XRD patterns of synthesized ANA and JBW from the different starting materials. A pure phase of JBW was observed from RK whose Al coordination was changed from octahedral to tetrahedral by the dissolution of kaolin (Reyes et al., 2011), while a pure phase of ANA was obvious from synthesis with DK24.

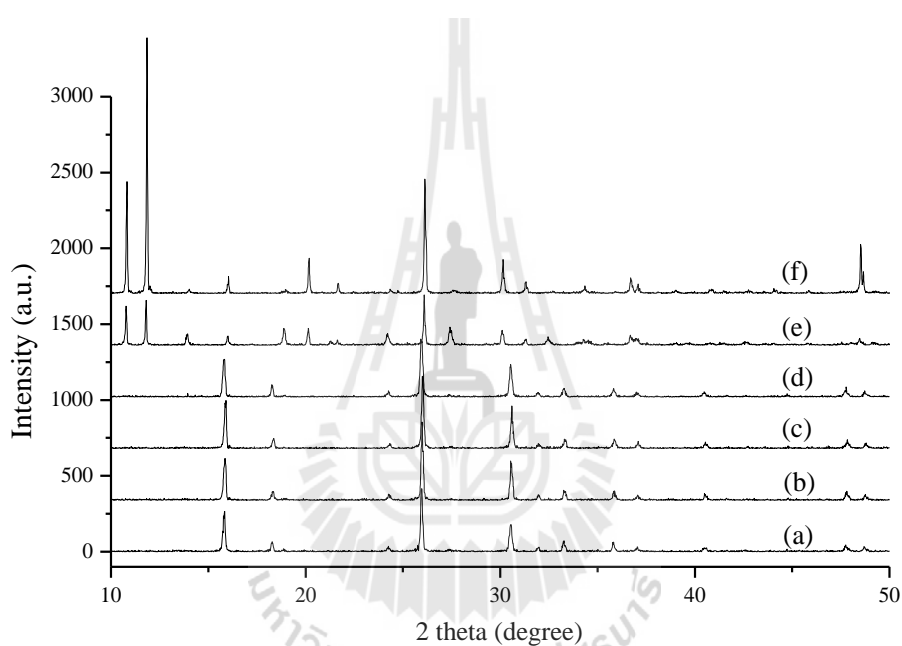


Figure 3.3 XRD patterns of sodium zeolites from different starting materials; DK24 with different reaction periods such as 6 h (a), 12 h (b), 24 h (c) and 48 h (d); MK (e) and RK (f) with reaction period of 48 h.

The diffractograms of synthesized ANA are matched with the diffractograms of ANA from the collection of simulated XRD powder patterns as shown in Figure 3.4 (Treacy et al., 1996). The major refraction peak of ANA at $2\theta = 25.96^\circ$ corresponds to a basal spacing of $d_{400} = 3.43 \text{ \AA}$. From the collection of

simulated XRD powder patterns, the major refraction peak of JBW is $2\theta = 10.75^\circ$ corresponding to a basal spacing of $d_{100} = 8.23 \text{ \AA}$ (Figure 3.5), but the synthesized JBW showed the major refraction peak changed to a $2\theta = 11.84^\circ$ ($d_{100} = 7.47$) which is consistent with that reported by Lin et al. (2004).

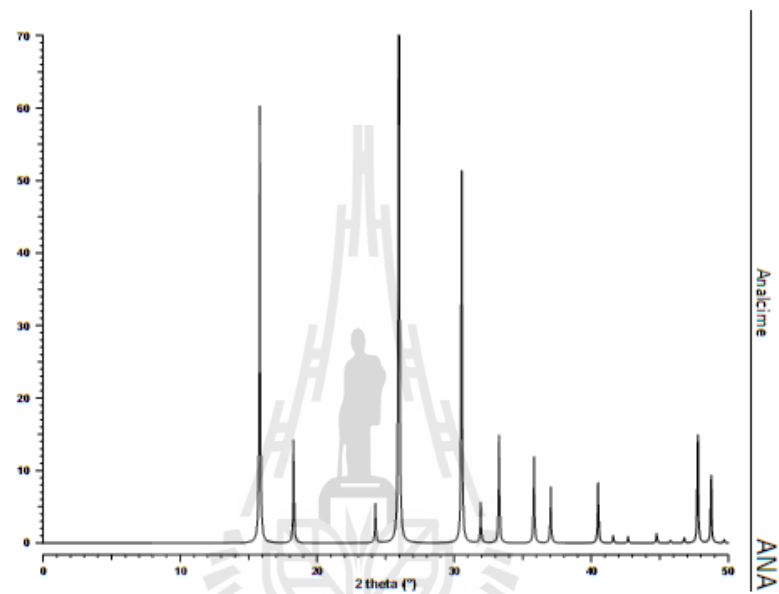


Figure 3.4 The simulated XRD powder pattern of ANA (Treacy et al., 1996).

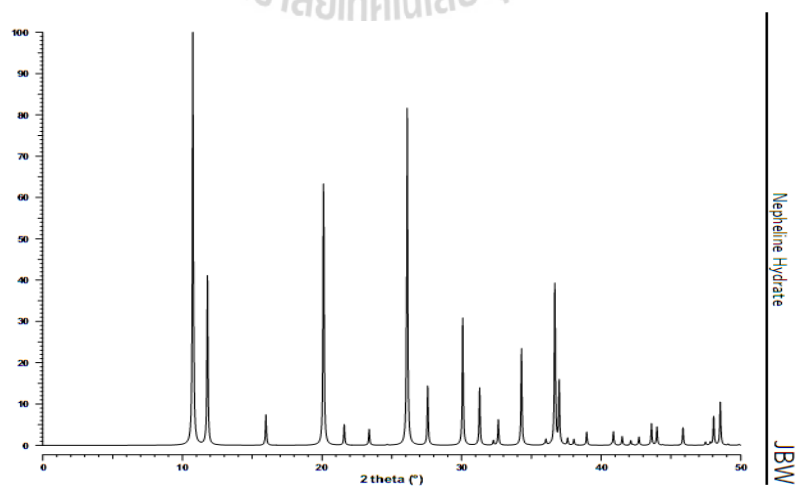


Figure 3.5 The simulated XRD powder pattern of JBW (Treacy et al., 1996).

The maximum intensity was observed with the reaction period of 24 h. When the reaction time was increased to 48 hours or decreased to 12 h, the percentage of crystallinity was slightly decreased (see Table 3.3). SEM image shows that a morphology of ANA was trapezohedral and a size of crystallinity varied between 5 to 14 μm (Figure 3.6). The variation of the particle sizes might have been resulted from the metal oxide (Atta et al., 2012) remained in DK24. When the synthesis of ANA in this study was compared with some reports elsewhere (Atta et al., 2012; Hegazy et al., 2010) the achievement of a smaller particle size (5-14 μm) of ANA and its pure phase with well crystallinity under a shorter reaction period (6-24 h) had occurred. The obtained smaller crystal size can be explained that the dealumination of kaolin affects the increase of pore volume in order to fasten its dissolved process (Colina and Llorens, 2007), as well as the growth of the crystals

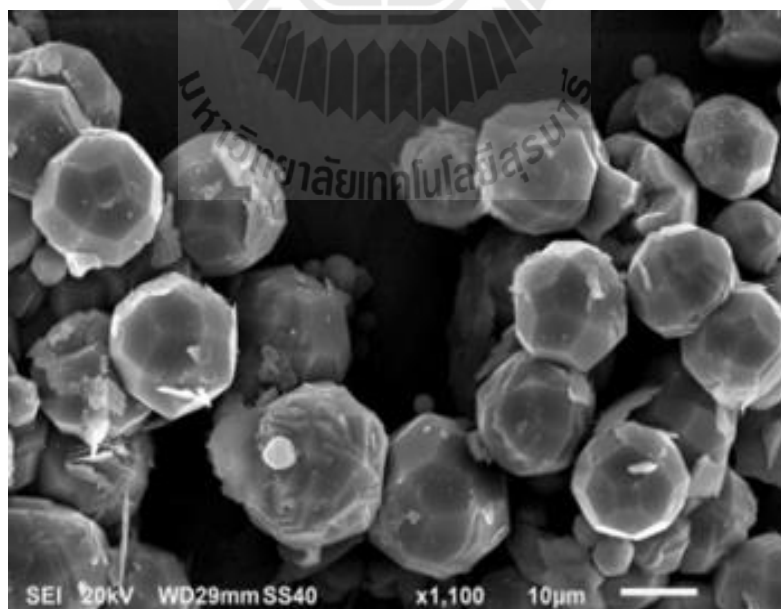


Figure 3.6 SEM image of ANA from DK24 with reaction period of 24 h.

When using DK4.5-6 with $\text{SiO}_2/\text{Al}_2\text{O}_3$ mole ratio between 7.3-13.5 as starting materials for synthesizing ANA, the mixed phase of ANA and SiO_2 was observed (Figure 3.7). The morphologies of ANA and amorphous SiO_2 were shown in Figure 3.8.

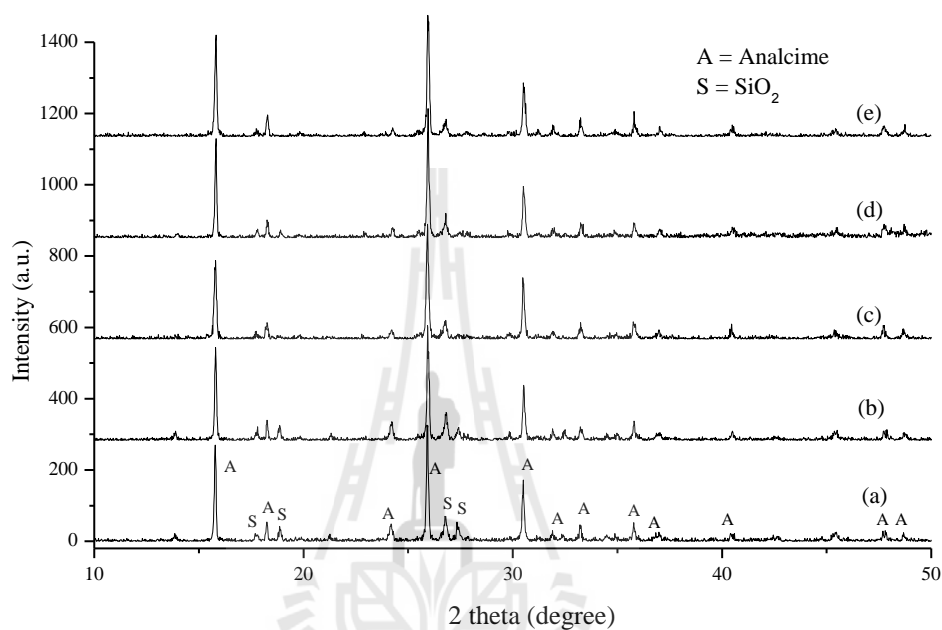


Figure 3.7 XRD patterns of ANA zeolite and SiO_2 from DK4.5 (a), DK5 (b), DK5.5 (c) and DK6 (d) with reaction period 6 h and from DK6 with reaction period 48 h (e).

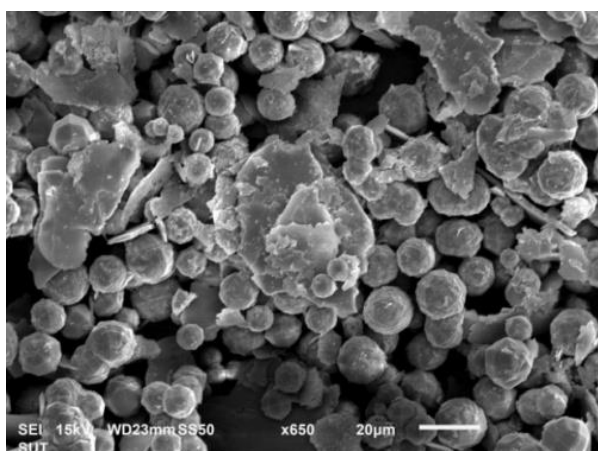


Figure 3.8 SEM image of ANA from DK5.5 with reaction period 6 h.

Figure 3.9 exhibits XRD patterns of JBW with different reaction periods including a purity phase of JBW which was observed with the reaction period of 6 h. The crystallinity was increased dramatically with the reaction period from 12 to 24 h. The crystallinity was decreased with the extended reaction period of 48 hours while the highest yield was observed with the reaction period of 24 hours. A long prismatic lath-like morphology of JBW was shown in Figure 3.10.

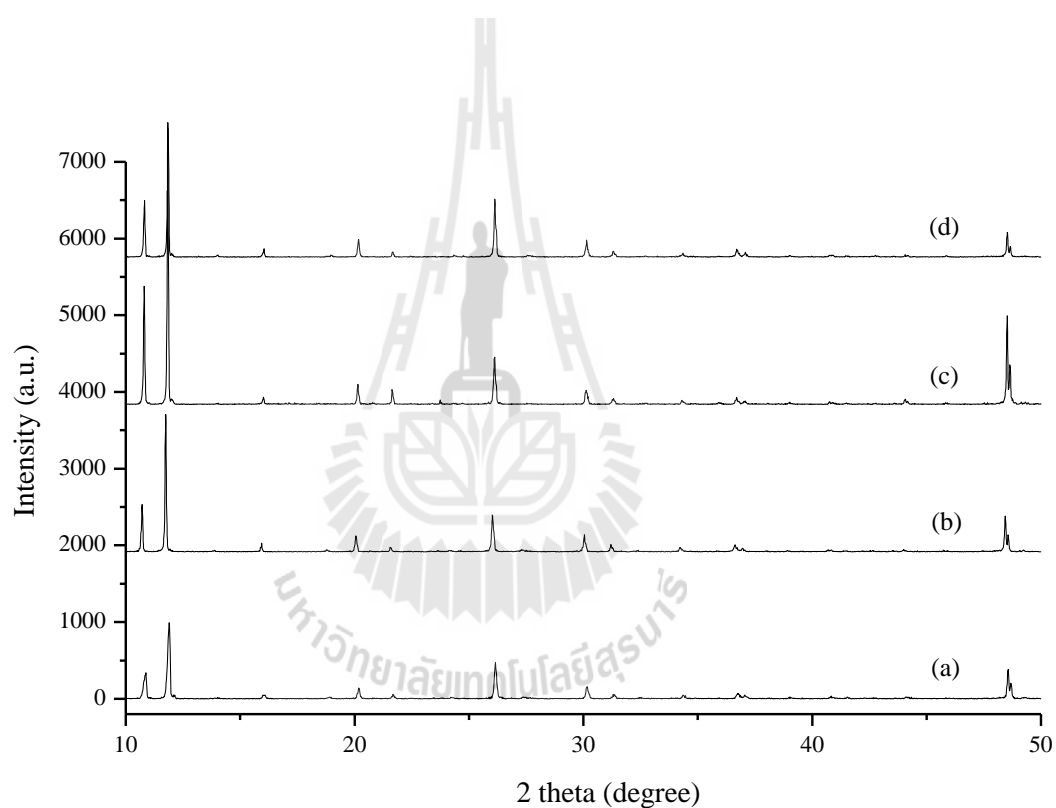


Figure 3.9 XRD patterns of JBW zeolite (a) with different reaction period such as 6 h (a), 12 h (b), 24 h (c) and 48 h (d).

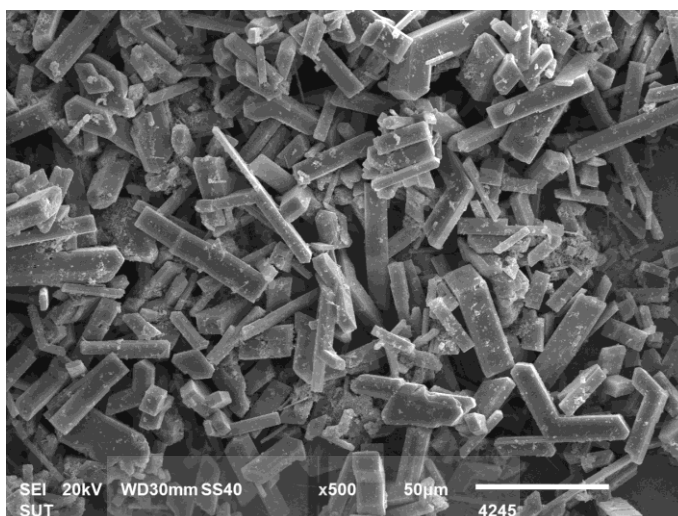


Figure 3.10 SEM image of JBW from RK with reaction period 24 h.

The pure phase and well crystallinity of JBW was achieved at a shorter reaction time compared to those reported by Lin et al. (2004) and Healey et al. (2000) in which a pure phase of JBW was obtained with the reaction period of 96 h and 2 days, respectively, using metakaolin as starting material.

3.4.2.2 Synthesis of CAN and SOD

Figure 3.11 illustrates XRD patterns of synthesized zeolite from different starting materials. A pure phase of CAN obtained from DK24 mixed with $\text{Al}(\text{OH})_3$ showed the maximum intensity at reaction period 12 h. The diffractogram of synthesized CAN are matched with the diffractogram from the collection of simulated XRD powder patterns as shown in Figure 3.12 (Treacy et al., 1996). The major refraction peak at $2\theta = 18.91^\circ$ corresponds to a basal spacing of $d_{101} = 4.69 \text{ \AA}$, while a mixed phase of CAN and SOD appeared if using RK and MK as starting materials. At high alkali concentration it showed a pure phase of CAN (see Table 3.3).

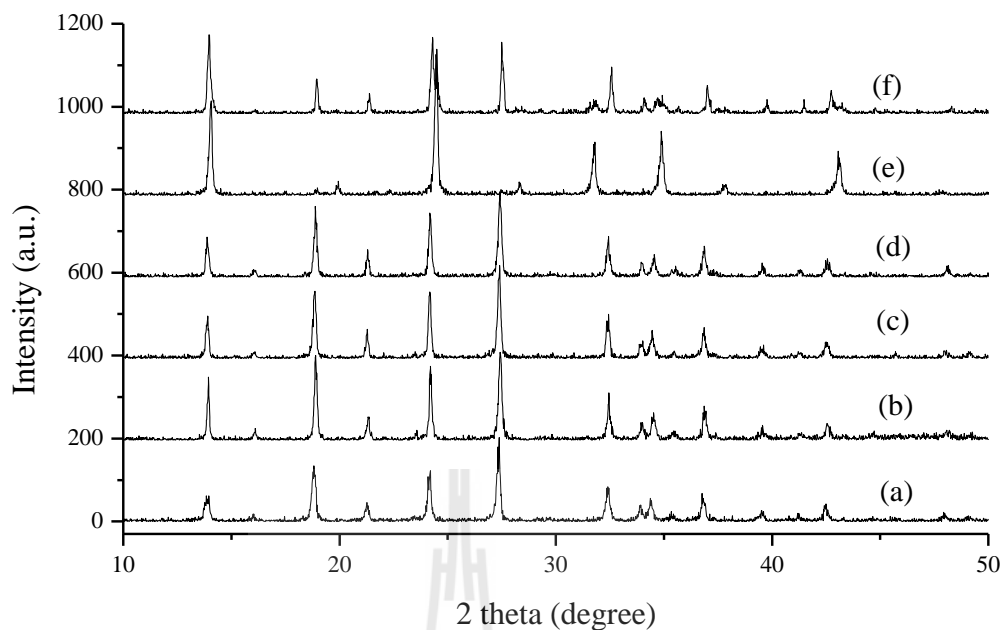


Figure 3.11 XRD patterns (A) of CAN from different starting materials; DK24 with different reaction periods such as 6 h (a), 12 h (b), 24 h (c) and 48 h (d); MK (e) and RK (f) with reaction period of 48 h.

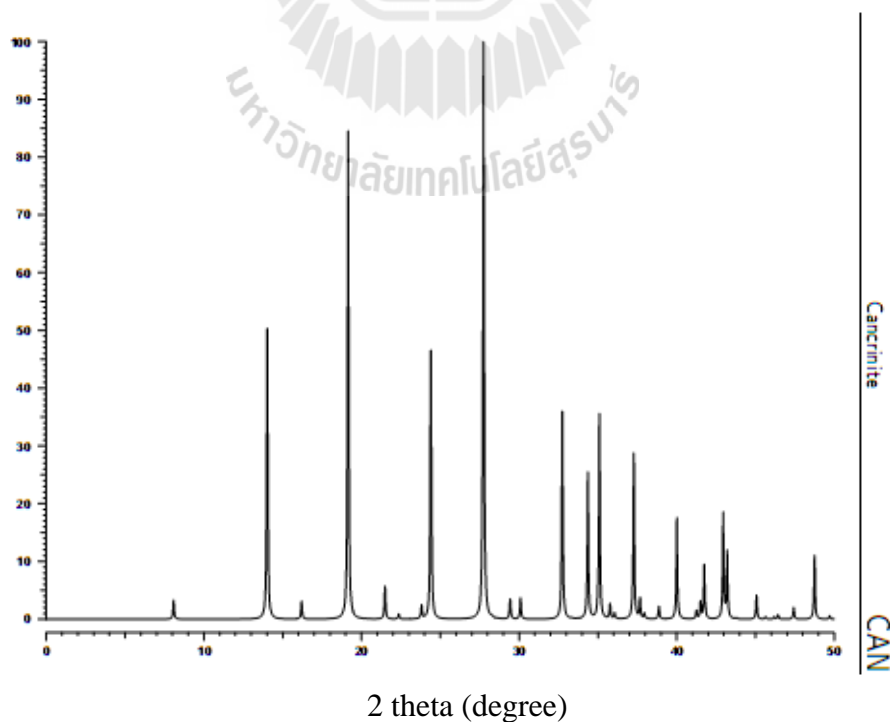


Figure 3.12 The simulated XRD powder pattern of CAN (Treacy et al., 1996).

SEM demonstrates a morphology of CAN being long rod-like (Figure 3.13) obtained at the reaction period of 12 h. According to other related research like Lin et al. (2004), a synthesized pure phase of CAN from metakaolin was succeeded with the reaction time of 192 h, however, in this work, a pure phase of CAN (crystallinity (84%)) has been obtained from DK24 within the reaction period of 6 h.

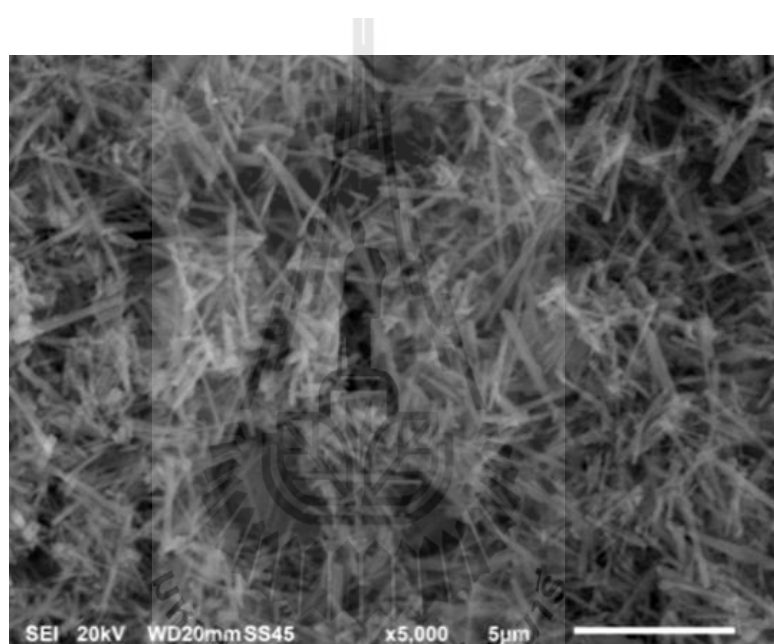


Figure 3.13 SEM image of CAN from DK5.5 with reaction period 12 h.

Furthermore, when using DK5 and DK5.5 as starting material, a higher percentage of crystallinity of CAN could be observed compared to using DK24 plus $\text{Al}(\text{OH})_3$ (see in Figure 3.14 and Table 3.3). In addition, DK5.5 without adding $\text{Al}(\text{OH})_3$ represents the highest crystallinity with the reaction period of 12 h. This clearly indicated the less energy consumption in CAN synthesis with DK5.5.

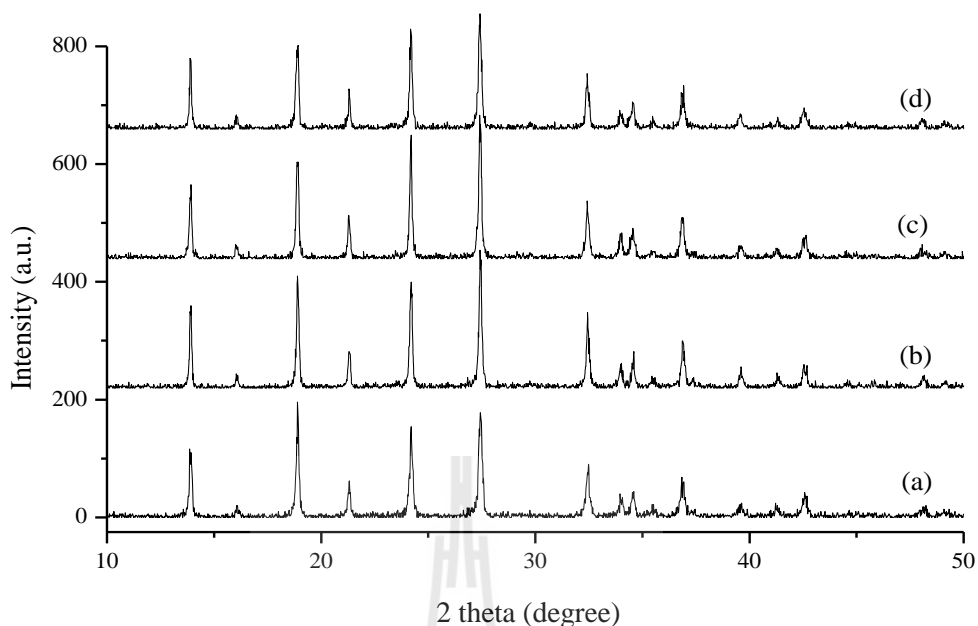


Figure 3.14 XRD patterns of CAN from DK5 with reaction period of 12 h (a) and from DK5.5 with different reaction periods such as 6 h (b), 12 h (c) and 24 h (d).

Figure 3.15 displays XRD patterns of synthesized SOD with different reaction periods. The diffractogram of synthesized SOD are matched with the diffractogram from the collection of simulated XRD powder patterns for zeolite as shown in Figure 3.16 (Treacy et al., 1996). The major refraction peak at $2\theta = 24.54^\circ$ corresponds to a basal spacing of $d_{211} = 3.62 \text{ \AA}$. The maximum intensities had been obtained with a reaction period of 12 h. The morphology of SOD was wedge-shape blade (Figure 3.17(a)). When the reaction period was prolonged to 24 h, a multiphase of SOD and CAN appeared. The minor peak at 18.89° and 27.74° exhibited CAN peaks and the typical SEM image revealed co-crystallization of SOD and CAN (see Figure 3.17(b)). The result obviously indicates that a phase transition of dissolved SOD phase to CAN phase occurs. This clearly corresponds to other related research like that of Barnes et al. (1999).

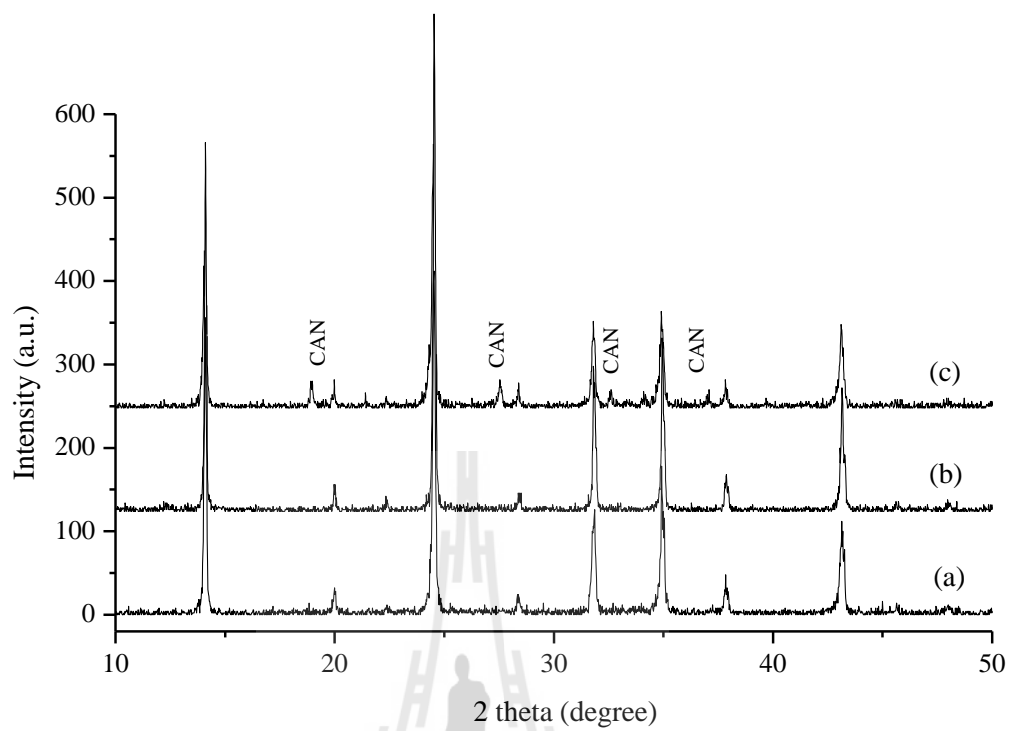


Figure 3.15 XRD patterns of product in synthesis SOD zeolite at reaction period of 6 h (a), 12 h (b) and 24 h (c).

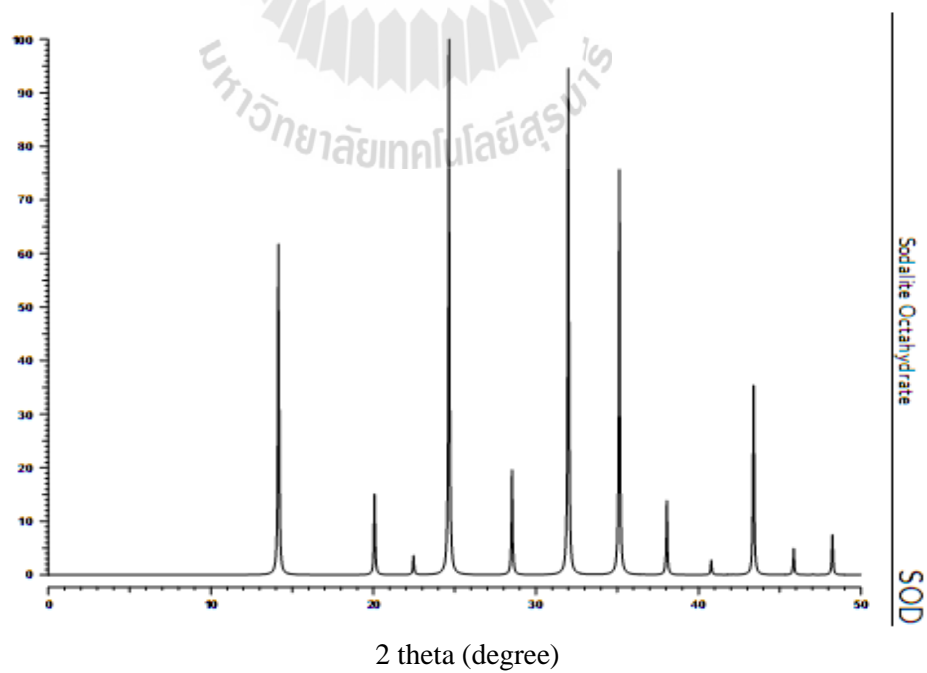


Figure 3.16 The simulated XRD powder pattern of SOD (Treacy et al., 1996).

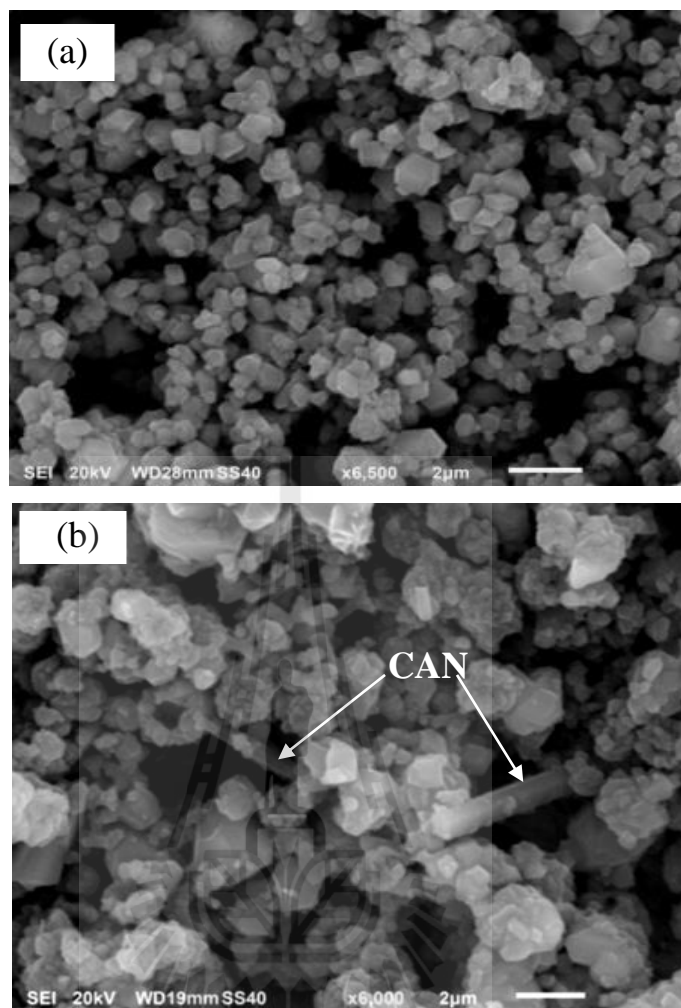


Figure 3.17 SEM image of SOD with reaction period of 12 h (a) and the mixed phase of SOD and CAN with reaction period of 24 h (b).

3.4.3 Acidity analysis by NH_3 -TPD

Figure 3.18 reveals NH_3 -TPD patterns of various sodium zeolites. The desorption peak of NH_3 on ANA showed a distinction desorption peak at 376 °C. JBW obviously showed two desorption peaks at the high and low temperature of 365 °C and 186 °C, respectively. In the case of CAN and SOD, a big desorption peak appeared at low temperature at 179 °C for CAN and a broad centered around 219 °C for SOD.

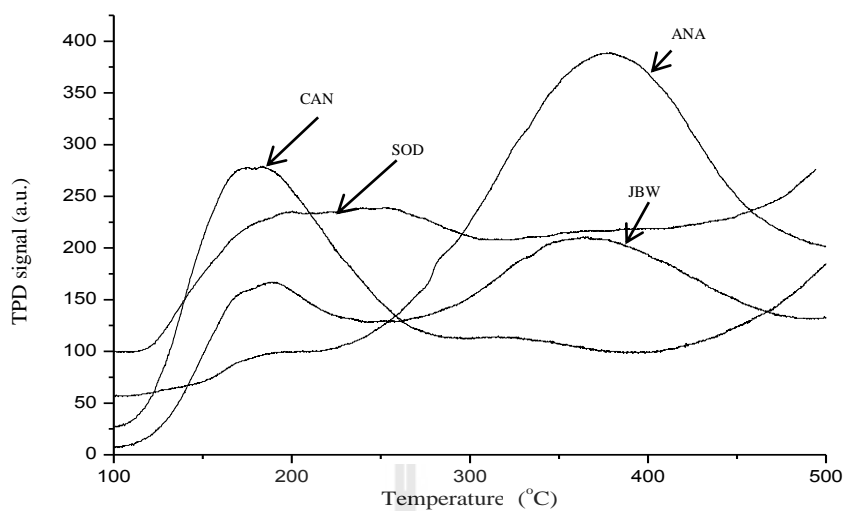


Figure 3.18 NH_3 -TPD patterns of ANA, JBW, CAN and SOD.

The desorption peak at the high temperature of ANA and JBW indicated that ANA and JBW had stronger Lewis acid site than that of CAN and SOD. The Lewis acid site assigned to the extraframework cations of Na^+ that is coordinated with lone-electron pair of the nitrogen atoms of NH_3 . The strength of the Lewis acid site depends on distribution of cations site of each zeolite framework (Auroux et al., 1995). The high temperature of desorption peak might be resulted from the Na^+ cation in those positions strongly coordinated with NH_3 .

The result of XRF proves the Si/Al mole ratio of these zeolites increasing in the sequence of ANA>JBW>CAN>SOD which is inversely proportional to an existence of Na^+ cations (see Table 3.4). Based on the quantity of Na^+ in the zeolites, we expected that the higher the Na is, the greater the amount of NH_3 is adsorbed. On the opposite, ANA showed the highest amount of NH_3 adsorbed in spite of having a lower Na^+ content. This result might have been the effect of an average number of coordinated NH_3 to Na^+ in ANA which was higher than that of the other sodium zeolites due to its higher strength of Lewis acid sites.

Table 3.4 Total amount of adsorbed NH₃ related to Na⁺ and ratio of Si/Al of sodium zeolites.

Zeolites	Pore size* (Å)	Si/Al mole ratio	Na⁺ cation (mol)	Total NH₃ desorbed (mmol/g)
ANA	1.6×4.2	2.37	0.53	0.234
JBW	3.7×4.8	1.68	0.68	0.146
CAN	5.9×5.9	1.47	0.86	0.122
SOD	2.6	1.32	0.89	0.144

* Baerlocher, 2001.

3.4.4 Thermal analysis

After the sodium zeolites were dried overnight at 120 °C, it was left to cool down in desiccators before being analyzed by TG (thermogravimetry). TG and DTG (differential thermogravimetry) curves of water loss in sodium zeolites with temperatures between 50 to 395 °C are shown in Figure 3.19. DTG curves of different zeolite types uncovered different temperatures of dehydration peaks. DTG of ANA evidently showed dehydration peak at the highest temperature about 328 °C. A sharp peak of JBW appeared at 213 °C and a large broad band of CAN and SOD centered at about 189 °C and 231 °C, respectively.

This suggested a strong interaction of water molecules was mostly in ANA. At these dehydration temperatures, the water losses resulted from the water located in zeolite cavities and bound to nonframework cations (Castaldi et al., 2005). This strongly indicated that water molecules in ANA bound to sodium ions is stronger than that in the other sodium zeolites. This result was consistent to that of NH₃-TPD suggesting that sodium ions in ANA are stronger Lewis acid than those in the other zeolites.

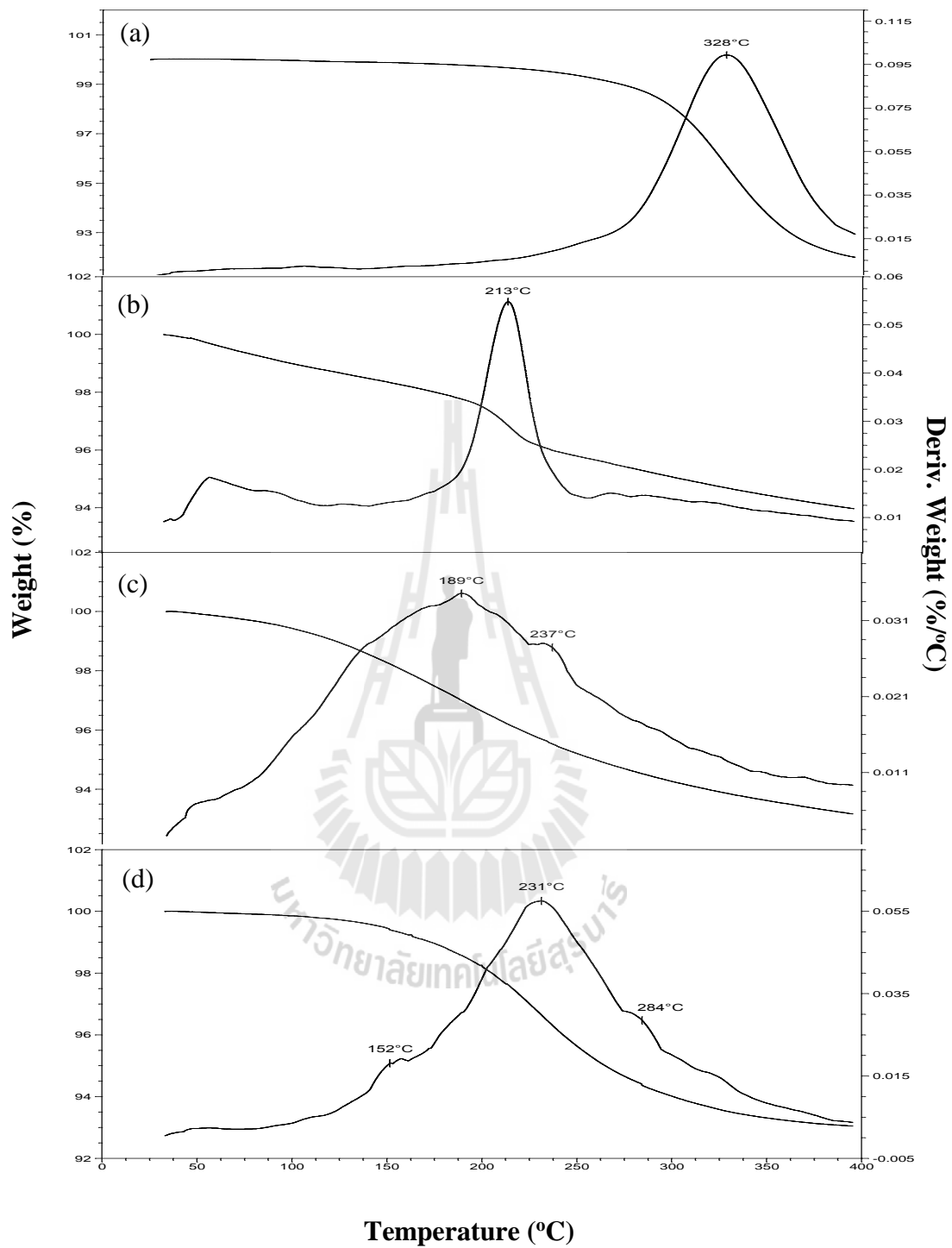


Figure 3.19 TGA/DTG curves of ANA (a), JBW (b), CAN (c) and SOD (d).

The sharp band of JBW specifies that water molecule in JBW is mainly a single type of hydrate water. The stronger interaction of water molecule may be explained in term of bond distance between Na^+ and H_2O depending on the strength of polarization of water molecule by sodium ion. A stronger polarization of water molecule leads to the shorter bond distance of Na^+ and H_2O resulting in the greater thermal stability of water as in ANA.

In contrast, the large broad band of dehydration with a peak centered at the lowest temperature was observed in CAN indicating no clear differences regarding the coordination of water to sodium ions as in ANA and in JBW. The dehydration of CAN in this range was assigned to water loss from the ϵ cages (Linares et al., 2005). It seems that the interaction of water in SOD is stronger than that in CAN and JBW according to DTA of SOD.

3.4.5 Dehydration in ethanol solution

Figure 3.20 showed the abilities of sodium zeolite in dehydration of ethanol solution with various ethanol concentrations. All sodium zeolites can be used as adsorbents for the dehydration. Above all, ANA showed the best performance to dehydrate under the experiment concentration ranges (85.0%-97.0% v/v ethanol solutions) compared to the other sodium zeolites which can be dehydrated at 97.0% v/v ethanol solution to yield an absolute ethanol. This result corresponds to that of NH_3 -TPD and DTG suggesting that sodium ions in ANA are stronger Lewis acid than those in the other zeolites. The dehydration ability of SOD appeared to be the lowest. The result differed from the DTG curves of water suggesting that water molecules preferred in SOD more than those in CAN and JBW. This might have been affected by the zeolite pore structure that dominantly determines the infiltration

mechanism of water into the pore. SOD structure contains very small pore openings (a diameter 2.6 Å) compared to CAN (5.9×5.9 Å) and JBW (3.7×4.8 Å) (Baerlocher, 2001). The smaller the zeolite pore is, the more difficult the infiltration is likely to occur.

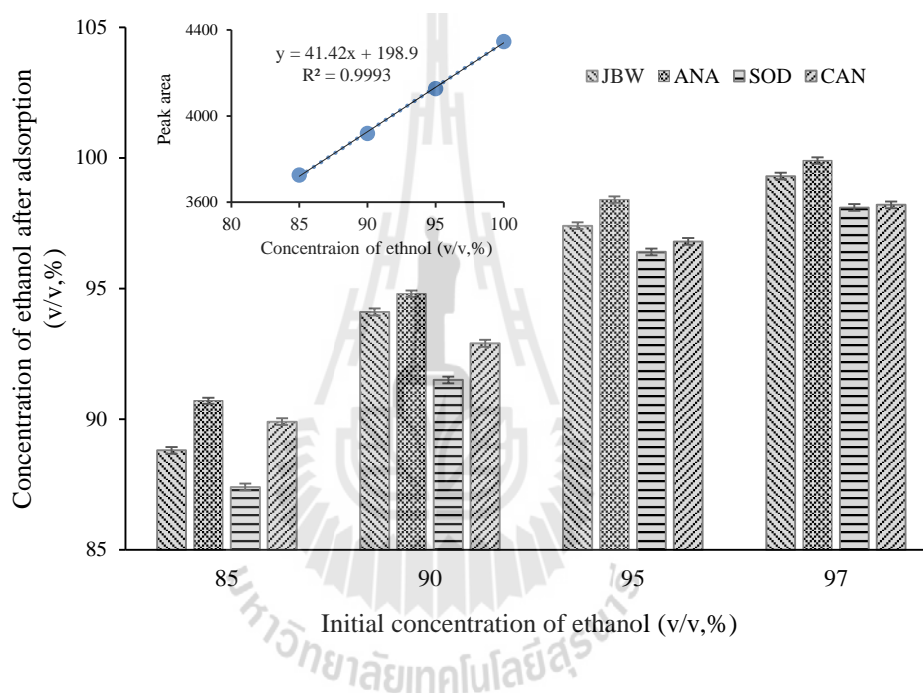


Figure 3.20 Adsorption of water from various ethanol concentrations.

3.5 Conclusions

A pure phase and high crystallinity of ANA, JBW, CAN and SOD have been successfully obtained through a shorter reaction period compared to those from other related research. The NH_3 -TPD characterization proved to be considerably absorbed with the extreme number of adsorption sites into ANA. DTG curve indicated strong interaction of water into ANA. Generally, ANA was compared with zeolite NaA for

dehydration (Muenpoowank and Rangriwatanonon, 2012) showing that zeolite NaA produced high concentrations of ethanol solution from 85.0 to 88.2%v/v and 95.0 to 97.9%v/v by batch method. However, in this present study, ANA exhibited a more effective adsorbent to dehydration in ethanol from 85.0 to 90.4 and 95.0 to 98.6%v/v. Moreover, ANA can dehydrate in ethanol solutions from 97.0%v/v to 99.9%v/v. Besides ANA, JBW is an alternative interesting adsorbent for dehydration in ethanol solution with its simplest way to synthesize and its cost effectiveness as well as its better performance than those of CAN and SOD for increasing ethanol concentration from 90.0, 95.0 and 97.0%v/v to 94.1, 97.4 and 99.3%v/v, respectively. The adsorption capacity of zeolite mainly relies on the strength of Lewis acid sites and pore structure. For ANA, it does appear that the acid strength is predominated, while the pore structure for SOD limits its water adsorption capacity.

3.6 References

- Ali Memon, S., Yiu Lo, T., Shi, X., Barbhuiya, S. and Cui, H. (2013). Preparation, characterization and thermal properties of Lauryl alcohol/Kaolin as novel form-stable composite phase change material for thermal energy storage in buildings. **Applied Thermal Engineering**. 59: 336-347.
- Alkan, M., Hopa, Ç., Yilmaz, Z. and Güler, H. (2005). The effect of alkali concentration and solid/liquid ratio on the hydrothermal synthesis of zeolite NaA from natural kaolinite. **Microporous and Mesoporous Materials**. 86: 176-184.
- Atta, A. Y., Jibril, B. Y., Aderemi, B. O. and Adefila, S. S. (2012). Preparation of analcime from local kaolin and rice husk ash. **Applied Clay Science**. 61: 8-13.

- Auroux, A., Huang, M. and Kaliaguine, S. (1995). Crystallinity dependence of Lewis acidity and Lewis basicity in Na zeolites. **Journal of Physical Chemistry**. 99: 9952-9959.
- Baerlocher, C., Meier, W. M. and Olson, D. H. (2001). Atlas of zeolite framework types. **Structure Commission of the International Zeolite Association**.
- Barnes, M. C., Addai-Mensah, J. and Gerson, A. R. (1999). The mechanism of the sodalite-to-cancrinite phase transformation in synthetic spent Bayer liquor. **Microporous and Mesoporous Materials**. 31: 287-302.
- Castaldi, P., Santona, L., Cozza, C., Giuliano, V., Abbruzzese, C., Nastro, V. and Melis, P. (2005). Thermal and spectroscopic studies of zeolites exchanged with metal cations. **Journal of Molecular Structure**. 734: 99-105.
- Castellano, M., Turturro, A., Riani, P., Montanari, T., Finocchio, E., Ramis, G. and Busca, G. (2010). Bulk and surface properties of commercial kaolins. **Applied Clay Science**. 48: 446-454.
- Chaisena, A. and Rangsrivatananon, K. (2005). Synthesis of sodium zeolites from natural and modified diatomite. **Materials Letters**. 59: 1474-1479.
- Cho, C. H., Oh, K. Y., Yeo, J. G., Kim, S. K. and Lee, Y. M. (2010). Synthesis, ethanol dehydration and thermal stability of NaA zeolite/alumina composite membranes with narrow non-zeolitic pores and thin intermediate layer. **Journal of Membrane Science**. 364: 138-148.
- Colina, F. G. and Llorens, J. (2007). Study of the dissolution of dealuminated kaolin in sodium-potassium hydroxide during the gel formation step in zeolite X synthesis. **Microporous and Mesoporous Materials**. 100: 302-311.

- Dyer, A., Tangkawanit, S. and Rangriwatananon, K. (2004). Exchange diffusion of Cu^{2+} , Ni^{2+} , Pb^{2+} and Zn^{2+} into analcime synthesized from perlite. **Microporous and Mesoporous Materials**. 75: 273-279.
- Farmer, V. C. (2000). Transverse and longitudinal crystal modes associated with OH stretching vibrations in single crystals of kaolinite and dickite. **Spectrochimica Acta, Part A**. 56: 927-930.
- Haelssig, J. B., Tremblay, A. Y. and Thibault, J. (2012). A new hybrid membrane separation process for enhanced ethanol recovery: Process description and numerical studies. **Chemical Engineering Science**. 68: 492-505.
- Heah, C. Y., Kamarudin, H., Mustafa Al Bakri, A. M., Bnhussain, M., Luqman, M., Khairul Nizar, I., Ruzaidi, C. M. and Liew, Y. M. (2012). Study on solids-to-liquid and alkaline activator ratios on kaolin-based geopolymers. **Construction and Building Materials**. 35: 912-922.
- Healey, A. M., Johnson, G. M. and Weller, M. T. (2000). The synthesis and characterisation of JBW-type zeolites.: Part A: Sodium/potassium aluminosilicate, $\text{Na}_2\text{K}[\text{Al}_3\text{Si}_3\text{O}_{12}]\cdot 0.5\text{H}_2\text{O}$. **Microporous and Mesoporous Materials**. 37: 153-163.
- Hegazy, E. Z., El Maksod, I. H. A. and El Enin, R. M. M. A. (2010). Preparation and characterization of Ti and V modified analcime from local kaolin. **Applied Clay Science**. 49: 149-155.
- Lalik, E., Mirek, R., Rakoczy, J. and Groszek, A. (2006). Microcalorimetric study of sorption of water and ethanol in zeolites 3A and 5A. **Catalysis Today**. 114: 242-247.

- Lin, D. C., Xu, X. W., Zuo, F. and Long, Y. C. (2004). Crystallization of JBW, CAN, SOD and ABW type zeolite from transformation of meta-kaolin. **Microporous and Mesoporous Materials**. 70: 63-70.
- Linares, C. F., Sánchez, S., Urbina de Navarro, C., Rodríguez, K. and Goldwasser, M. R. (2005). Study of cancrinite-type zeolites as possible antacid agents. **Microporous and Mesoporous Materials**. 77: 215-221.
- Liu, Q., Navrotsky, A., Jove-Colon, C. F. and Bonhomme, F. (2007). Energetics of cancrinite: Effect of salt inclusion. **Microporous and Mesoporous Materials**. 98: 227-233.
- Liu, Y., Yang, Z., Yu, C., Gu, X. and Xu, N. (2011). Effect of seeding methods on growth of NaA zeolite membranes. **Microporous and Mesoporous Materials**. 143: 348-356.
- Lu, L., Shao, Q., Huang, L. and Lu, X. (2007). Simulation of adsorption and separation of ethanol–water mixture with zeolite and carbon nanotube. **Fluid Phase Equilibria**. 261: 191-198.
- Madejová, J. (2003). FTIR techniques in clay mineral studies. **Vibrational Spectroscopy**. 31: 1-10.
- Makó, É., Senkár, Z., Kristóf, J. and Vágvölgyi, V. (2006). Surface modification of mechanochemically activated kaolinites by selective leaching. **Journal of Colloid and Interface Science**. 294: 362-370.
- Muenpoowank, K. and Rangsrivananon, K. (2012). Elimination of water from ethanol solution by zeolites. **The Pure and Applied Chemistry International Conference**. 1225-1228.

- Panda, A. K., Mishra, B. G., Mishra, D. K. and Singh, R. K. (2010). Effect of sulphuric acid treatment on the physico-chemical characteristics of kaolin clay. **Colloids and Surfaces A: Physicochemical and Engineering Aspects**. 363: 98-104.
- Qiu, W. and Zheng, Y. (2009). Removal of lead, copper, nickel, cobalt, and zinc from water by a cancrinite-type zeolite synthesized from fly ash. **Chemical Engineering Journal**. 145: 483-488.
- Reyes, C. R., Williams, C. D. and Roberts, C. (2011). Synthesis and characterisation of SOD-, CAN- and JBW-Type structures by hydrothermal reaction of kaolinite at 200 °C. **Dyna**. 166: 39.
- Ríos, C. A., Williams, C. D. and Fullen, M. A. (2009). Nucleation and growth history of zeolite LTA synthesized from kaolinite by two different methods. **Applied Clay Science**. 42: 446-454.
- Sato, K., Aoki, K., Sugimoto, K., Izumi, K., Inoue, S., Saito, J., Ikeda, S. and Nakane, T. (2008). Dehydrating performance of commercial LTA zeolite membranes and application to fuel grade bio-ethanol production by hybrid distillation/vapor permeation process. **Microporous and Mesoporous Materials**. 115: 184-188.
- Tatlier, M., Barış Cigizoglu, K., Tokay, B. and Erdem-Şenatalar, A. (2007). Microwave vs. conventional synthesis of analcime from clear solutions. **Journal of Crystal Growth**. 306: 146-151.
- Treacy, M. M., Ballmoos, R. V. and Higgins, J. B. (1996). **Collection of simulated XRD powder pattern for zeolite**. International zeolite Association. Elsevier. 500-581.

- Wang, L., Luo, Z. and Shahbazi, A. (2013). Optimization of simultaneous saccharification and fermentation for the production of ethanol from sweet sorghum (*Sorghum bicolor*) bagasse using response surface methodology. **Industrial Crops and Products**. 42: 280-291.
- Yamamoto, T., Kim, Y. H., Kim, B. C., Endo, A., Thongprachan, N. and Ohmori, T. (2012). Adsorption characteristics of zeolites for dehydration of ethanol: Evaluation of diffusivity of water in porous structure. **Chemical Engineering Journal**. 181-182: 443-448.
- Yang, S., Vlessidis, A. G. and Evmiridis, N. P. (1997). Synthesis of zeolites in the system $\text{Na}_2\text{O-SiO}_2\text{-Al}_2\text{O}_3\text{-H}_2\text{O}$ -glycerol. **Microporous Materials**. 9: 273-286.
- Yingling, B., Li, C., Honglin, W. and Zongcheng, Y. (2013). Application of an integrated statistical design to optimize the cold enzyme hydrolysis conditions for ethanol production. **Biochemical Engineering Journal**. 74: 27-35.
- Zhang, J. and Liu, W. (2011). Thin porous metal sheet-supported NaA zeolite membrane for water/ethanol separation. **Journal of Membrane Science**. 371: 197-210.
- Zhao, H., Deng, Y., Harsh, J. B., Flury, M. and Boyle, J. S. (2004). Alteration of kaolinite to cancrinite and sodalite by simulated Hanford tank waste and its impact on cesium retention. **Clays and Clay Minerals**. 52: 1-13.

CHAPTER IV

FACILE HYDROTHERMAL SYNTHESIS OF ZEOLITIC ANA MEMBRANE FROM RAW KAOLIN, DEALUMINATED KAOLIN AND CHEMICAL SOURCE

4.1 Abstract

Successful and facile hydrothermal synthesis of zeolitic ANA (analcime) membrane on the porous ceramic support was carried out using *in situ* synthesis method. Raw kaolin, dealuminated kaolin and also chemical were selected as starting material source. X-ray diffraction (XRD) and scanning electron microscope (SEM) were used to characterize ANA membranes. An appropriated ANA membrane was synthesized on the suitable ceramic support which was prepared from the ingredient of 10.0 wt% cristobalite, 2.5 wt% activated carbon, 2.5 wt% calcite and 85.0 wt% raw kaolin. The small crystals (20-37 μm) and thin layer of ANA (45-67 μm) were obtained by raw kaolin with aging while using dealuminated kaolin and chemical appeared small crystals and thin layer of ANA without aging. It seems that the longer hydrothermal time is, the more obvious the crystals tightly bound with the support becomes.

4.2 Introduction

Recently, the field of zeolite membranes significantly attracts various kinds of applications (Pina et al., 2011) in gas or liquid separations (Maghasoudi et al., 2014), membrane reactors (Tavolaro et al., 2011) and sensors (Vilaseca et al., 2007; Baimpos et al., 2012) not only because of its selective absorption, uniform but also its molecular size pore. More importantly, zeolite membrane also has high mechanical strength, thermal and chemical stability compared to organic membranes. The hydrophilic zeolite membranes such as NaA zeolite (Zhang and Liu, 2011; Shao et al., 2014; Liu et al., 2011; Kunnakorn et al., 2011; Kondo et al., 2010; Cho et al., 2010; Basak et al., 2014), hydroxylsodalite (H-SOD) (Kazemimoghdam and Mohammadi, 2011), faujasite-type zeolite (X and Y) (Kita et al., 2001), and mordenite (Navajas et al., 2002) membrane have been widely applied to break the azeotrope of ethanol and water for preparation anhydrous ethanol, especially NaA zeolite membrane. However, the previous work (in chapter III) found that ANA showed the best performance to dehydrate of ethanol solution compared to JBW, CAN and SOD. Therefore, ANA zeolite should be a good alternative absorbent for separation applications. In addition, ANA consists of the aperture of the 8-ring pore opening $1.6 \times 4.2 \text{ \AA}$. Therefore, small pore size of ANA makes the separation of small molecules by difference in size possible. Thus, small water molecules as about 2.6 \AA are expected to be separated from bigger molecule of ethanol as 4.4 \AA . The synthesis of ANA with natural raw materials such as diatomite (Chaisena and Rangriwatananon, 2005), perlite (Dyer et al., 200; Kongkachuichay and Lohsoontorn, 2004) and kaolin (Atta et al., 2012; Hegazy et al., 2010) is more economically advantageous than the synthesis with chemicals because of its cost effectiveness.

by leaching with strong alkali solutions (Kazemimoghadam and Mohammadi, 2011; Abbasi et al., 2010).

Until now, there are only few studies focusing on how to prepare zeolite layer from solid phase like kaolin on mullite support. What has been publicly reported is just the synthesis of hydroxysodalite (H-SOD) from metakaolin on porous mullite tubular support (Kazemimoghadam and Mohammadi, 2011). Thus, this gives rise to this present research whose aim focuses on simple preparation of high crystalline hydrophilic ANA membrane with raw kaolin which is one of the cheapest and most abundantly available silica and alumina source in our country, Thailand, for water/ethanol separation in a future towards separation/pervaporation performance. In addition, dealuminated kaolin and chemical source were also studied as starting materials for synthesizing ANA.

4.3 Experiment

4.3.1 Materials

Raw kaolin (RK) and dealuminated kaolin (DK24) (from chapter III) was used as starting material from local source for synthesis of ANA. In addition, ANA were also synthesized from chemical source with mixture of colloidal silica sol (Ludox HS-40 from Dupont, 40% SiO₂) and Al(OH)₃ (Carlo Erba). As well as pellets of sodium hydroxide (Merck) were used as alkaline solution in the synthesis of ANA. RK were used for the preparing of porous ceramic supports, it was sieved with 63 μm mesh before being used in the later steps. In this process, cristobalite prepared from rice husk and hydrochloric acid (Merck), activated carbon and CaCO₃ were purchased from Panreac and QRëC, respectively.

4.3.2 Preparation of porous ceramic support

4.3.2.1 Preparation of cristobalite

Cristobalite, one of the ingredients is needed for making the ceramic discs as it helps to maintain a thermal expansion coefficient of ceramic plate to be constant (Geus et al., 1992). These following steps were taken to prepare cristobalite from rice husk. Firstly, rice husk (10.0 g) was washed with tap water followed by deionized water (DI) and dried at 110 °C. Then it was reacted with 100.0 mL of 1 M HCl solution and boiled for 3 hours. Later, the obtained solid was washed with DI water until pH was 7 and dried at 110 °C. After that it was calcined at 700 °C for 4 h to eliminate organic compound (Yalçın and Sevinç, 2001). After white powders of pure silica were obtained, then, silica was sieved with 63 µm mesh and followed by calcined at 1400 °C to transform silica into cristobalite (Wahl et al., 1961).

4.3.2.2 Preparation of porous ceramic disc

The followings are the ingredients for preparing the porous ceramic discs i.e. 10.0 wt% of cristobalite, 2.5 wt%, 5.0 wt% and 10.0 wt% of activated carbon and CaCO₃ as pore former and 80.0-87.5 wt% of kaolin. Moreover, the mixture of only kaolin (90.0 wt%) and cristobalite (10.0 wt%) was prepared as a porous ceramic disc. The ingredients of preparing the porous ceramic discs are summarized in Table 4.1. The main stages of the preparation of the ceramic discs used in this work are described in Figure 4.1. Generally, to start with, DI water was added into the ingredient followed by sonication for 60 min, and then it was heated, stirred and evaporated until the mixtures became slurry. When the slurry was dried in an oven at 110 °C, 13.0 g of the obtained sample was later ground and compressed as a

disc (5.5 cm diameter×0.5 cm thick) about 1000 psi by uniaxial dry pressing. Next, the disc was put on crucible and sintered at 1400 °C in the furnace for 90 min with a heating and cooling rate of 2.0 °C/min to burn off the organic or inorganic to transform the mixture into porous ceramic supports. Then the porous ceramic supports was cleaned with DI water and dried at 110 °C. All the supports were carried out by using gloves. The percent of shrinkage of all the prepared supports were about 24%.

Normally, the apparent porosity was conducted by analytical balance and Archimedes' method (Souza et al., 2011). The porous ceramic supports were prepared from pore former of 2.5, 5.0 and 10.0 wt% of activated carbon and 2.5, 5.0 and 10.0 wt% of CaCO₃ denoted as 2.5A, 5A and 10A and 2.5Ca, 5Ca and 10Ca, respectively. Similarly, the porous ceramic support from the mixture of pore former of 2.5 wt% activated carbon and 2.5 wt% calcite was denoted as 2.5ACa.

Table 4.1 The compositions of the ingredients (wt%) for preparation of porous ceramic discs.

No.	Kaolin (g)	Cristobalite (g)	CaCO ₃ (g)	Activated Carbon (g)
1	100.00	-	-	-
2	90.00	10.00	-	-
3	87.50	10.00	2.50	-
4	87.50	10.00	-	2.50
5	85.00	10.00	5.00	-
6	85.00	10.00	-	5.00
7	85.00	10.00	2.50	2.50
8	80.00	10.00	10.00	-
9	80.00	10.00	-	10.00

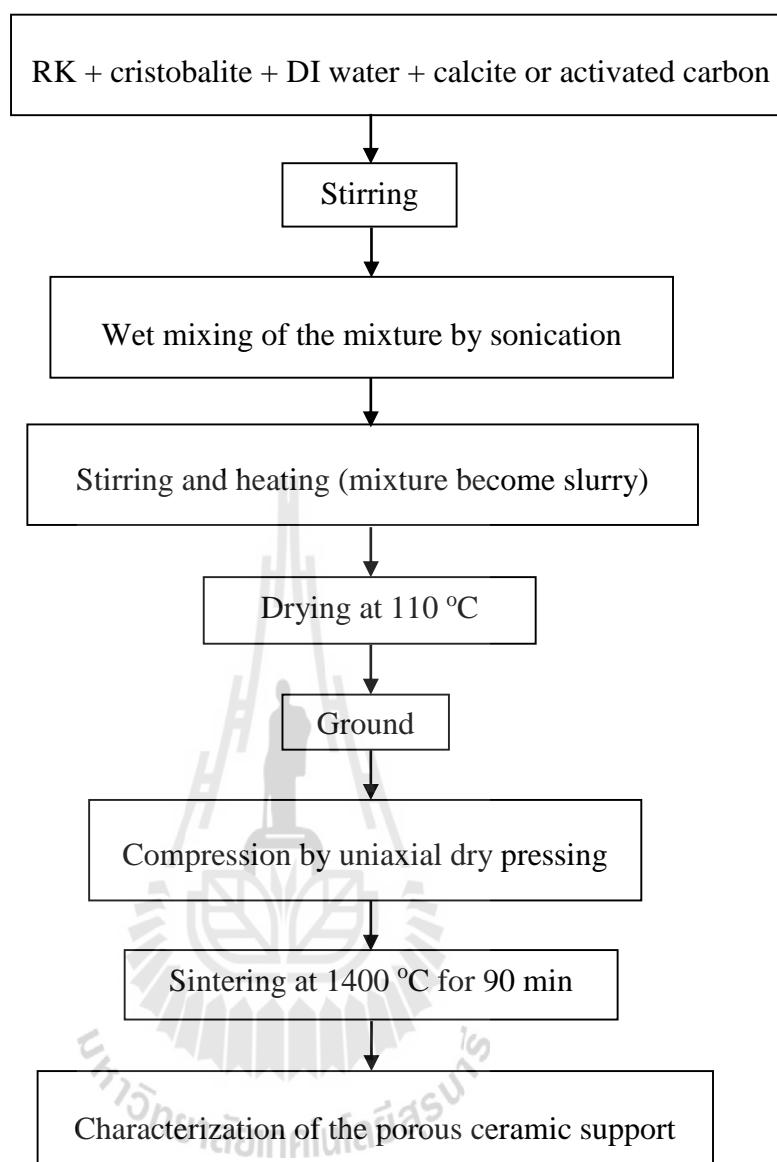


Figure 4.1 The main stages of the preparation for the porous ceramic discs.

4.3.3 ANA membranes synthesis

4.3.3.1 ANA membrane from porous ceramic supports

The porous ceramic supports were placed in a stainless steel autoclave followed by transferring of NaOH solution. The concentration of NaOH solutions were used as 7.5% and 10.0% w/v. Then the autoclave was placed in an oven

at 200 °C with the reaction time for 24 h. ANA membrane was washed with DI water until pH = 7 and dried at 110 °C. The results showed in appendix.

4.3.3.2 The ANA membranes were synthesized by using RK, DK24 and chemical as starting material

ANA membrane from RK source; To begin with, the mixture of RK and NaOH solution (the molar composition as in synthesis of JBW in chapter III) was stirred for 1 h, and then it was transferred into a stainless steel autoclave followed by immersing porous ceramic supports into the mixture with the condition of no aging and with aging of 1, 2 and 3 days at an ambient temperature. After that, autoclave was placed in an oven at 200 °C with the reaction time of 12, 18 and 24 h. Then the autoclave was cooled down to room temperature. Finally, the products were washed with DI water until pH 7 and dried at 110 °C.

ANA membrane from DK24 source; the mixture of DK24, Al(OH)₃ and NaOH solution (the molar composition as in synthesis of ANA in chapter III) were stirred for 1 h. The typical processes were performed same condition of RK as starting material.

ANA membrane from chemical source; Colloidal silica sol and Al(OH)₃ were used as SiO₂ and Al₂O₃ source, respectively. The mixture of 1.04 g Al(OH)₃, 1.93 g NaOH and DI water were stirred and heated until Al(OH)₃ dissolved. After that add 2.31 g colloidal silica into mixture and stirred, producing a homogeneous clear solution. The molar composition is Al₂O₃:2.3SiO₂:3.6Na₂O:140.4H₂O. The typical processes were performed as condition of RK as starting material.

4.3.4 Characterization

The X-ray diffraction (XRD) patterns were collected using a Bruker D2 Phaser with Cu-K α radiation (40 kV and 40 mA). Data collection was carried out in the 2θ rang 10-45° at step size of 0.02°. Micrographs of scanning electron microscope (SEM) different samples were performed with JSM-6010LV model (JEOL) operating with an accelerating voltage of 20 kV. Thermal analysis was simultaneously performed on a Model SDT 2960 at 5 °C/min up to 1000 °C, in air.

4.4 Results and discussion

4.4.1 Characteristic of porous ceramic support

The XRD patterns of amorphous silica and cristobalite were shown in Figure 4.2. The XRD patterns of RK, calcined kaolin and calcined mixture of raw kaolin and 10 %wt cristobalite (10cristobalite) were shown in Figure 4.3. Figure 4.3(a) shows the main refraction peak of raw kaolin and impurity phase of quartz at 20.8° and 26.6° (Zhou et al., 2013). Figure 4.3(b) demonstrates a sharp peak of cristobalite and mullite phase after calcinations of raw kaolin at 1400 °C. Figure 4.3(c) indicates intensity of mullite and cristobalite phase was decreased and showed distinct amorphous phase. It can be described that the addition of cristobalite to raw kaolin may effect to cristobalite diffused into kaolin then disturbed the transformation of kaolin to mullite and cristobalite phase.

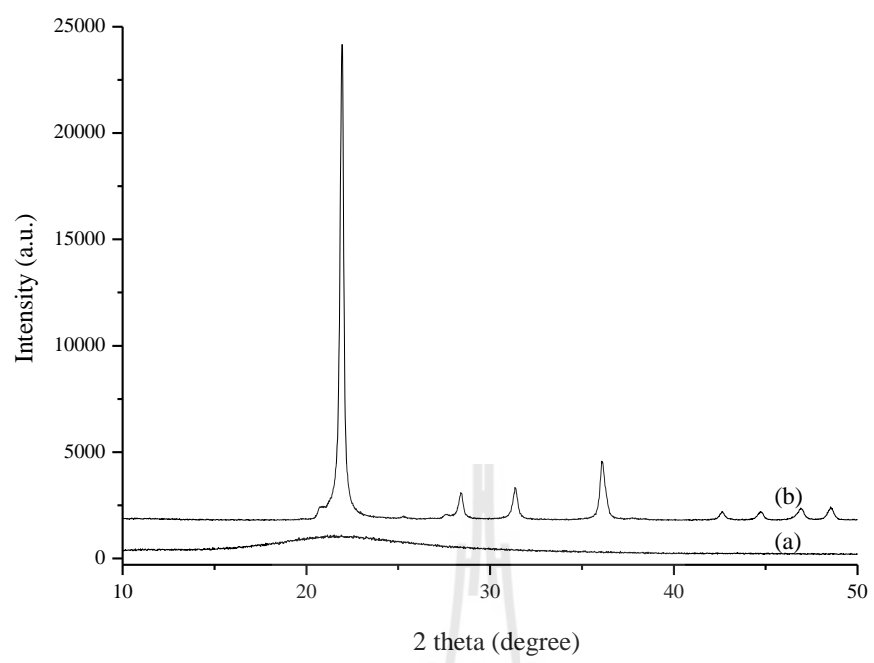


Figure 4.2 XRD patterns of (a) amorphous silica and (b) cristobalite from rice husk.

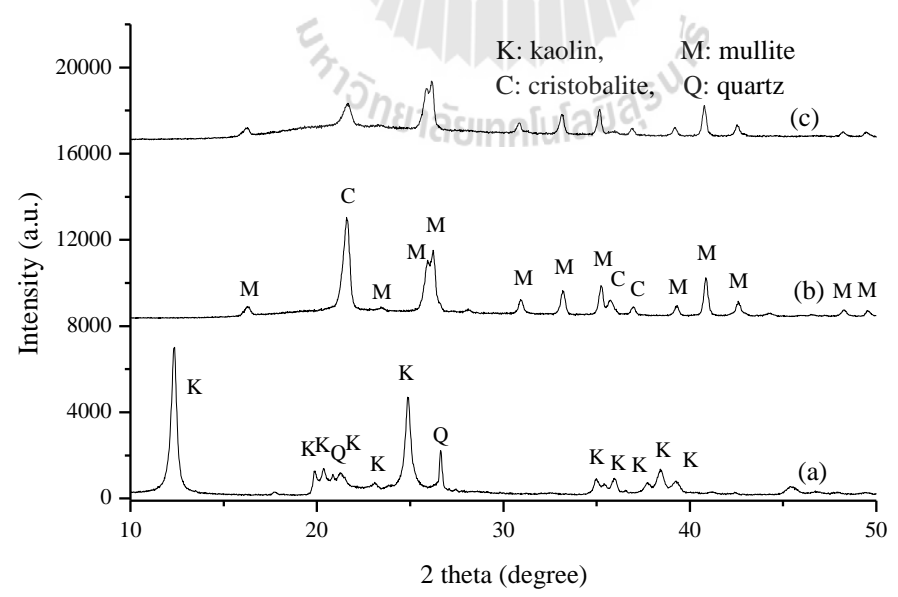


Figure 4.3 XRD patterns of (a) raw kaolin, (b) calcined kaolin and (c) 10 cristobalite.

Scanning electron micrograph of calcined kaolin is shown in Figure 4.4. The SEM micrograph of surface appeared scraggly surface with fracture (Figure 4.4(a)). The microstructure is uniform with a small grain size (Figure 4.4(b)). The cross section presented pore with inconsistent distribution (Figure 4.4(c)).

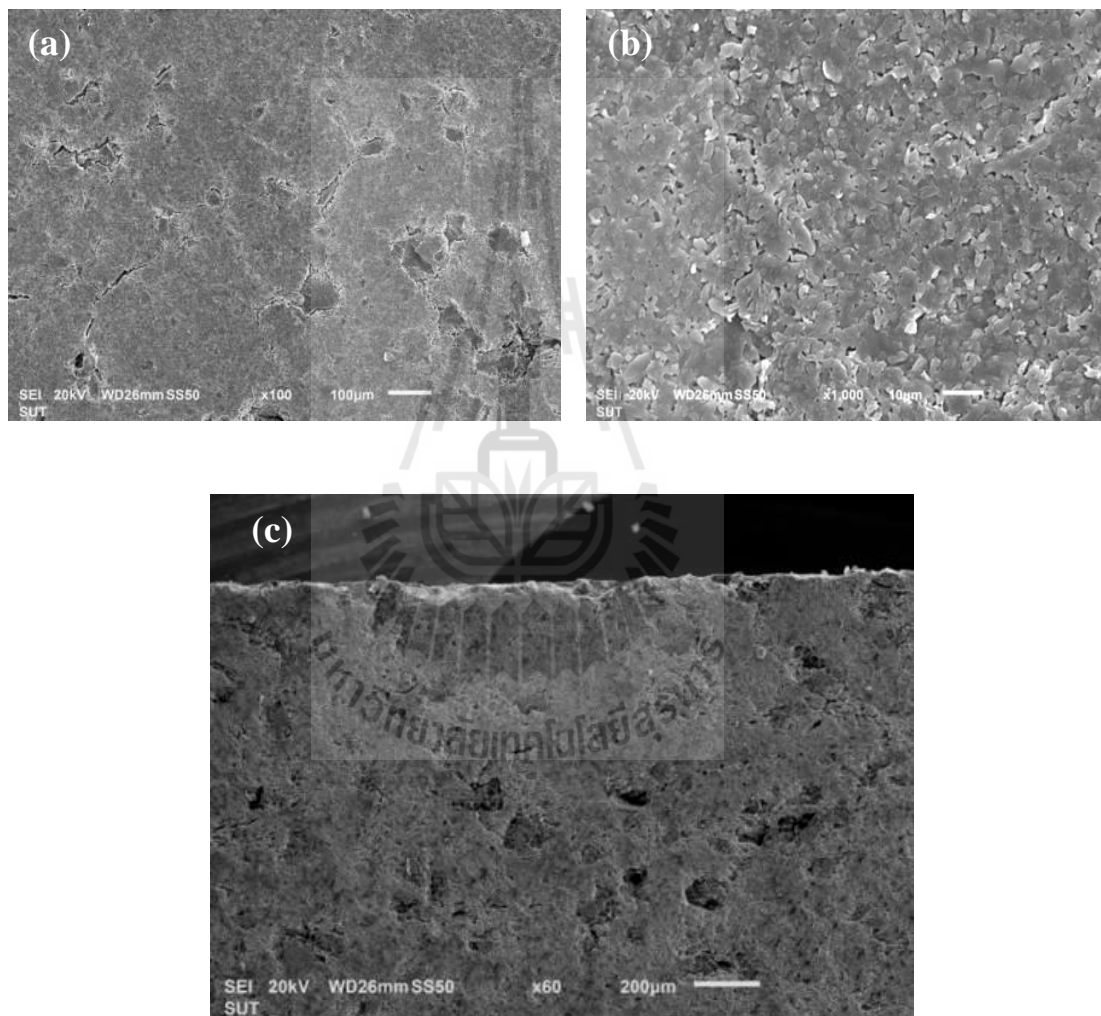


Figure 4.4 SEM micrograph of calcined kaolin disc: (a, b) top view, (c) cross section view.

Figure 4.5 shows XRD pattern of sintering of 2.5A, 5A and 10A. With all supports presented the mullite phase and cristobalite phase while 5A and 10A showed existence of an impurity phase of quartz. The intensity of cristobalite phase was increased with increasing of activated carbon amount. It was found that the activated carbon promoted cristobalite phase and restricted the transformation of quartz phase.

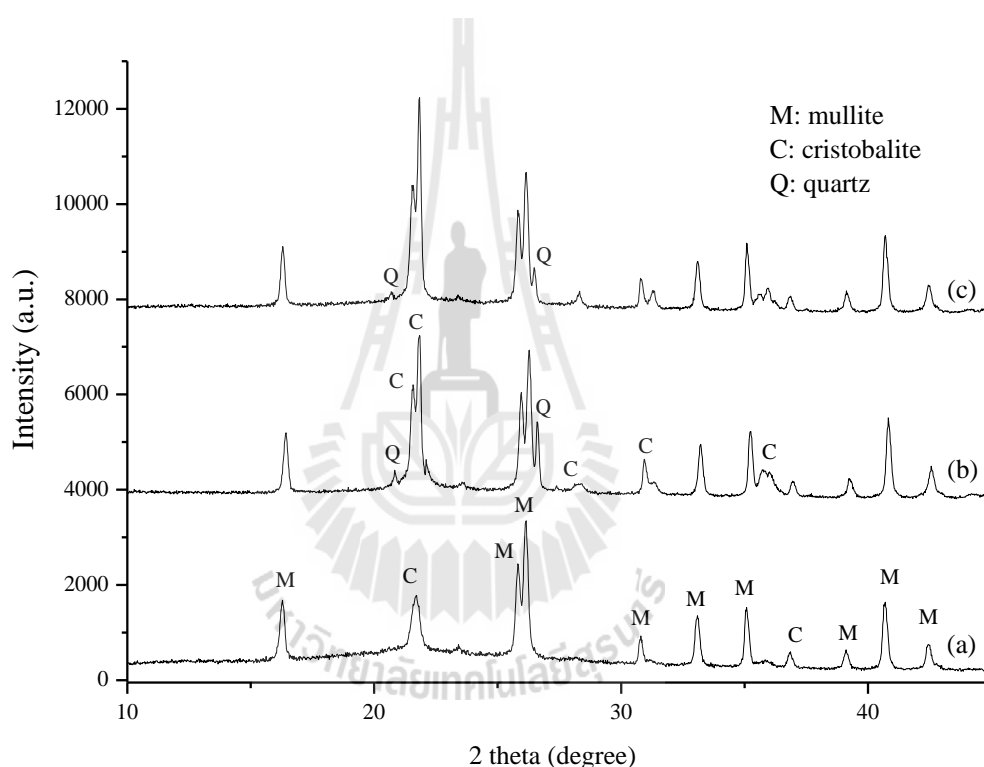


Figure 4.5 XRD patterns of porous ceramic support (a) 2.5A (b) 5A and (c) 10A.

The surface and cross-section SEM micrographs of 2.5A, 5A and 10A were shown in Figure 4.6. The sintering of these supports at 1400 °C, activated carbon was decomposed to CO₂ then produced pore throughout disc. By carbon and organic compound in kaolin were burn at about 450 °C (Yan et al., 2011). The 5A showed both small spherical pore and also elongated became bigger within the range

60-80 μm than those of 2.5A (20-40 μm). While, the 10A showed the fracture surface a rough morphological structure with a wide range about 40-140 μm . The cross-sections showed clearly distribution of the pore through into body. The density and sizes of pore were increased with increasing amount of activated carbon.

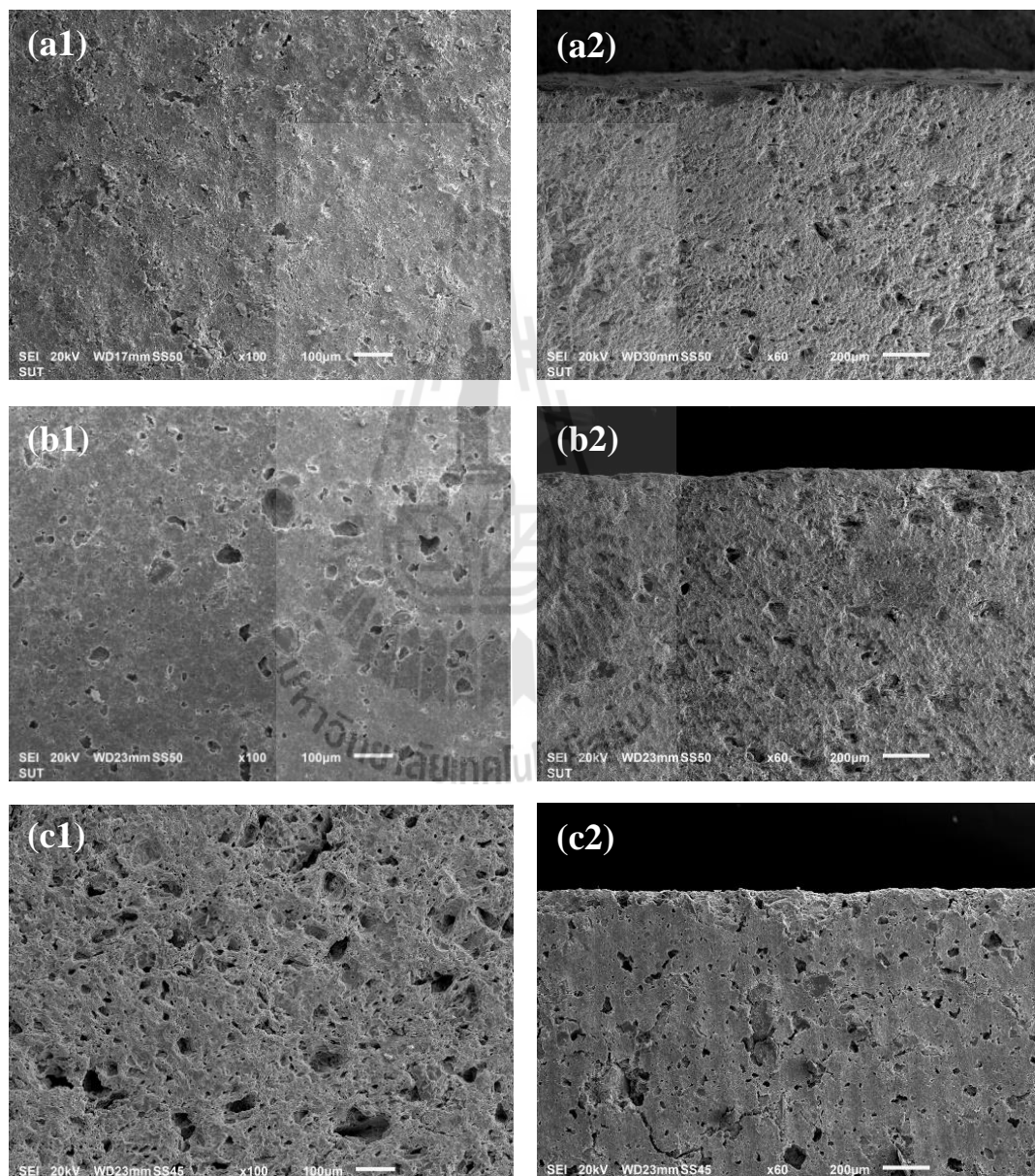


Figure 4.6 Top view and cross sectional SEM micrograph of porous ceramic support for 2.5A ((a1) and (a2)), 5A ((b1) and (b2)) and 10A ((c1) and (c2)).

Figure 4.7 shows the XRD patterns of 2.5Ca, 5Ca and 10Ca. All supports showed mullite phase, cristobalite phase and anorthite phase. In addition, the support of 5Ca presented one peak of wollastonite at 35.2° while 10Ca showed many peaks of wollastonite at 22.4°, 23.2°, 27.0° and 27.6°. The intensity of mullite phase was decreased of 10Ca. It was found that CaCO₃ affect to transformation of kaolin to mullite phase and promoted anorthite phase and wollastonite phase. The reaction of CaCO₃ with cristobalite and kaolin were presented by according to equation (4.2) and (4.3).

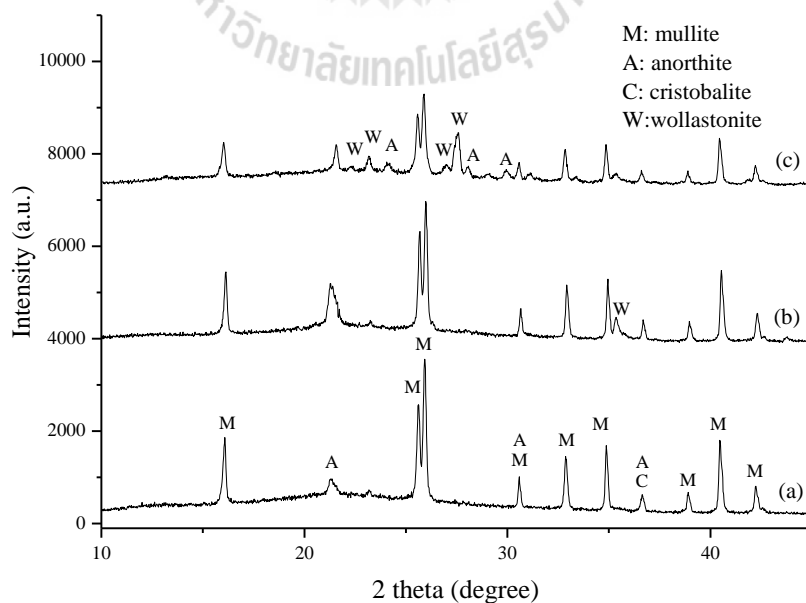


Figure 4.7 XRD patterns of porous ceramic plate (a) 2.5Ca, (b) 5Ca and (c) 10Ca.

Figure 4.8 demonstrates SEM micrographs of the surface and cross-section of 2.5Ca, 5Ca and 10Ca. The support of 10Ca showed spherical pore as elongated or ellipsoid with larger pore size than those of 5Ca and 2.5Ca with the pore size within the range of 30-100 μm , 20-60 μm and 10-30 μm , respectively.

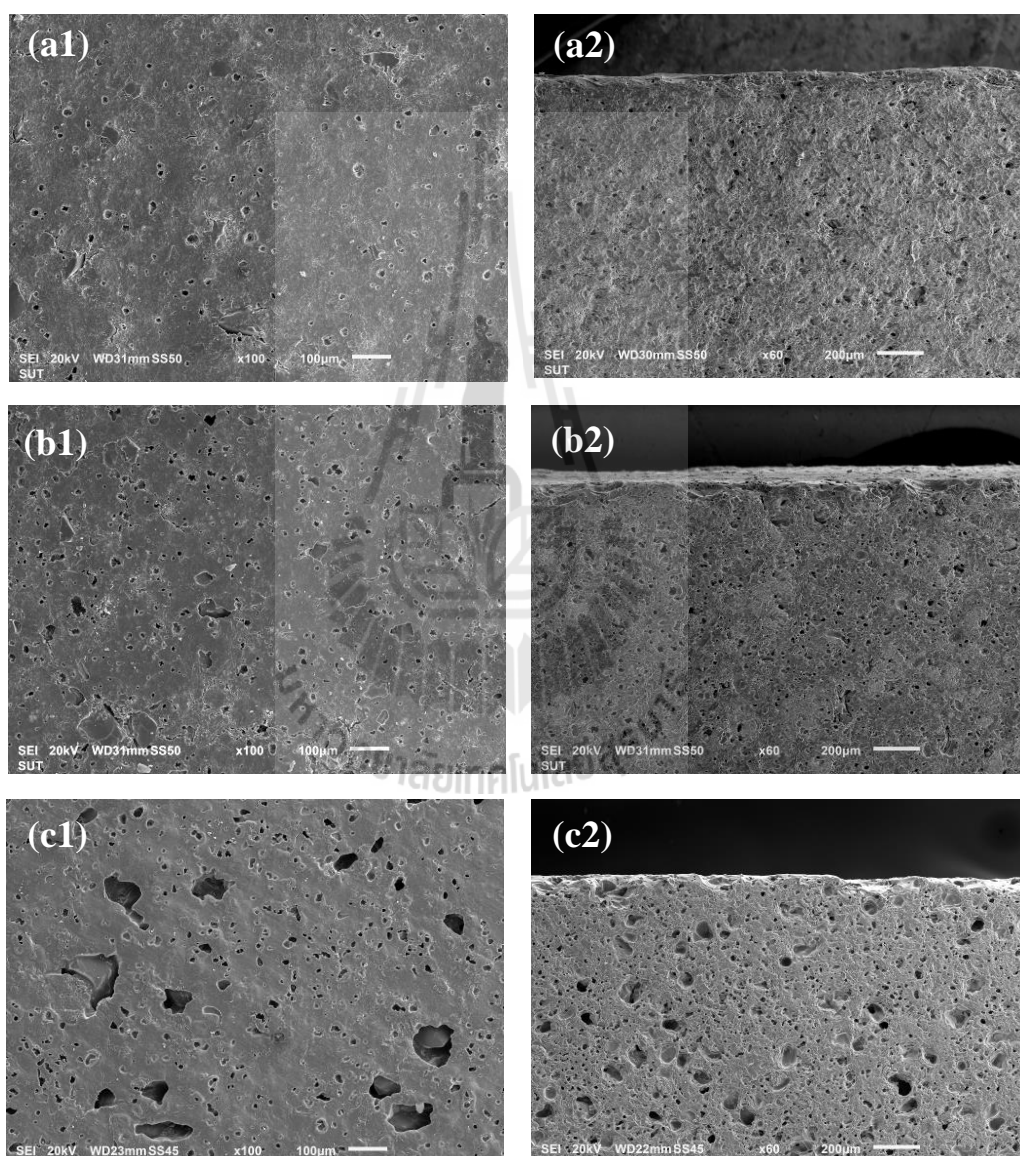


Figure 4.8 Top view and cross sectional SEM photographs of porous ceramic support for 2.5Ca ((a1) and (a2)), 5Ca ((b1) and (b2)) and 10Ca ((c1) and (c2)).

The apparent pore of those supports can be explained in term of calcinations of CaCO_3 . At high temperature regime corresponding to decomposition of CaCO_3 into CaO and release CO_2 gas then CO_2 gas created the porous texture (Nandi et al., 2008; Harabi et al., 2014). Thermal analyses of calcite were showed in Figure 4.9. It presented only endothermic peak in the temperature regime of 650 to 800 °C with mass loss of 45.07%. The large pore of 10Ca due to high concentration of calcite influence to the particle agglomerated then decarbonation generating residual entrapped gas more than at low concentration. In the case of cross-sectional of these porous ceramic supports showed pore spread through the body.

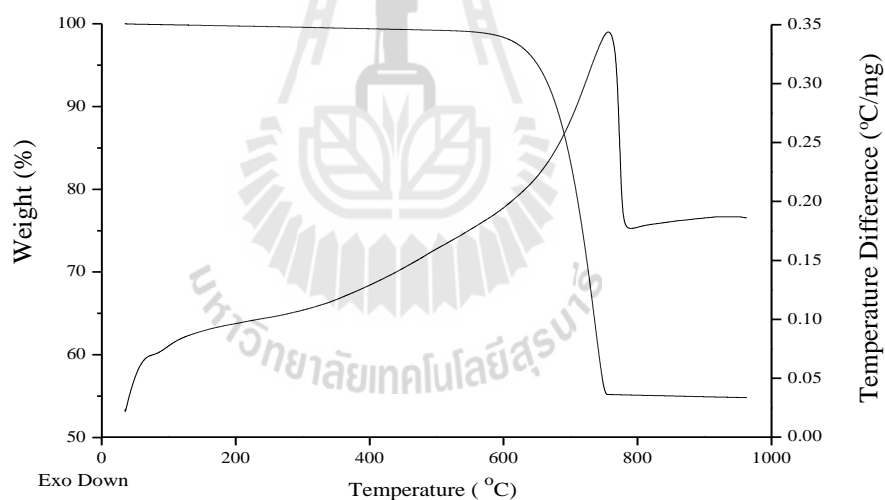


Figure 4.9 TGA and DTA curve of CaCO_3 .

In addition, SEM micrographs of surface and cross section of 2.5ACa were shown in Figure 4.10. The small spherical pore and elongated pore were presented within the range of 20-50 μm in size. The mixed phase of mullite, anorthite, cristobalite and wollastonite were showed in Figure 4.11.

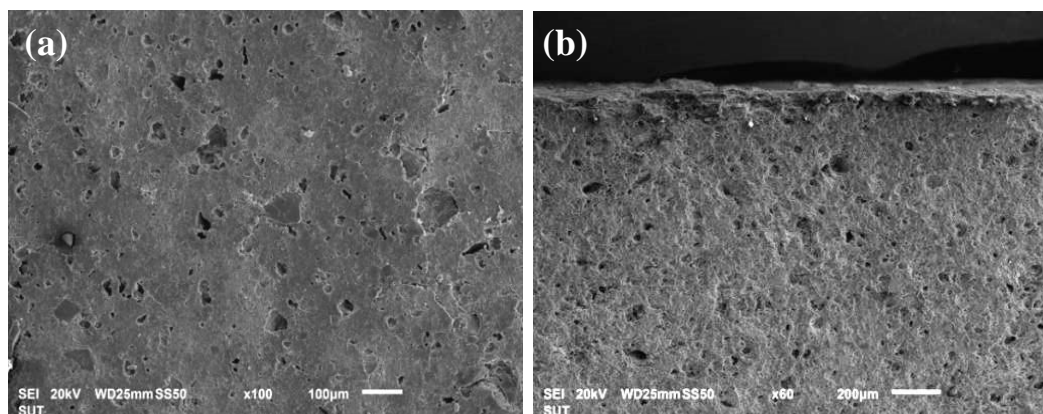


Figure 4.10 Top view (a) and cross sectional (b) SEM photographs of the 2.5ACa.

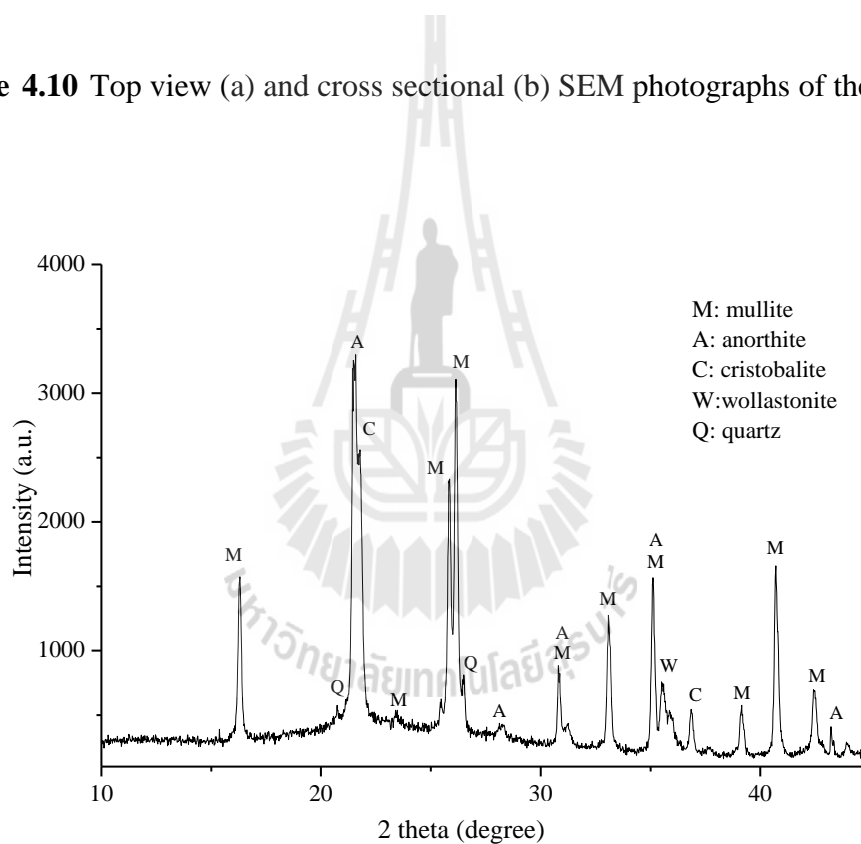


Figure 4.11 XRD patterns of 2.5ACa.

The pore size and the porosity of all the porous ceramic supports are summarized in Table 4.2. Comparison of the percent porosity of porous ceramic support between activated carbon and calcite as pore former were showed in Figure 4.12. The average pore size and percent porosity were increased with increasing of

activated carbon and CaCO_3 amount. The activated carbon produced percent porosity in support larger than calcite.

Table 4.2 The average pore size and percentage of porosity of porous ceramic supports.

Porous ceramic supports	2.5A	2.5Ca	2.5ACa	5A	5Ca	10A	10Ca
The range pore size (μm)	20-40	10-30	20-50	60-80	20-60	40-140	30-100
Porosity (%)	14.6	10.0	22.6	26.3	23.9	51.1	48.7

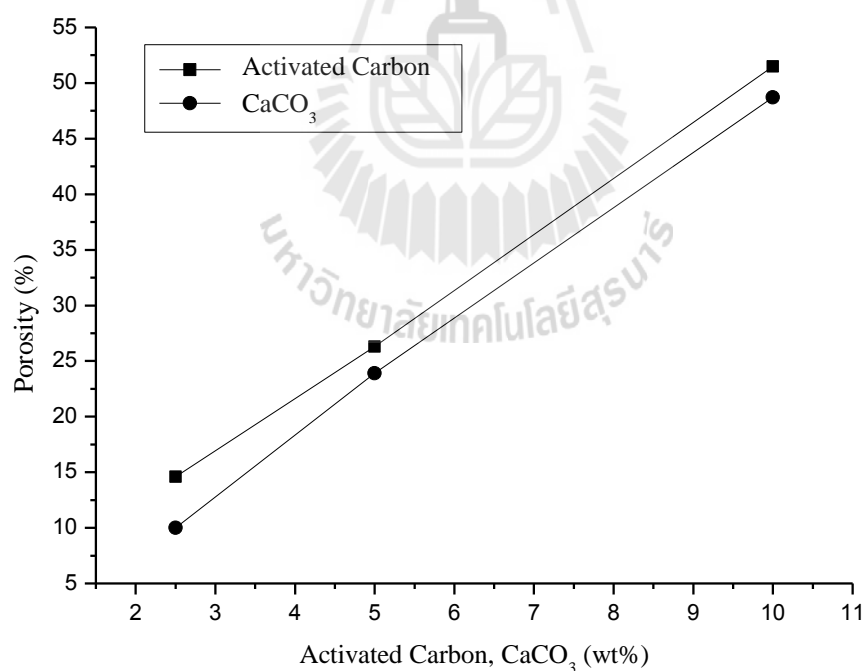


Figure 4.12 Percentage of porosity of porous ceramic supports from activated carbon and CaCO_3 as pore formers.

4.4.2 Characteristics of ANA membrane

4.4.2.1 ANA membrane from RK source

1) Effect of porous ceramic support

The XRD patterns in Figure 4.13(a)-(c) show only a single phase of ANA on 2.5A, 2.5Ca and 2.5ACa, but the sharpest peak of XRD with the highest intensity of ANA was observed in 2.5ACa indicating that a crystal is perfect with more amounts of ANA crystals. These results are consistent with those of SEM (see Figure 4.14 and 4.15). The appearance of mixed phase of ANA and cristobalite on 5A and 5Ca (Figure 4.13(d)-(e)) may be due to the better leaching of silica with NaOH solution resulting in larger porous ceramic and higher porosity like 5A and 5Ca.

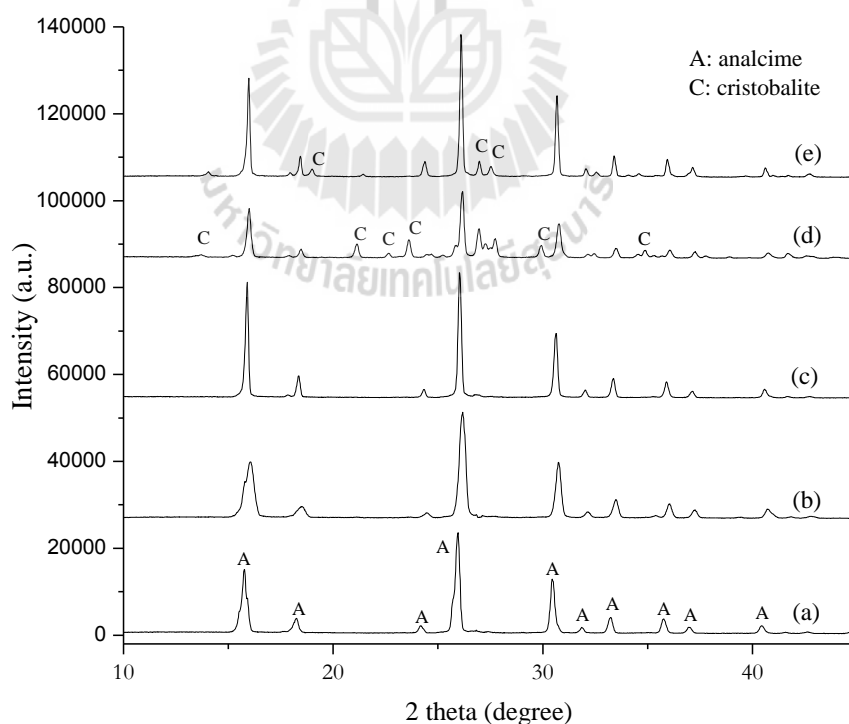


Figure 4.13 XRD patterns of ANA membrane on (a) 2.5A, (b) 2.5Ca, (c) 2.5ACa, (d) 5A and (e) 5Ca for 24 h.

Figure 4.14 shows SEM micrographs of ANA membrane on 2.5A and 2.5Ca. The surface of 2.5A was covered by continuously and increasingly growing ANA crystals while the surface of 2.5Ca obviously showed the space between ANA crystals. The cross-section of the porous ceramic disc demonstrates the crystal layers of both 2.5A and 2.5Ca bound with the disc.

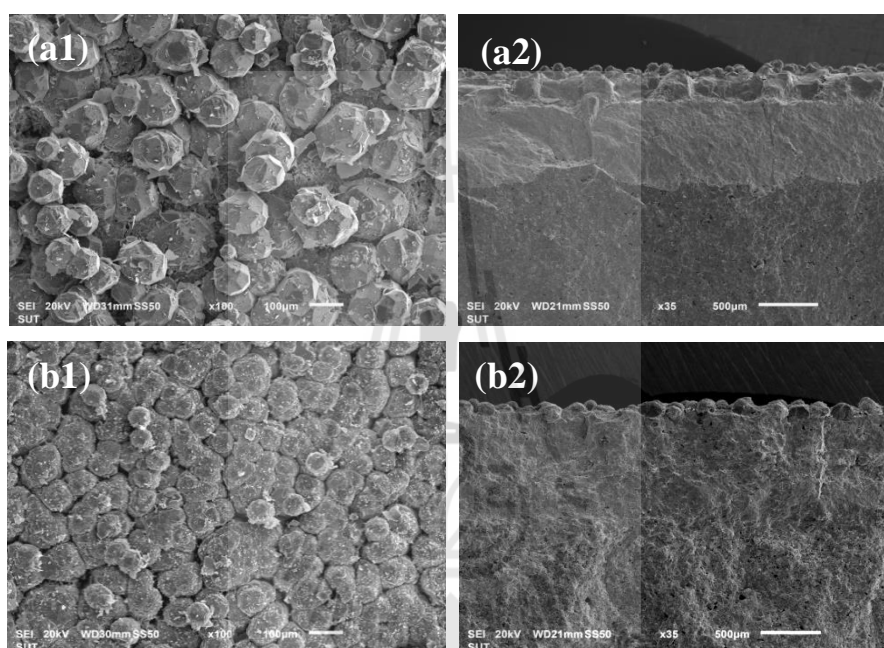


Figure 4.14 Surface and cross-sectional SEM micrographs of the ANA membrane on 2.5A ((a1) and (a2)) and 2.5Ca ((b1) and (b2)) for 24 h.

Figure 4.15 illustrates SEM micrographs of ANA crystals covering on 2.5ACa, 5A and 5Ca. ANA crystals completely cover on the surface of 2.5ACa over 5A and 5Ca which are partially covered by ANA crystals, corresponding to the results of XRD (Figure 4.13(c)-(e)). The cross-section of ceramic disc of 5A indicates a horizontal crevice from the top plate about 500 µm but it was not observed in 5Ca and 2.5ACa because of the sample of 5A which has higher porosity (26.3%)

and larger pore size (60-80 μm) compared to the other supports (2.5A, 2.5Ca, 2.5ACa and 5Ca). However, these supports contained ANA layer bound with the ceramic disc. When ANA was synthesized on the support 10A and 10Ca, ANA membrane of 10A was cracked easily while the zeolite membrane of 10Ca showed a rough surface (see in appendices). It can be concluded from all of the results that 2.5ACa is suitable as porous ceramic support for in situ synthesis method with the raw kaolin in order to prepare ANA membrane.

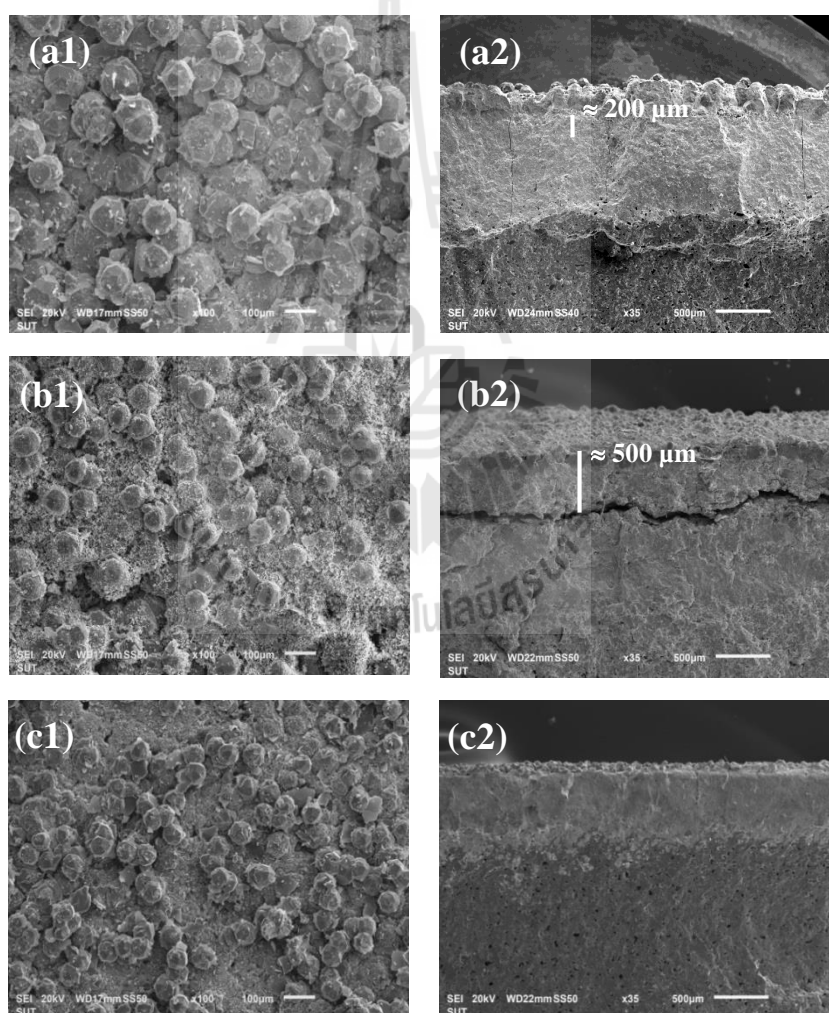


Figure 4.15 Surface and cross-sectional SEM micrographs of the ANA membrane on 2.5ACa ((a1) and (a2)), 5A ((b1) and (b2)) and 5Ca ((c1) and (c2)) for 24 h.

In addition, Figure 4.16 shows element lines of aluminium and silicon in cross section of ANA membrane by SEM analysis. The intensity of those elements was divided into 3 segments. The intensity of aluminium seems to be constant while it is different in silicon. The segment 1 showed a higher intensity of silicon than the segment 3 and 2. It can be described that the silicon of the support in the segment 2 is dissolved by NaOH solution and reacted with RW after that the crystallization of ANA occurred at segment 1. From SEM image as shown in Figure 4.17, the thickness of ceramic support is not changed compared between before and after ANA synthesis. It was found that the porous ceramic support is not erosion but only silicon was dissolved.

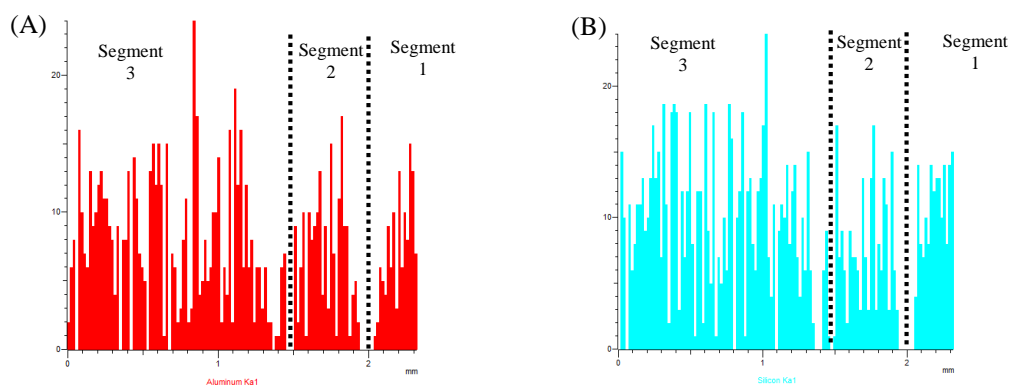
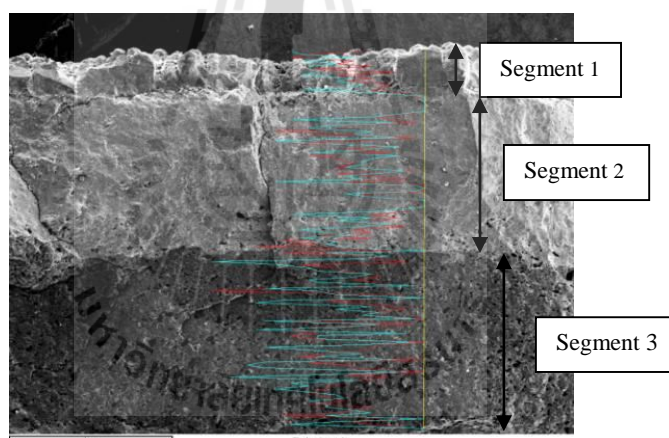


Figure 4.16 Cross-sectional SEM micrograph of the ANA membrane on 2.5AC for 24 h and the results of element line analysis for aluminium (A) and silicon (B).

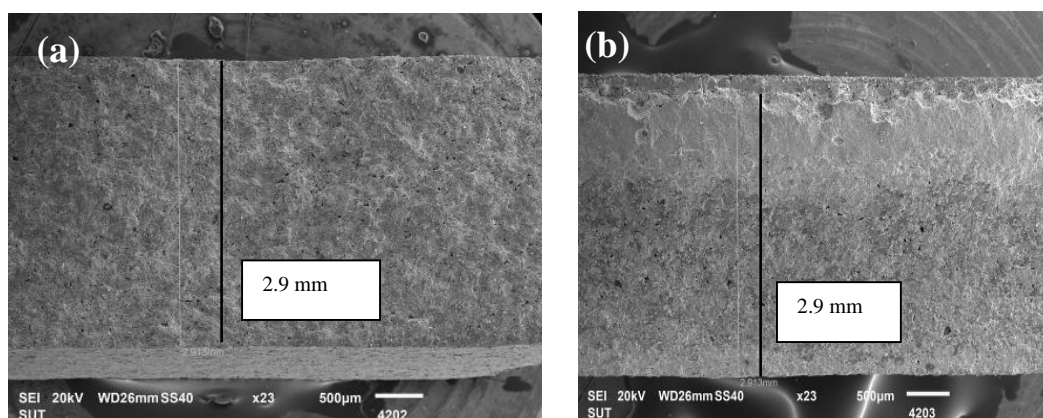


Figure 4.17 Cross-sectional SEM micrographs of 2.5ACa; before (a) and after (b) synthesized ANA membrane.

2) Effect of hydrothermal time

SEM micrographs of the synthesized ANA on 2.5ACa at different hydrothermal times of 18 and 24 h were shown in Figure 4.18. They indicate that the longer hydrothermal time was, the bigger the crystal size became. This was consistent with the elsewhere report (Shan et al., 2011). The sizes of crystals were about 40-84 μm and 112-152 μm for hydrothermal time of 18 and 24 h, respectively. However, ANA membrane could not be synthesized with hydrothermal time of 12 h due to the occurrence of peeling of ANA layer out of the ceramic disc.

Figure 4.18(a2) illustrates SEM micrographs of the cross-sections of ANA membrane with 18 h of hydrothermal time. The thickness of the ANA layer is about 220 μm . This includes a layer between ANA layer and the disc which looks like its seam. If the hydrothermal time is extended to 24 h, the internal growth of crystals was allowed to be sufficiently done. This caused the crystals to bind with the disc resulting in layer thickness about 200 μm (Figure 4.18(b2)). This

might be influenced by the increased amount of the elution of the support to alkaline solution causing the intermediate layer to be packed densely with zeolite and mullite (Kondo and Kita, 2010).

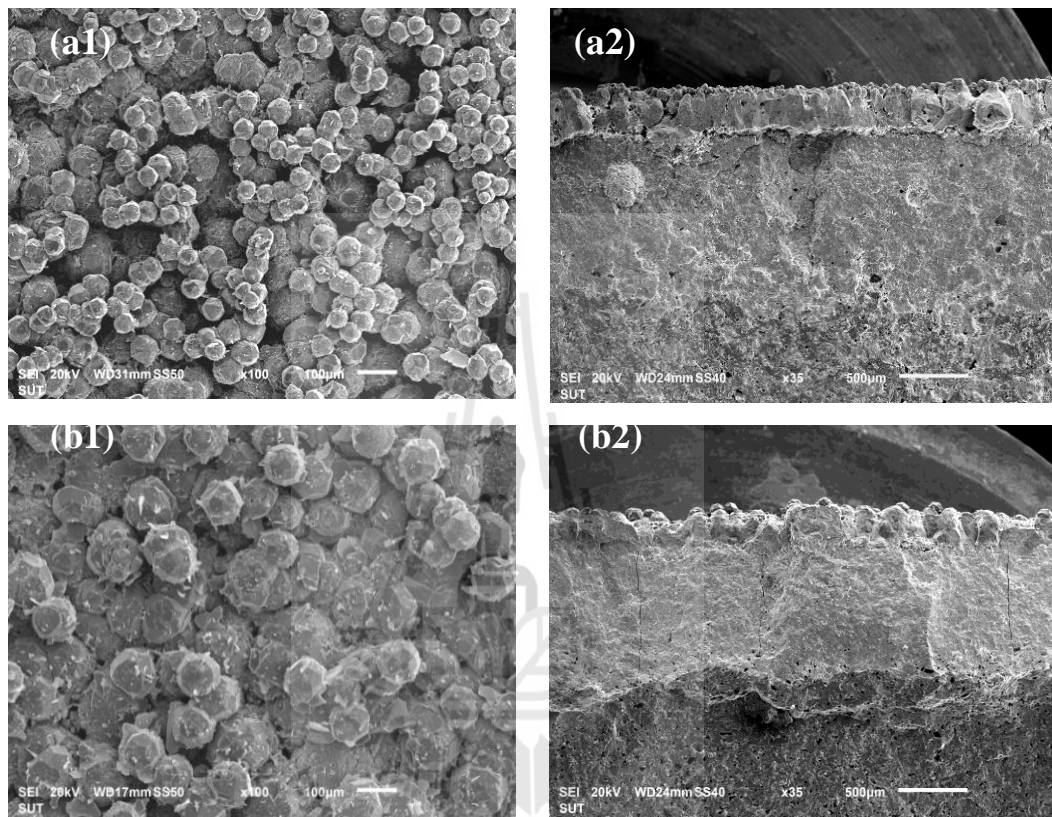


Figure 4.18 Surface and cross-sectional SEM micrographs of the ANA membrane on 2.5ACa at hydrothermal time of 18 h ((a1) and (a2)) and 24 h ((b1) and (b2)).

The chemical composition of JBW used to synthesize ANA membrane was not the same molar composition used to synthesize ANA powder. But it was synthesized with the same molar composition as synthesized JBW powder. This can be explained by the dissolution of silica from the support to lead to the molar composition that can be synthesized ANA layer. The occurrence of crystalline ANA on 2.5ACa from RK was shown in three steps with a diagram in Figure 4.19.

- (1) The dissolution of cristobalite in 2.5ACa by NaOH solution
- (2) The crystallization of ANA crystal from RK reacting with SiO_2
- (3) The intergrowth of ANA layer adhered onto 2.5ACa

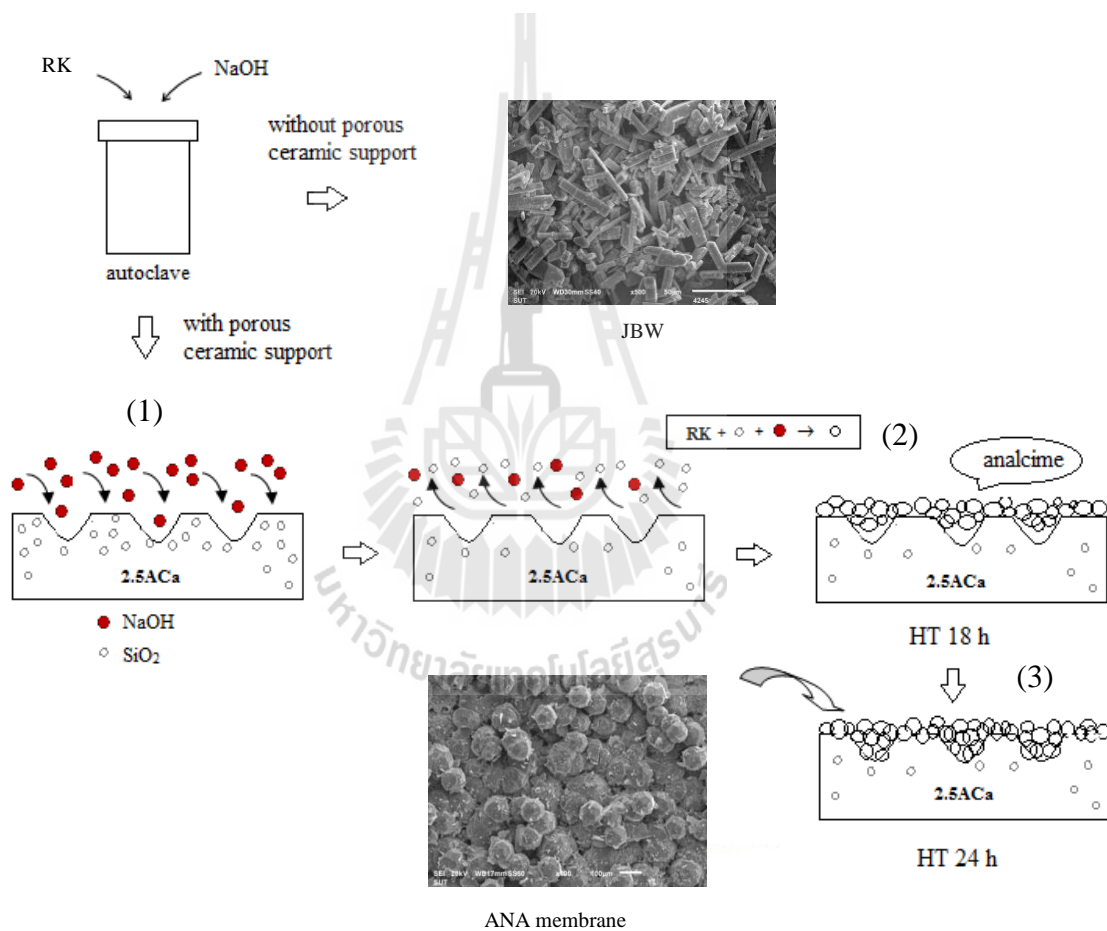


Figure 4.19 The diagram of crystallization of ANA layer on 2.5ACa from RK.

3) Effect of aging time

Figure 4.20 shows that SEM micrographs of ANA membrane with the effect of precursor aging varied from 1 day to 3 days. The average crystal size is about 25-37 μm . It is noticeable that the size of ANA crystals is within the range of pore size of 2.5ACa (20-50 μm). The comparison of the crystal size in the ANA membrane synthesis with and without aging indicates that the smaller size of the crystal was obtained with aging while a larger size occurred without aging (Figure 4.18(a1)).

This may result from increasing number of nuclei or nuclei precursors in the synthesis with aging resulting in the smaller zeolite crystals and an increase in the amount of zeolite (Jülide Koroğlu et al., 2002; Zhang et al., 2002). The small crystal size and a number of zeolite crystals increase instruct the number and the size of the gaps in the membrane reduce. The small crystal zeolite membrane were proposed to form multi-layers compared with large crystal zeolite membrane, the layer of crystal can close gaps and cracks of the preceding layer (Zhang et al., 2002). Possibility, the diffusion of polar group as water molecules enhance with smaller crystal size and number of crystals. The very thin cross-section of ANA layer (Figure 4.20(a2)) is about 50 μm compared to that about 220 μm without aging. The decreasing of zeolite thickness affect to the increasing of water flux of the pervaporation system due to rapid diffusion of water molecules from the retentate side to the permeate side (Kalyani et al., 2008; Malepour et al., 2008; Kunnakorn et al., 2011).

The XRD patterns of 1 day and 2 days of aging (Figure 4.21 (a)-(b)) exhibit both the sharp peaks of ANA phase and the small broad peak of

mullite at 23.7° . Nevertheless, the broad peak disappeared with 3 days aging (Figure 4.21(c)) indicating that the occurring crystals overspread completely on the surface of the support. The coverage of ANA crystals through the disc presented quality in terms of maximum surface coverage, interlocked crystal arrangement and rendering better separation factor for water/ethanol mixture (Basak et al., 2014). Therefore, ANA membranes prepared with aging is effective increasingly for separation of water from ethanol.

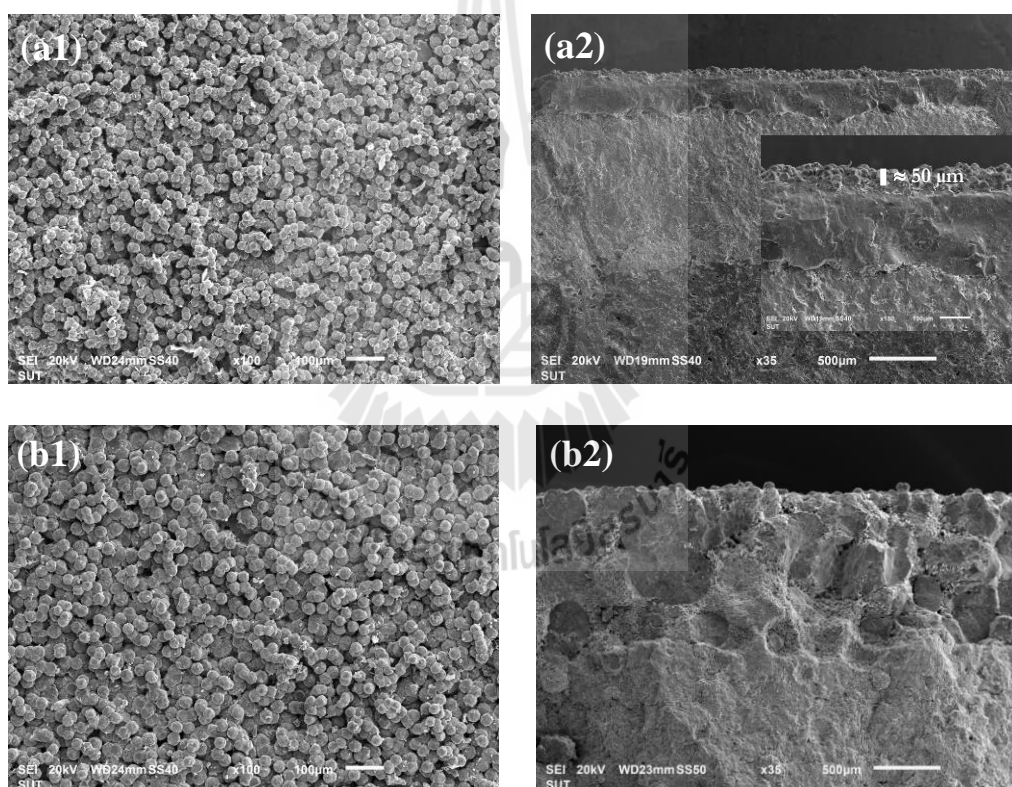


Figure 4.20 Surface and cross-sectional SEM micrographs of the ANA membrane on 2.5ACa with reaction time of 18 h using precursor aged 1 day ((a1) and (a2)), 2 days ((b1) and (b2)) and 3 days ((c1) and (c2)).

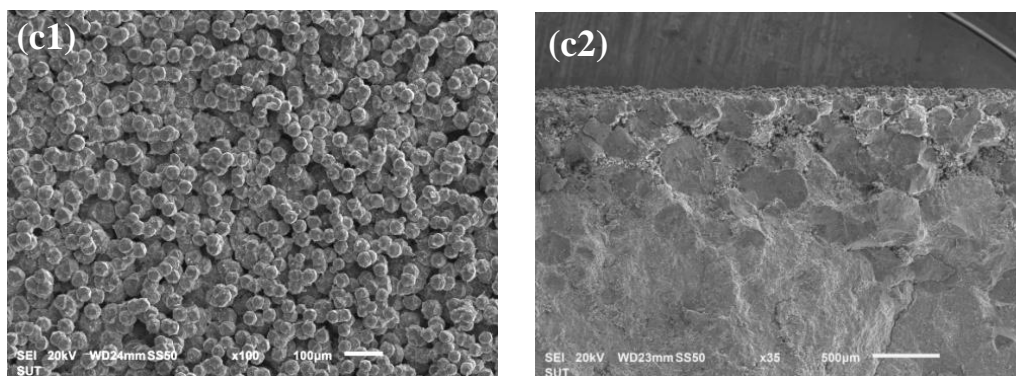


Figure 4.20 Surface and cross-sectional SEM micrographs of the ANA membrane on 2.5ACa with reaction time of 18 h using precursor aged 1 day ((a1) and (a2)), 2 days ((b1) and (b2)) and 3 days ((c1) and (c2)) (Continued).

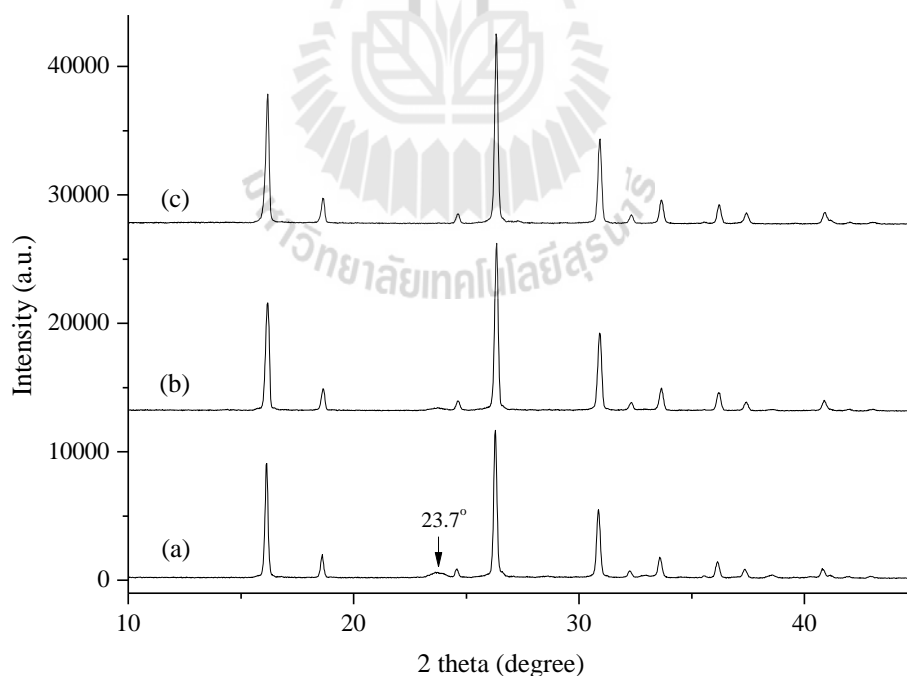


Figure 4.21 XRD patterns of the ANA membrane on 2.5ACa with reaction time of 18 h using precursor aged (a) 1 day, (b) 2 days and (c) 3 days.

4.4.2.2 ANA membrane from DK24 source

1) Effect of hydrothermal time

Figure 4.22 shows the surface SEM micrograph of ANA membrane on 2.5ACa with various hydrothermal times such as 12, 18 and 24 h. It was found that the crystal size of ANA was increased with an increase in hydrothermal time (Shan et al., 2011). The crystal sizes were about 11 μm , 19 μm and 32 μm at hydrothermal time of 12, 18 and 24 h, respectively. Figure 4.23 shows the SEM micrograph of ANA membrane cross-sections. The hydrothermal time of 18 h, the thickness of ANA layer was about 77.6-168.0 μm and it clearly observed that the small crystals of ANA were agglomerated and appeared a space between crystals. With longer hydrothermal time to 24 h, a dense inter-grown zeolite crystal layer was formed onto 2.5ACa with about 54 μm in thickness. It indicated that the longer the hydrothermal time is the shorter the thickness of the ANA layer appears. The XRD patterns show only a single phase of ANA crystals within the considered reaction times of 12-24 h (see in Figure 4.24). The ANA layer was completely covered on 2.5ACa with hydrothermal time only 12 h and a smaller crystal size of ANA was observed when compared with using RW as starting material (Figure 4.15(a)). The crystallization of ANA from DK24 with and without the support of 2.5ACa was shown in a diagram of Figure 4.25.

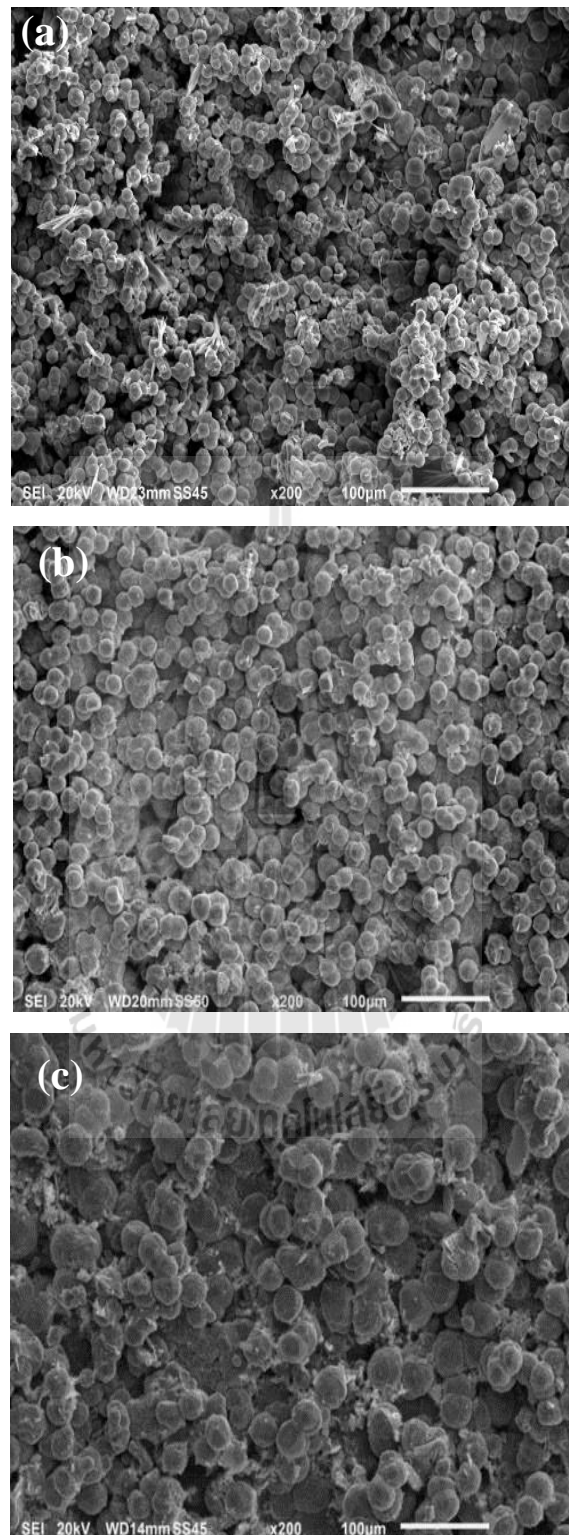


Figure 4.22 Surface SEM micrograph of the ANA membrane on 2.5ACa for (a) 12, (b) 18 and (c) 24 h.

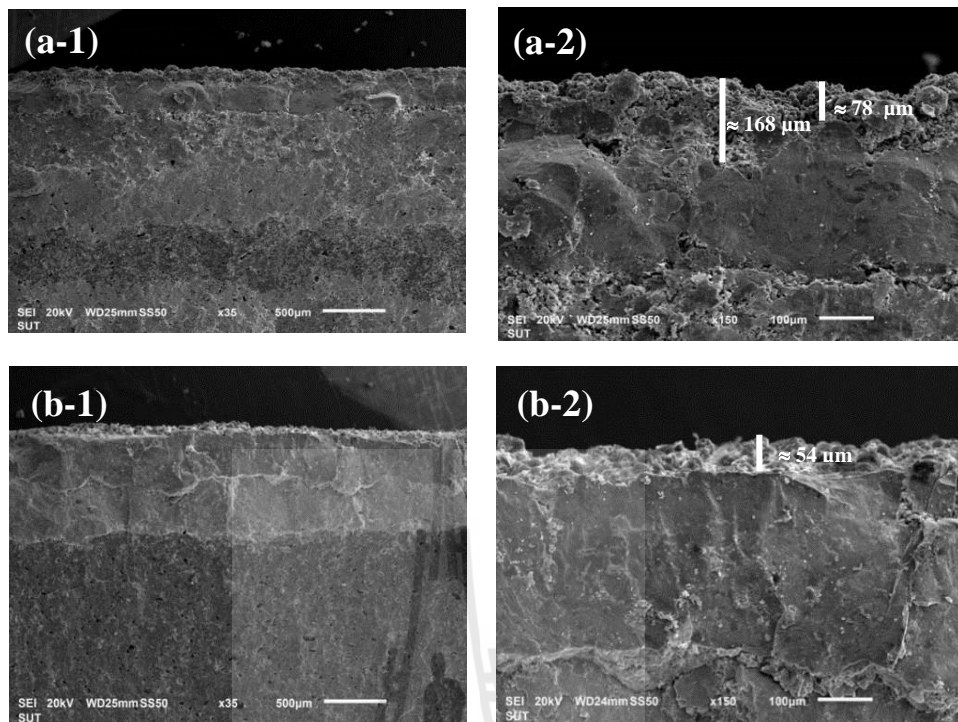


Figure 4.23 Cross-sectional SEM micrograph of the ANA membrane on (a-1, a-2) 2.5ACa for 18 h and (b-1, b-2) 24 h.

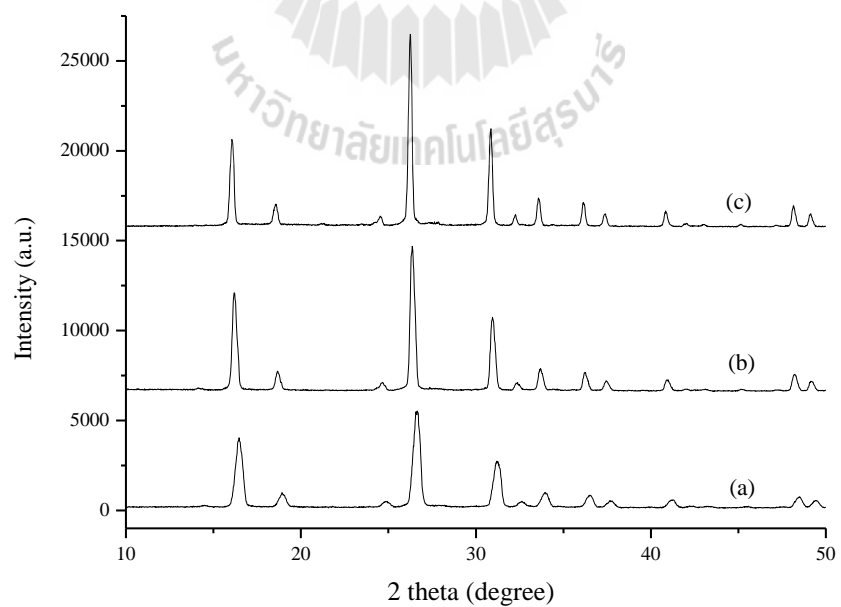


Figure 4.24 XRD patterns of ANA membrane on 2.5ACa for (a) 12, (b) 18 and (c) 24 h.

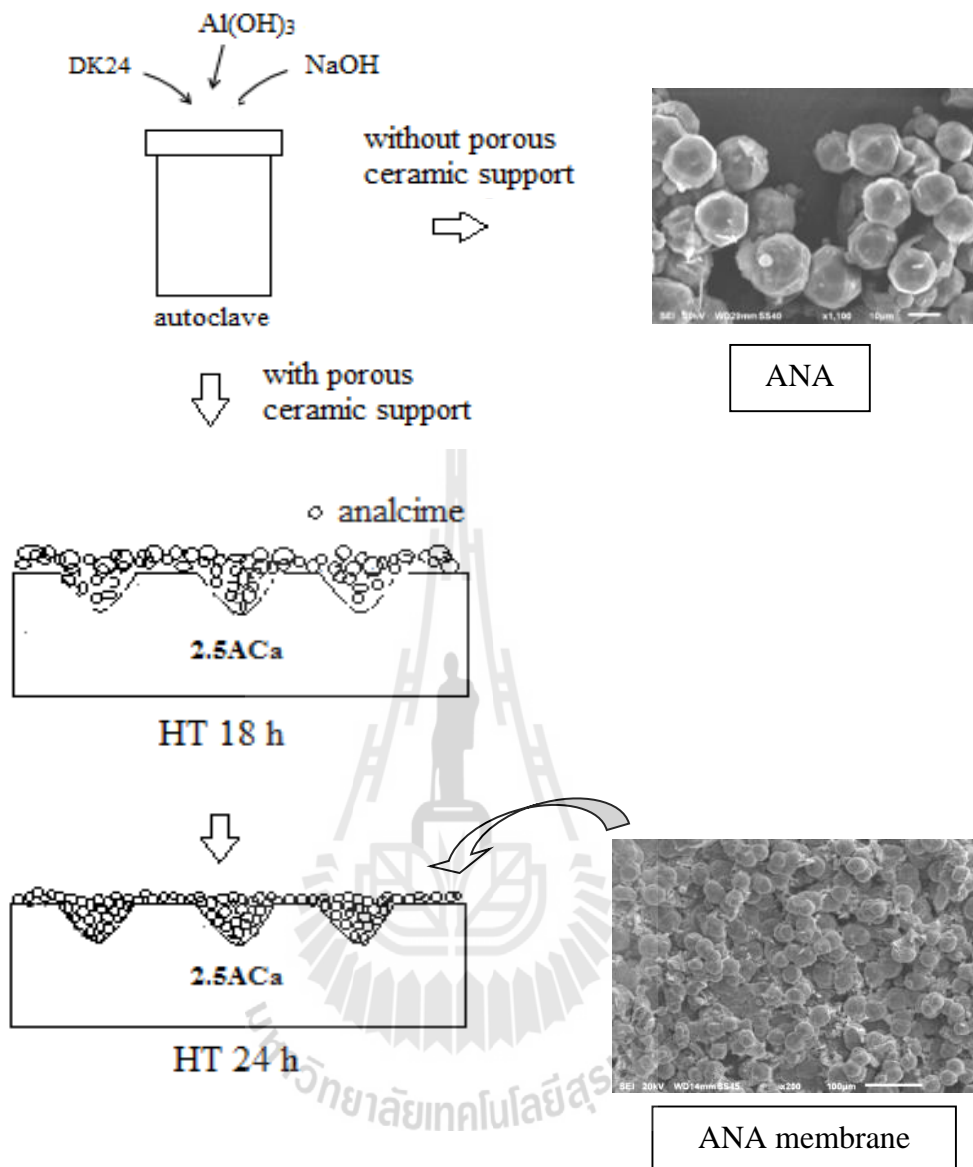


Figure 4.25 The diagram of crystallization of zeolites from DK24 with and without the support of 2.5ACa.

2) Effect of aging time

Figure 4.26 shows SEM micrographs of ANA membrane with aging 1 day and 2 days. The crystal sizes were increased with an increase in aging time. The average crystal size about $17 \mu\text{m}$ was obtained with aging for 1 day. With a

longer aging time to 2 days, the bigger crystals with an average crystal size about 76 μm was observed. The gaps between crystals of ANA membrane were present with both conditions and it is clearly observed from aging 2 days. In the membrane cross-section, the big crystals were interspersed inside the support with 2 days aging. The XRD pattern in Figure 4.27 showed both of analcime phase and cristobalite phase. It was found that the synthesis of ANA by using DK24 with aging is not suitable for preparing ANA membrane maybe an excess dissolution of cristobalite in support.

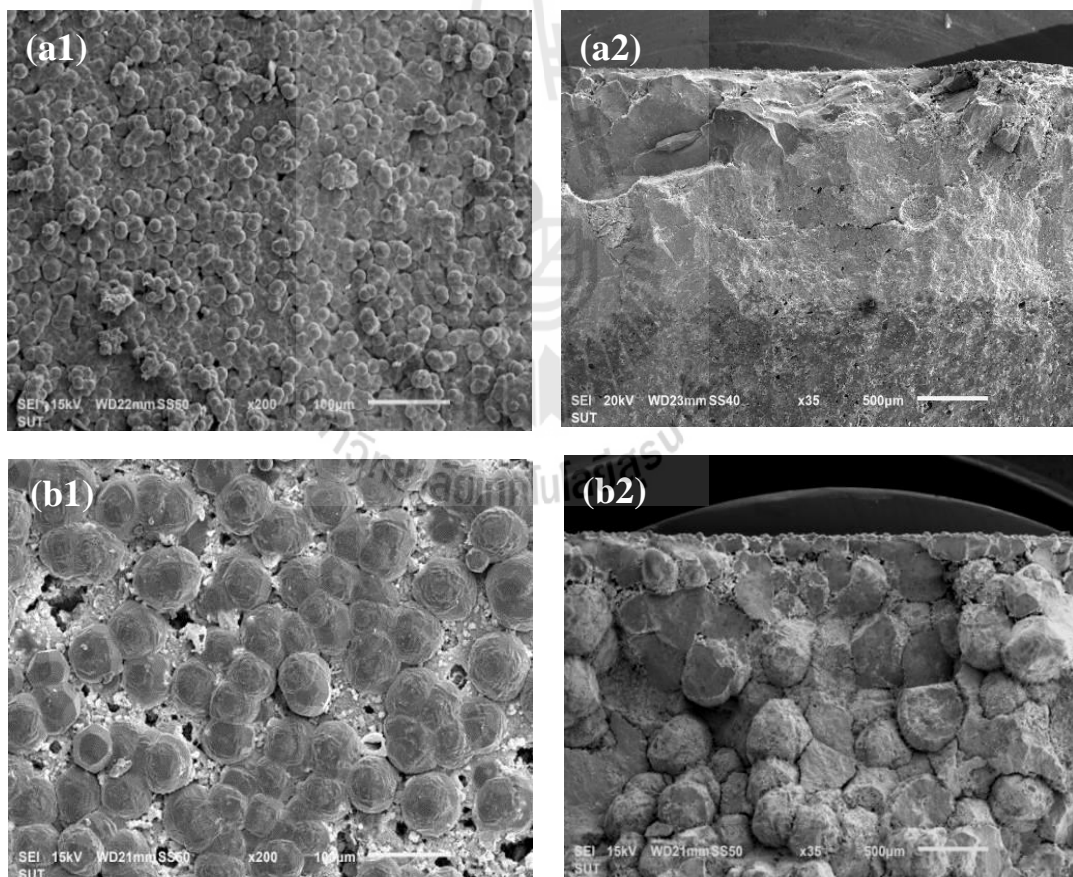


Figure 4.26 Surface and cross-sectional SEM micrograph of the ANA membrane on 2.5ACa for aging 1 day ((a1) and (a2)) and aging 2 days ((b1) and (b2)).

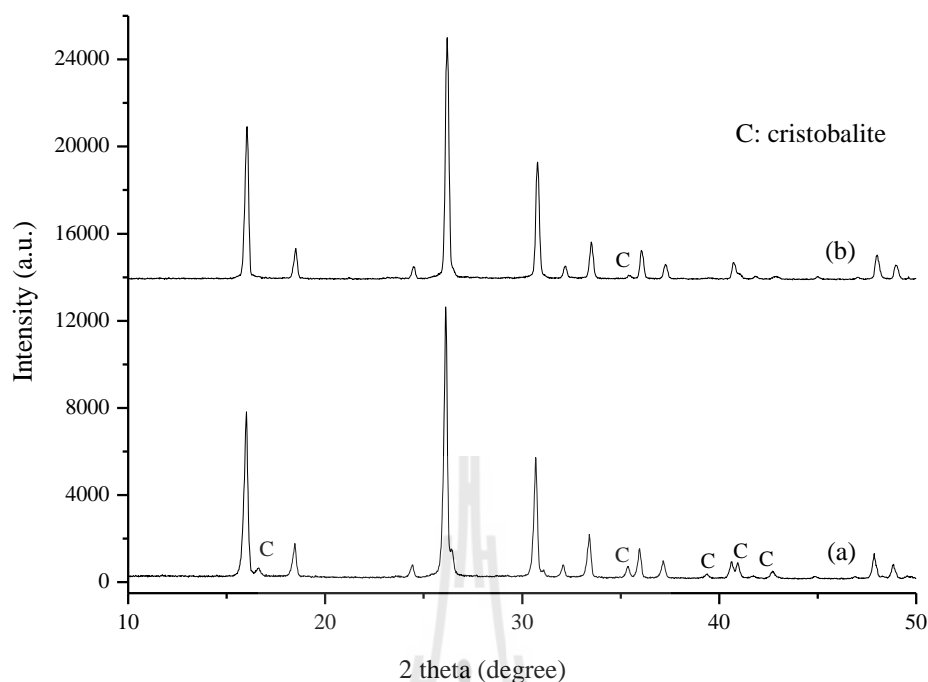


Figure 4.27 XRD patterns of ANA membrane on 2.5ACa prepared by aging (a) 1 day and (b) 2 days.

4.4.2.3 ANA membrane from chemical source

1) Effect of hydrothermal time

SEM micrographs of the synthesized ANA on 2.5ACa at different hydrothermal times of 18 h and 24 h were shown in Figure 4.28. The hydrothermal time of 18 hours showed big crystal and gaps between crystals while 24 hours showed crystalline ANA with small crystals and the thickness of the ANA layer is about 60 μm . The XRD pattern showed a mixed phase of ANA and mullite (35.7° , 41.2° and 43.0°) at 18 h of reaction time and single phase of ANA at 24 h (see in Figure 4.29). It indicates that with hydrothermal time of 24 h the ANA crystals overspread completely on the support.

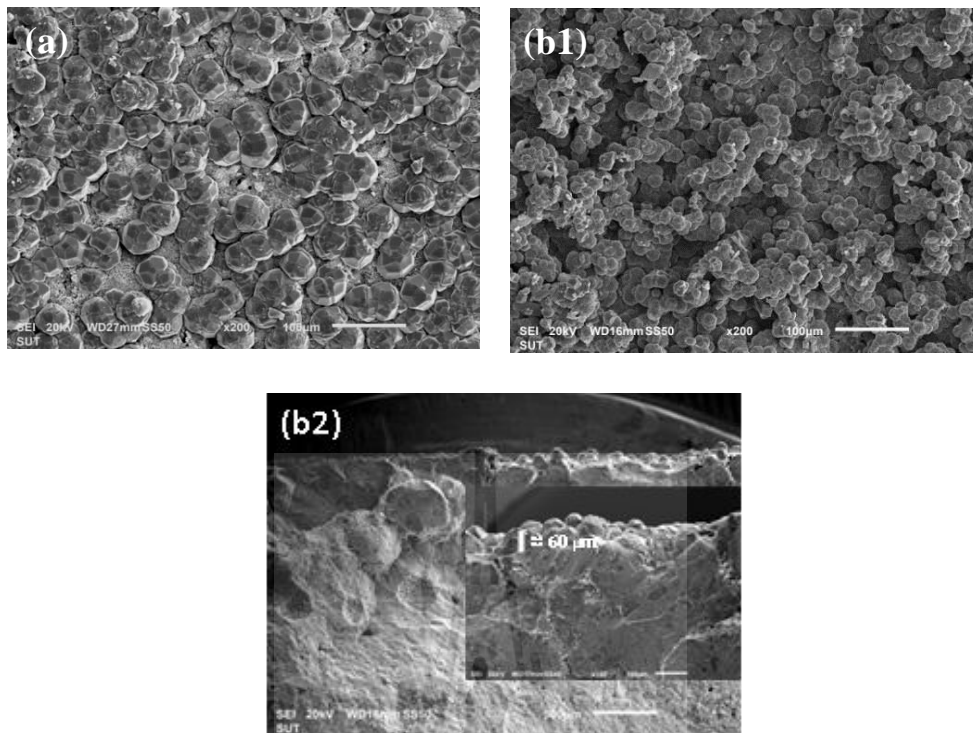


Figure 4.28 Surface and cross-sectional SEM micrograph of the ANA membrane on 2.5ACa for (a) 18 h and (b1) and (b2) 24 h.

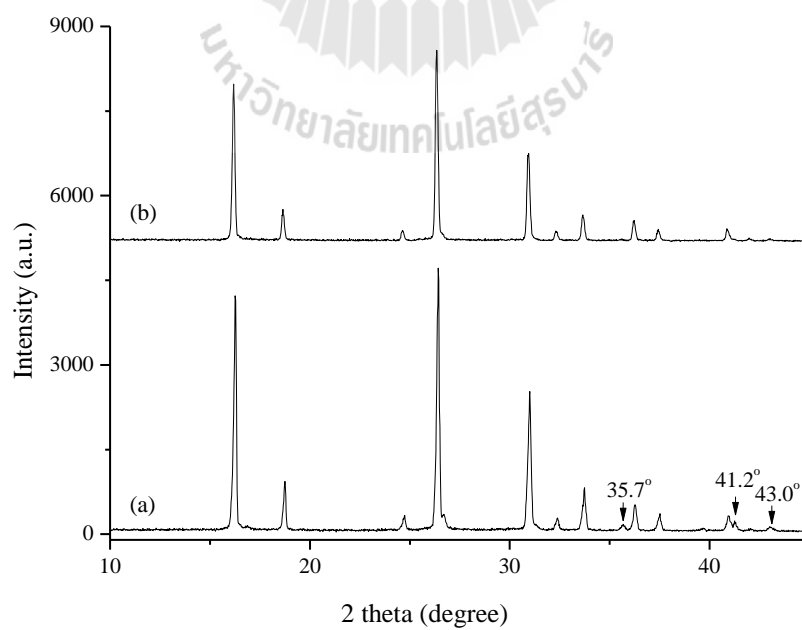


Figure 4.29 XRD patterns of the ANA membrane on 2.5ACa for (a) 18 h and (b) 24 h.

4.5 Conclusions

Zeolite membranes are usually synthesized from aqueous aluminosilicate gel of pure solutions of sodium silicate and sodium aluminates under hydrothermal system. We have demonstrated that ANA membrane was successfully produced from raw kaolin or dealuminated kaolin as starting material. In the preparation of ceramic support, the type and the amount of pore former (activated carbon and calcite) affect the average pore size, percent porosity and phase of the support. Moreover, they play a significant role on the dissolution of cristobalite from the support. The suitable ceramic support found in this work was prepared from the ingredient of 10.0 wt% cristobalite, 2.5 wt% activated carbon and 2.5 wt% calcite and 85.0 wt% raw kaolin.

In the synthesis of ANA membrane, the small crystal size (about 25-37 μm) and thin layer of ANA (about 45-50 μm) were obtained from raw kaolin with aging as well as using dealuminated kaolin without aging showed the small crystal size (about 11-32 μm) and thin layer (about 54 μm). In the case of using chemical as starting material showed smaller crystal size about 20 μm and 60 μm in thickness. This results indicate that the synthesis of ANA membrane from raw kaolin or dealuminated kaolin produce crystals size and layer thickness not much different from chemical. Therefore, using raw kaolin as starting material is a good alternative for reducing cost in synthesizing ANA membrane.

4.6 References

- Abbasi, M., Mirfendereski, M., Nikbakht, M., Golshenas, M. and Mohammadi, T. (2010). Performance study of mullite and mullite–alumina ceramic MF membranes for oily wastewaters treatment. **Desalination**. 259: 169-178.

- Asghari, M., Mohammadi, T., Aziznia, A., Danayi, M. R., Moosavi, S. H., Alamdari, R. F. and Agand, F. (2008). Preparation and characterization of a thin continuous faujasite membrane on tubular porous mullite support. **Desalination**. 220: 65-71.
- Atta, A. Y., Jibril, B. Y., Aderemi, B. O. and Adefila, S. S. (2012). Preparation of analcime from local kaolin and rice husk ash. **Applied Clay Science**. 61: 8-13.
- Bai, J. (2010). Fabrication and properties of porous mullite ceramics from calcined carbonaceous kaolin and α -Al₂O₃. **Ceramics International**. 36: 673-678.
- Baimpos, T., Gora, L., Nikolakis, V. and Kouzoudis, D. (2012). Selective detection of hazardous VOCs using zeolite/Metglas composite sensors. **Sensors and Actuators A**. 186: 21-31.
- Basak, S., Kundu, D. and Naskar, M. K. (2014). Low temperature synthesis of NaA zeolite membranes: The effect of primary and secondary crystallizations. **Ceramics International**. 40: 12923-12930.
- Chaisena, A. and Rangsrivatananon, K. (2005). Synthesis of sodium zeolites from natural and modified diatomite. **Materials Letters**. 59: 1474-1479.
- Chen, Y. F., Wang, M. C. and Hon, M. H. (2004). Phase transformation and growth of mullite in kaolin ceramics. **Journal of the European Ceramic Society**. 24: 2389-2397.
- Cho, C. H., Oh, K. Y., Yeo, J. G., Kim, S. K. and Lee, Y. M. (2010). Synthesis, ethanol dehydration and thermal stability of NaA zeolite/alumina composite membranes with narrow non-zeolitic pores and thin intermediate layer. **Journal of Membrane Science**. 364: 138-148.

- Dong, Y., Hampshire, S., Zhou, J. -e., Ji, Z., Wang, J. and Meng, G. (2011). Sintering and characterization of flyash-based mullite with MgO addition. **Journal of the European Ceramic Society**. 31: 687-695.
- Dyer, A., Tangkawanit, S. and Rangriwatananon, K. (2004). Exchange diffusion of Cu^{2+} , Ni^{2+} , Pb^{2+} and Zn^{2+} into analcime synthesized from perlite. **Microporous and Mesoporous Materials**. 75: 273-279.
- Esharghawi, A., Penot, C. and Nardou, F. (2009). Contribution to porous mullite synthesis from clays by adding Al and Mg powders. **Journal of the European Ceramic Society**. 29: 31-38.
- Geus, E. R., Den Exter, M. J. and van Bekkum, H. (1992). Synthesis and characterization of zeolite (MFI) membranes on porous ceramic supports. **Journal of the Chemical Society, Faraday Transactions**. 88: 3101-3109.
- Harabi, A., Zenikheri, F., Boudaira, B., Bouzerara, F., Guechi, A. and Foughali, L. (2014). A new and economic approach to fabricate resistant porous membrane supports using kaolin and CaCO_3 . **Journal of the European Ceramic Society**. 34: 1329-1340.
- Hegazy, E. Z., El Maksod, I. H. A. and El Enin, R. M. M. A. (2010). Preparation and characterization of Ti and V modified analcime from local kaolin. **Applied Clay Science**. 49: 149-155.
- Jülide Köroğlu, H., Sarioğlu, A., Tatlıer, M., Erdem-Şenatalar, A. and Tunç Savaşçı, Ö. (2002). Effects of low-temperature gel aging on the synthesis of zeolite Y at different alkalinities. **Journal of Crystal Growth**. 241: 481-488.
- Kalyani, S., Smitha, B., Sridhar, S. and Krishnaiah, A. (2008). Pervaporation separation of ethanol–water mixtures through sodium alginate membranes. **Desalination**. 229: 68-81.

- Kazemimoghadam, M. and Mohammadi, T. (2011). Preparation of nano pore hydroxysodalite zeolite membranes using of kaolin clay and chemical sources. **Desalination**. 278: 438-442.
- Kita, H., Fuchida, K., Horita, T., Asamura, H. and Okamoto, K. (2001). Preparation of Faujasite membranes and their permeation properties. **Separation and Purification Technology**. 25: 261-268.
- Kongkachuichay, P. and Lohsoontorn, P. (2006). Phase diagram of zeolite synthesized from perlite and rice husk ash. **ScienceAsia**. 32: 13-16.
- Kondo, M. and Kita, H. (2010). Permeation mechanism through zeolite NaA and T-type membranes for practical dehydration of organic solvents. **Journal of Membrane Science**. 361: 223-231.
- Kunnakorn, D., Rirksomboon, T., Aungkavattana, P., Kuanchertchoo, N., Atong, D., Hemra, K., Kulprathipanja, S. and Wongkasemjit, S. (2011). Optimization of synthesis time for high performance of NaA zeolite membranes synthesized via autoclave for water-ethanol separation. **Desalination**. 280: 259-265.
- Li, Y. and Yang, W. (2008). Microwave synthesis of zeolite membranes: A review. **Journal of Membrane Science**. 316: 3-17.
- Liu, Y., Yang, Z., Yu, C., Gu, X. and Xu, N. (2011). Effect of seeding methods on growth of NaA zeolite membranes. **Microporous and Mesoporous Materials**. 143: 348-356.
- Maghsoudi, H. and Soltanieh, M. (2014). Simultaneous separation of H₂S and CO₂ from CH₄ by a high silica CHA-type zeolite membrane. **Journal of Membrane Science**. 470: 159-165.

- Malekpour, A., Millani, M. R. and Kheirkhah, M. (2008). Synthesis and characterization of a NaA zeolite membrane and its applications for desalination of radioactive solutions. **Desalination**. 225: 199-208.
- Mohammadi, T. and Pak, A. (2003). Effect of calcination temperature of kaolin as a support for zeolite membranes. **Separation and Purification Technology**. 30: 241-249.
- Nandi, B. K., Uppaluri, R. and Purkait, M. K. (2008). Preparation and characterization of low cost ceramic membranes for micro-filtration applications. **Applied Clay Science**. 42: 102-110.
- Navajas, A., Mallada, R., Téllez, C., Coronas, J., Menéndez, M. and Santamaría, J. (2002). Preparation of mordenite membranes for pervaporation of water-ethanol mixtures. **Desalination**. 148: 25-29.
- Pina, M. P., Mallada, R., Arruebo, M., Urbiztondo, M., Navascués, N., de la Iglesia, O. and Santamaria, J. (2011). Zeolite films and membranes. Emerging applications. **Microporous and Mesoporous Material**. 144: 19-27.
- Shan, L., Shao, J., Wang, Z. and Yan, Y. (2011). Preparation of zeolite MFI membranes on alumina hollow fibers with high flux for pervaporation. **Journal of Membrane Science**. 378: 319-329.
- Shao, J., Zhan, Z., Li, J., Wang, Z., Li, K. and Yan, Y. (2014). Zeolite NaA membranes supported on alumina hollow fibers: Effect of support resistances on pervaporation performance. **Journal of Membrane Science**. 451: 10-17.
- Souza, A. E., Teixeira, S. R., Santos, G. T. A., Costa, F. B. and Longo, E. (2011). Reuse of sugarcane bagasse ash (SCBA) to produce ceramic materials. **Journal of Environmental Management**. 92: 2774-2780.

- Tavolaro, A. and Tavolaro, P. (2007). LTA zeolite composite membrane preparation, characterization and application in a zeolitic membrane reactor. **Catalysis Communications**. 8: 789-794.
- Vida-Simiti, I., Jumate, N., Moldovan, V., Thalmaier, G. and Sechel, N. (2012). Characterization of gradual porous ceramic structures obtained by powder sedimentation. **Journal of Materials Science and Technology**. 28: 362-366.
- Vilaseca, M., Coronas, J., Cirera, A., Cornet, A., Morante, J. R. and Santamaria, J. (2007). Gas detection with SnO₂ sensors modified by zeolite films. **Sensors and Actuators, B**. 124: 99-110.
- Wahl, F., Grim, R. and Graf, R. (1961). Phase transformations in silica as examined by continuous X-ray diffraction. **American Mineralogist**. 46: 196-208.
- Yan, W., Li, N. and Han, B. -q. (2011). Preparation and characterization of porous ceramics prepared by kaolinite gangue and Al(OH)₃ with double addition of MgCO₃ and CaCO₃. **International Journal of Minerals, Metallurgy, and Materials**. 18: 450-454.
- Zhang, J. and Liu, W. (2011). Thin porous metal sheet-supported NaA zeolite membrane for water/ethanol separation. **Journal of Membrane Science**. 371: 197-210.
- Zhang, Y., Xu, Z. and Chen, Q. (2002). Synthesis of small crystal polycrystalline mordenite membrane. **Journal of Membrane Science**. 210: 361-368.
- Zhou, H. M., Qiao, X. C. and Yu, J. G. (2013). Influences of quartz and muscovite on the formation of mullite from kaolinite. **Applied Clay Science**. 80-81: 176-181.

CHAPTER V

THE PERVAPORATION FOR SEPARATION

WATER/ETHANOL MIXTURE THROUGH ZEOLITIC

ANA MEMBRANES

5.1 Abstract

Zeolitic ANA membranes were obtained from using raw kaolin and dealuminated kaolin as silica and alumina source under synthesis with in situ synthesis method. These ANA membranes were used for separation of water from ethanol solution. The performances of zeolitic ANA membrane were investigated with various temperatures at 55 °C, 65 °C and 75 °C and ethanol concentrations at 90.0 wt% and 95.0 wt%. It was found that the performance of ANA membrane showed a high selectivity of water with the separation factor was high as >10,000 for ethanol feed concentration of 90.0 wt% and 95.0 wt%. Consequently, the concentration of ethanol solution was close to >99.8 wt%. The total water flux decreases with a decrease in a temperature and an increase in thickness of ANA membrane including an increase in concentration of ethanol mixture in feed. The best ANA membrane was prepared with raw kaolin under aging 3 days. It showed the highest total water flux of 0.27 kg/m²h compared to ANA membrane from raw kaolin with aging 1 day, dealuminated kaolin and chemical source whose total water flux was 0.25 kg/m²h, 0.22 kg/m²h and 0.19 kg/m²h, respectively. ANA membrane

obtained from raw kaolin is a good alternative adsorbent for separation of water/ethanol mixture due to its simple synthesis and its low cost-effective.

5.2 Introduction

The various technologies have been used for produced anhydrous ethanol such as azeotrope distillation, pressure swing adsorption of water on molecular sieves and pervaporation or vapor permeation of water through hydrophilic membranes. Pervaporation is used to solve this problem because it consumes less energy and environmental friendly. The separation of water from ethanol with pervaporation depends on the diffusion coefficient and correlation of each component in the membrane. Moreover, the zeolite membrane has high mechanical strength, thermal and chemical stability compared to organic membranes.

Especially, in the separation area, many types of zeolite were studied to break the azeotrope of ethanol and water mixture by pervaporation such as zeolite X, Y, T, mordenite and hydroxysodalite. Zeolite A membrane is the suitable in those applications. In previous work (chapter III), analcime (ANA) is a better adsorbent for dehydration of ethanol more than zeolite NaA and also sodalite because it has stronger Lewis acid sites, so its interaction with water is stronger than that of the others. Moreover, ANA has a small pore size of 8-ring pore opening aperture 1.6×4.2 Å, so it makes the separation of small molecules by difference in size possible. Small water molecule about 2.6 Å is expected to be separated from bigger molecule of ethanol as 4.4 Å.

Therefore, the performances of the zeolitic ANA membranes in the separation of the water/ethanol mixtures by pervaporation was focused in this chapter. The

synthesized ANA membranes as mentioned in the chapter IV were utilized in the pervaporation process.

5.3 Experiment

5.3.1 Materials

ANA membranes obtained from different starting materials source and porous ceramic supports as mentioned in the chapter IV were used for separation of water/ethanol mixture by pervaporation.

5.3.2 Pervaporation tests

Pervaporation tests were carried out using a laboratory-made set-up. A schematic layout of the experimental set-up used in this study is described in Figure 5.1.

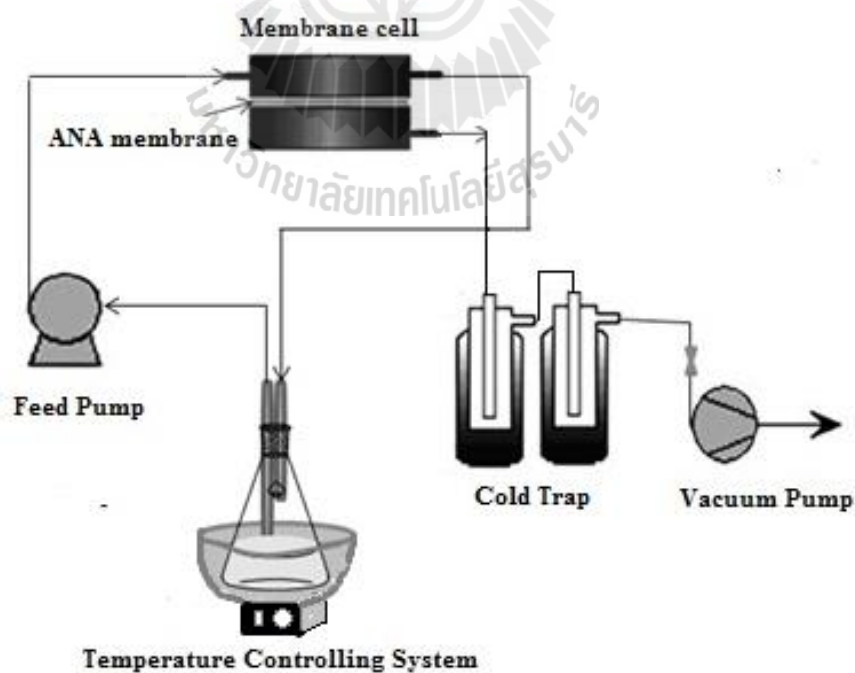


Figure 5.1 Scheme of a laboratory-made set-up for the pervaporation experiment.

The feed mixture of 90 %wt water/ethanol was used in this work with a total amount of throughput of 140 mL. The experiments were carried out at temperature of 75 °C and pressure of 7 mbar at the permeate side and a period of 30 min. The feed is continuously circulated from feed tank to the upstream side of the membrane by peristaltic pump with adjustable function of flow rate for 46 mL/min. Vapor of permeate is condensed and collected in a cold trap immersed in liquid nitrogen via a hose to condense permeate. The effective membrane area was 38.0 cm². The effect of operating temperature on pervaporation performance is carried out at a series of constant temperature, regulated by thermostatic bath. Feed and permeate concentration have been determined by gas chromatography (GC) using Hewlett Packard model HP-6890. A capillary column of HP-INNOWax Polyethylene Glycol (30 m × 0.32 mm) and FID detector were used. The membrane performance was evaluated by a separation factor (α) and total water flux (J in kg/(m²h)). It can be calculated from the following equation.

The total water flux (J) was calculated from the following equation (5.1):

$$J = \frac{G}{S\Delta t} \quad (5.1)$$

Where, G is the weight of water

S is the effective membrane area (m²)

Δt is the measuring time

The separation factor ($\alpha_{\text{H}_2\text{O}/\text{EtOH}}$) was calculated by equation (5.2):

$$\alpha_{\text{H}_2\text{O}/\text{EtOH}} = \frac{Y_{\text{EtOH}}/Y_{\text{H}_2\text{O}}}{X_{\text{EtOH}}/X_{\text{H}_2\text{O}}} \quad (5.2)$$

Where, X is the weight fractions of the permeate

Y is the weight fractions of the feed

5.4 Results and discussion

ANA membrane made by porous ceramic supports, raw kaolin with aging and without aging, dealuminated kaolin without aging and chemical were used for separation water from ethanol solution. The pervaporation performances of these ANA membrane were summarized in Table 5.1. ANA membrane obtained from porous ceramic supports and raw kaolin without aging could not dehydrate ethanol solution. The result showed a high concentration of ethanol in permeates and also ethanol concentration in feed was not change. This is a result of the surface of those ANA membranes existing apparent gaps between crystals, hence both water and ethanol molecules pass easily thorough non-zeolitic pore of ANA membrane (see in Figure 5.2) giving a rapid flux of ethanol solution.

Table 5.1 Pervaporation performance of ANA membranes.

No.	Porous ceramic supports	Starting material source	Separation factor	Flux (kg/m ² h)
1	2.5A	-	-	-
2	2.5Ca	-	-	-
3	2.5ACa	-	-	-
4	2.5A	Raw kaolin	-	-
5	2.5Ca	Raw kaolin	-	-
6	5A	Raw kaolin	-	-
7	5Ca	Raw kaolin	-	-
8	2.5ACa	Raw kaolin	-	-
9	2.5A	Raw kaolin (aging 1 day)*	-	-
10	2.5Ca	Raw kaolin (aging 1 day)*	-	-
11	5A	Raw kaolin (aging 1 day)**	-	-
12	2.5ACa	Raw kaolin (aging 1 day)	>10,000	0.25
13	2.5ACa	Raw kaolin (aging 3 days)	>10,000	0.27
14	2.5ACa	Dealuminated kaolin	>10,000	0.22
15	2.5ACa	Chemical	>10,000	0.19

* Peeling of ANA layer out of the ceramic disc.

** ANA membrane was cracked.

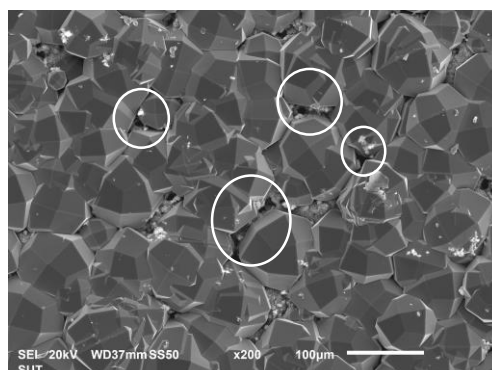


Figure 5.2 Surface SEM micrograph of ANA membrane from 2.5ACa with 10% NaOH.

ANA membranes were prepared by raw kaolin with aging, dealuminated kaolin without aging and chemical showed a very high selectivity to water (Table 5.1). It produced a concentration of ethanol >99.8 wt% from 90.0 wt% with high level of separation factor as >10,000. Possibly, in the preparation of ANA membrane with those conditions giving small crystals of ANA (20-37 μm) which can produce a multi-layer ANA, as a result a non-zeolitic pore disappeared indicating that small crystal sizes in this range (20-37 μm) supplement the separation factor of ANA membrane.

ANA membrane obtained from raw kaolin with aging 1 day, raw kaolin with aging 3 day, dealuminated kaolin without aging and chemical exhibited a layer thickness about 50 μm , 45 μm , 58 μm and 60 μm with total water flux as 0.25 $\text{kg}/(\text{m}^2\text{h})$, 0.27 $\text{kg}/(\text{m}^2\text{h})$, 0.20 $\text{kg}/(\text{m}^2\text{h})$ and 0.19 $\text{kg}/(\text{m}^2\text{h})$, respectively. The ANA membrane obtained from raw kaolin with aging 3 days showed the highest total water flux. It seems that a total water flux decreases with an increase in zeolite thickness. The thickness of zeolite layer increased means that the distance between permeate side and the retentate side increased likewise. Consequently, the diffusion of water molecules from retentate side to permeate side is low. This result agrees with elsewhere report such as Kalyani et al. (2008) reporting that the zeolite thickness was increased from 20 μm to 120 μm with a decrease in water flux from 0.1 $\text{kg}/(\text{m}^2\text{h})$ to 0.016 $\text{kg}/(\text{m}^2\text{h})$. Malekpour et al., 2008 and Kunnakorn et al., 2011 found that the total water flux for water/ethanol mixture was decreased with an increase in membrane thickness.

From the results of this study recommend that ANA membranes can be used for separation of water from ethanol solution by pervaporation. The ANA membrane synthesized from raw kaolin with aging or dealuminated kaolin or chemical showed

its good performance for water/ethanol separation. For reducing the cost, a raw kaolin or dealuminated kaolin is a good choice as a cheap source of silica and alumina in synthesizing ANA membrane. Although ANA membrane obtained from raw kaolin with aging 3 days showed a total water flux higher than raw kaolin with aging 1 day and dealuminated kaolin without aging, ANA membrane prepared with aging 1 day should be preferably used because of its shorter period of nucleation and it is easy to synthesize. Therefore, ANA membrane obtained from raw kaolin with aging 1 day was used to study the effect of temperature and concentration of ethanol in the feed.

The temperatures were varied with the range from 55 to 75 °C and ethanol solutions were 90 wt% and 95 wt%. The total water fluxes of the pervaporation system were increased with an increase in the temperature and the separation factor was quite constant at 10,000 (Figure 5.3). The temperature at 55 °C, 60 °C and 75 °C, gave the total water fluxes to 0.08 kg/(m²h), 0.18 kg/(m²h) and 0.25 kg/(m²h), respectively. The high water vapor at high temperature condenses rapidly through the capillary condensation mechanism in the zeolitic and nonzeolitic pores and it is high vaporized at the downstream side of the membrane. It seems as though the temperature increases, desorption rate of water vapor at the downstream side of the membrane increases. At low temperature a water vapor content is very low in ANA membrane. Therefore, the water vapor is strongly adsorbed in the zeolitic and nonzeolitic pores and condensed here and it significantly inhibits permeation of other gases by blocking them from entering in the pore (Okamoto et al., 2001).

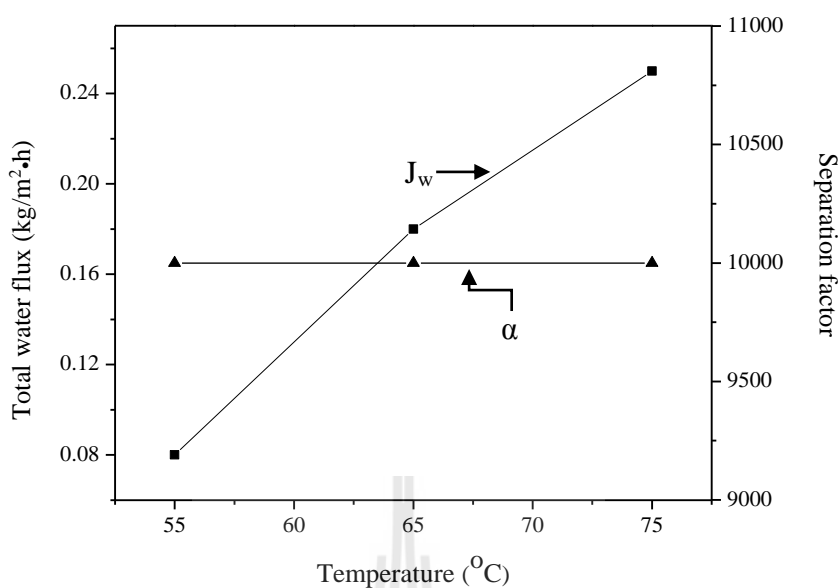


Figure 5.3 Effect of temperature on pervaporation performance of ANA membrane synthesized from raw kaolin with aging 1 day and using the feed of 90 wt% ethanol solution.

When considered the effect of ethanol concentration on that the pervaporation, it is obvious that the total water flux was decreased from 0.25 kg/(m²h) to 0.12 kg/(m²h) when ethanol concentration was increased from 90 wt% to 95 wt%. Kunnakorn et al. (2011) and Okamoto et al. (2001) also found that the total water flux of the pervaporation system for water-ethanol was decreased with an increase in concentration of ethanol in the feed mixture due to a low amount of water in feed mixture hence the vapor pressure of the water in the feed decreased resulting in reduction of driving force of vapor water through ANA membrane. In this study, it can be concluded that a feed mixture with high ethanol concentration and low temperature leads to a low total water flux of pervaporation of water-ethanol mixture. Table 5.2 summarizes pervaporation performance of zeolite membrane on mullite

support. As expected, a high separation factor and a high total water flux are demand for pervaporation with high quality of zeolite membrane. When compared the pervaporation performance of each type of zeolite membrane, it was found that ANA membranes yielded a low total water flux. However, the separation factor was still provided more than 10,000. Moreover, ANA membrane was synthesized from a cheap raw material and it was simple to prepare.

Table 5.2 Pervaporation performance of zeolite membranes on ceramic support.

EtOH:H₂O (mass ratio)	Method	Separation layer	Starting source	Separation factor	Flux (kg/m² h)	Ref.
90:10	Secondary	Hydroxy- sodalite	Chemical	>10,000	0.32	[1]
95:5	Secondary	Hydroxy- sodalite	Chemical	>10,000	0.27	[1]
90:10	Secondary	Hydroxy- sodalite	Metakaolin	>10,000	0.959	[1]
90:10	Secondary	NaA	Chemical	>10,000	1.69	[2]
90:10	Secondary	T-type	Chemical	>2,100	1.33	[2]
90:10	Secondary	Sodalite	Chemical	2	0.08	[3]
90:10	Secondary	NaY	Chemical	130	1.59	[3]
90:10	Secondary	NaX	Chemical	360	0.89	[3]
90:10	Secondary	NaA	Chemical	10,000	2.15	[3]
95:5	Secondary	Zeolite A	Chemical	>5000	2.35	[4]
90:10	In situ	Analcime	Raw kaolin	>10,000	0.25	This work

[1] Kazemimoghdam and Mohammadi, 2011; [2] Kondo and Kita, 2010 [3] Morigami et al., 2001; [4] Kondo et al., 2001.

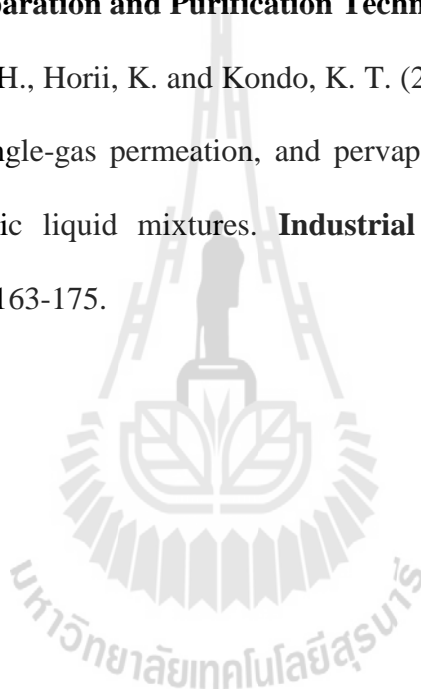
5.5 Conclusion

ANA membrane obtained from different starting materials such as raw kaolin, dealuminated kaolin and chemical source was successful used for separation of water from ethanol solution and it also showed a separation factors more than 10,000. The membrane from raw kaolin with aging for 3 days showed the highest total water flux of 0.27 kg/(m²h) while the others from raw kaolin with aging for 1 day, dealuminated kaolin and chemical source showed their water flux of 0.25 kg/m²h, 0.22 kg/m²h and 0.19 kg/m²h, respectively. According to their capabilities of separation and their water flux it confirmed that a low priced source as a raw kaolin can be used to synthesize a suitable ANA membrane for separation of water-ethanol mixture by pervaporation. Then ANA membrane from raw kaolin aging for 1 day was used in further study in considering the effect of temperature and ethanol concentration in feed mixture on a pervaporation. It was found that the total water fluxes of the pervaporation system increased with an increase in the temperature and the total water flux was decreased with an increase in ethanol concentration.

5.6 References

- Kazemimoghadam, M. and Mohammadi, T. (2011). Preparation of nano pore hydroxysodalite zeolite membranes using of kaolin clay and chemical sources. **Desalination**. 278: 438-442.
- Kondo, M. and Kita, H. (2010). Permeation mechanism through zeolite NaA and T-type membranes for practical dehydration of organic solvents. **Journal of Membrane Science**. 361: 223-231.

- Kunnakorn, D., Rirksomboon, T., Aungkavattana, P., Kuanchertchoo, N., Atong, D., Hemra, K., Kulprathipanja, S. and Wongkasemjit, S. (2011). Optimization of synthesis time for high performance of NaA zeolite membranes synthesized via autoclave for water–ethanol separation. **Desalination**. 280: 259-265.
- Morigami, Y., Kondo, M., Abe, J., Kita, H. and Okamoto, K. (2001). The first large-scale pervaporation plant using tubular-type module with zeolite NaA membrane. **Separation and Purification Technology**. 25: 251-260.
- Okamoto, K. -i., Kita, H., Horii, K. and Kondo, K. T. (2001). Zeolite NaA membrane: preparation, single-gas permeation, and pervaporation and vapor permeation of water/organic liquid mixtures. **Industrial & Engineering Chemistry Research**. 40: 163-175.



CHAPTER VI

CONCLUSIONS

The synthesis of hydrophilic sodium zeolites (ANA, JBW, CAN and SOD) with pure phase and high crystallinity were obtained through a shorter reaction period compared to those from other related researches (see in Table 6.1).

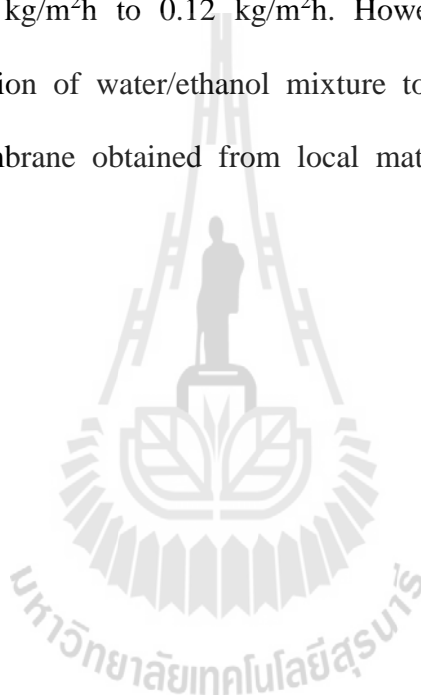
Table 6.1 Summarized the related researches on hydrothermal synthesis of sodium zeolites from different silica and alumina sources with different reaction periods.

Hydrophilic zeolites	SiO ₂ and Al ₂ O ₃ source	Temperature (°C)	Hydrothermal time; HT	References
ANA	kaolin, commercial sodium silicate	200	HT; 24 h	Hegazy et al. (2010)
ANA	metakaolin, rice husk ash	180	Aging; 3 days HT; 1 day	Atta et al. (2012)
JBW	metakaolin	200	HT; 4 days	Lin et al. (2004)
CAN			HT; 8 days	
SOD			HT; 2 days	
SOD + CAN	kaolin	200	HT; 6 h	Rios et al. (2011)
JBW			HT; 24 h	
ANA	dealuminated kaolin	200	HT; 6-48 h	In work
JBW	raw kaolin	200	HT; 6-48 h	In work
CAN	dealuminated kaolin	200	HT; 6-48 h	In work
SOD	calcined kaolin	200	HT; 6-12 h	In work

In the dehydration of ethanol solution with these sodium zeolites, ANA showed its adsorption capacity of water higher than that of the other sodium zeolites. The ethanol solution of 97.0%v/v was dehydrated to $99.9\pm 0.01\%$ v/v by ANA, while it was dehydrated to $99.3\pm 0.01\%$ v/v, $98.6\pm 0.01\%$ v/v and $97.8\pm 0.01\%$ v/v by JBW, CAN and SOD, respectively. However, all the sodium zeolites exhibited their own capabilities in dehydration of ethanol concentration of 85.0%v/v higher than that of a commonly used NaA (Muenpoowank and Rangriwatanonon, 2012). In addition, JBW is a good alternative adsorbent for dehydration of ethanol solution with its simplest way to synthesize and its cost effectiveness. ANA exhibited an extreme number of adsorption sites from the NH_3 -TPD characterization and stronger interaction of water from the DTG curve, so it showed the highest adsorption capacity of water in ethanol solution. SOD presented a high strength of Lewis acid site but it showed a low adsorption capacity maybe the pore structure limits. Therefore, the adsorption capacity of zeolite mainly relies on the strength of Lewis acid sites and pore structure.

In the case of the separations of water/ethanol mixture by membrane, ANA membranes were successfully performance with separation factor was high as $>10,000$. ANA membranes were obtained from raw kaolin with aging, dealuminated kaolin and chemical with no aging. It showed the small crystal size about 20-37 μm and thin layer about 45-67 μm . The suitable ceramic support were prepared from the ingredient of 10.0 wt% cristobalite, 2.5 wt% activated carbon, 2.5 wt% calcite and 85.0 wt% raw kaolin. In economically, ANA membrane from raw kaolin with aging 1 day is an alternative method of synthesis with a short reaction time and low cost of silica and alumina source. Therefore, ANA membrane obtained from this condition

was used to study the effect of temperature and concentration of feed mixture in the pervaporation process. It was found that a higher temperature resulted in a higher total water flux. The temperatures of 55 °C, 65 °C and 75 °C yielded a total water flux as 0.08 kg/m²h, 0.18 kg/m²h and 0.25kg/m²h, respectively. When considered the effect of ethanol concentration in feed mixture, it was found that an increase in the concentration of ethanol solution from 90.0 wt% to 95.0 wt% the total water flux was decreased from 0.25 kg/m²h to 0.12 kg/m²h. However, ANA membranes were successful for separation of water/ethanol mixture to produce anhydrous ethanol. Moreover, ANA membrane obtained from local material as raw kaolin and was synthesized easily.





APPENDIX

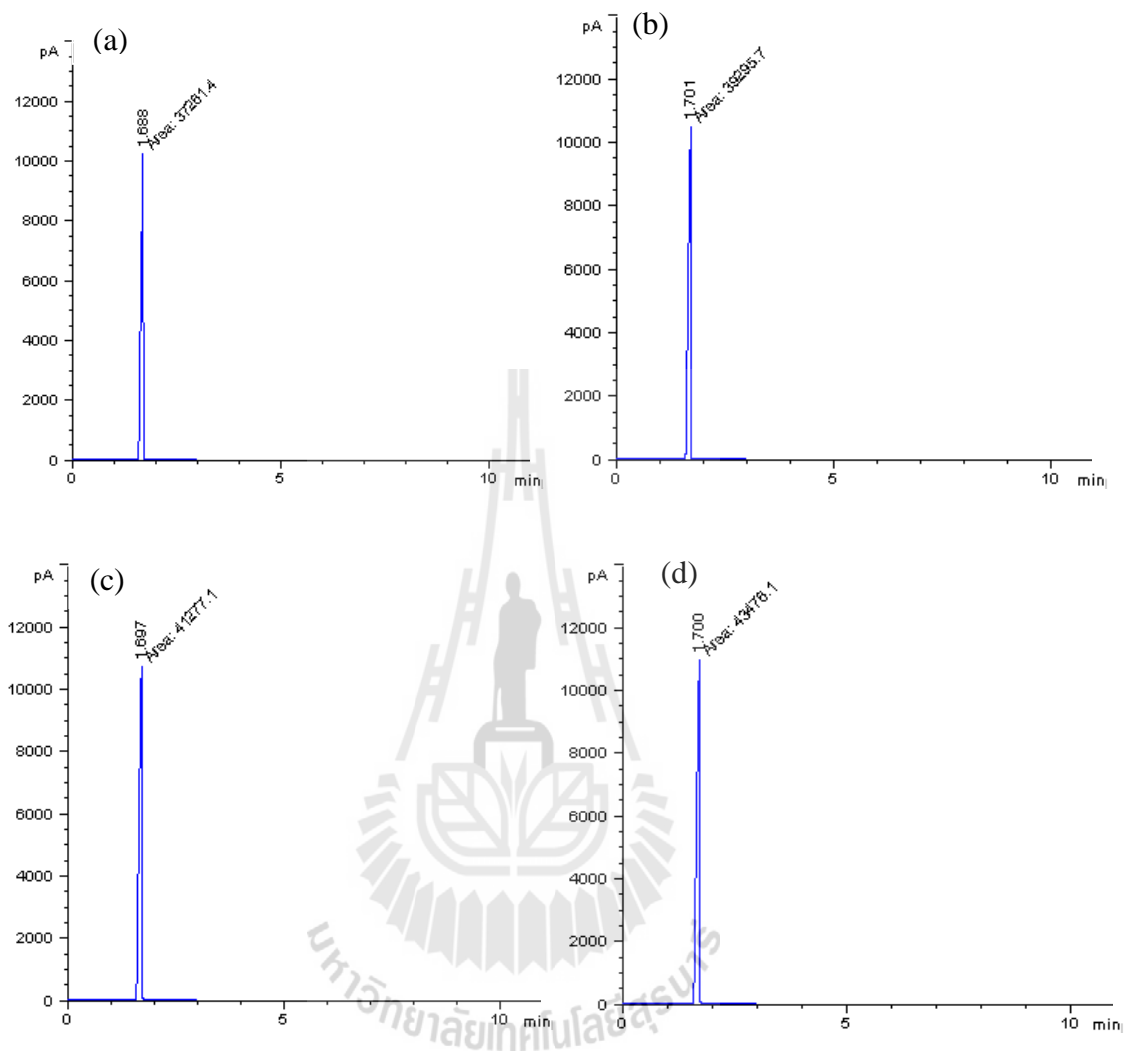


Figure A1 GC chromatograms of standard solutions of (a) 85% v/v, (b) 90% v/v, (c) 95% v/v and (d) 97% v/v of ethanol solutions

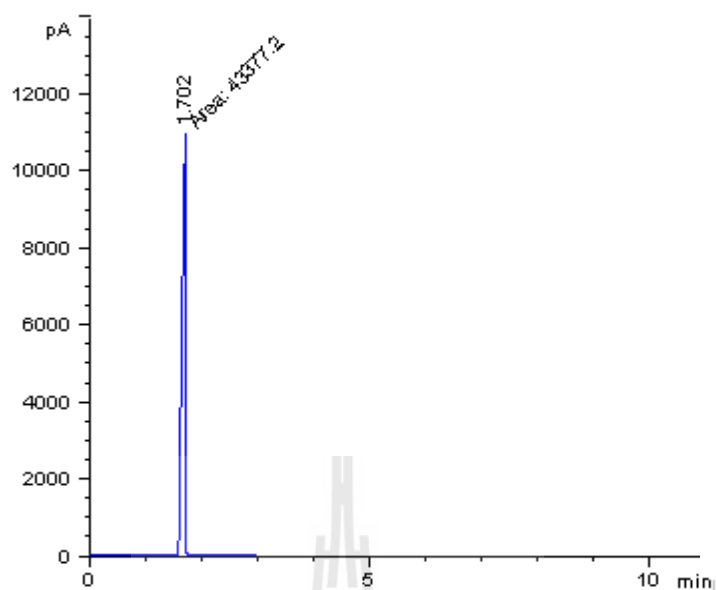


Figure A2 GC chromatograms of 97%v/v ethanol solution after adsorption by ANA.

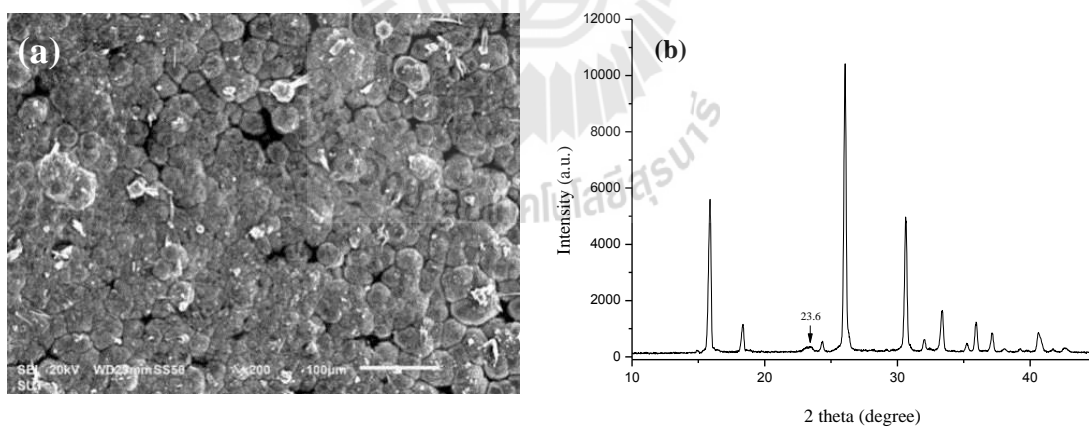


Figure A3 (a) Surface SEM micrograph and (b) XRD pattern of ANA membrane from kaolin sintered with 7.5% w/v NaOH.

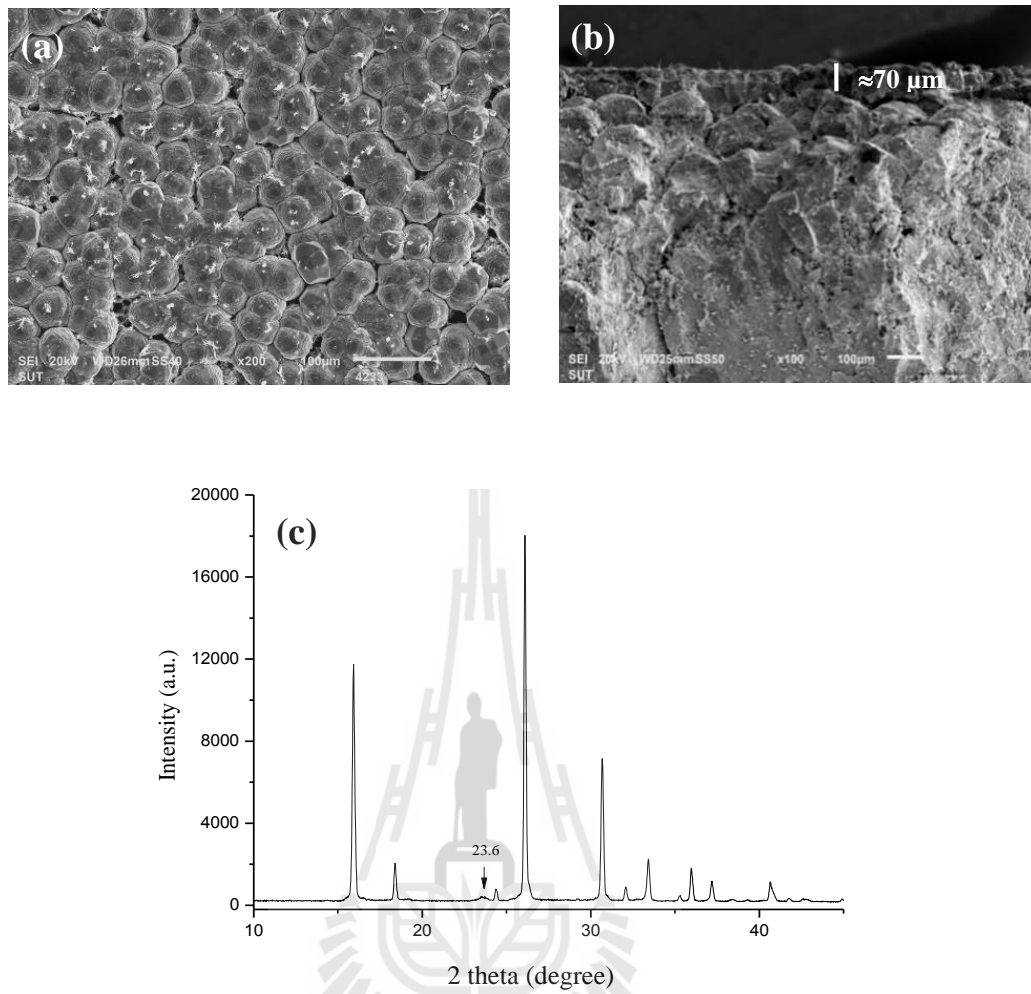


Figure A4 SEM micrograph ((a)-(b)) and XRD patterns (c) of ANA membrane from 10% cristobalite sintered with 7.5% w/v NaOH.

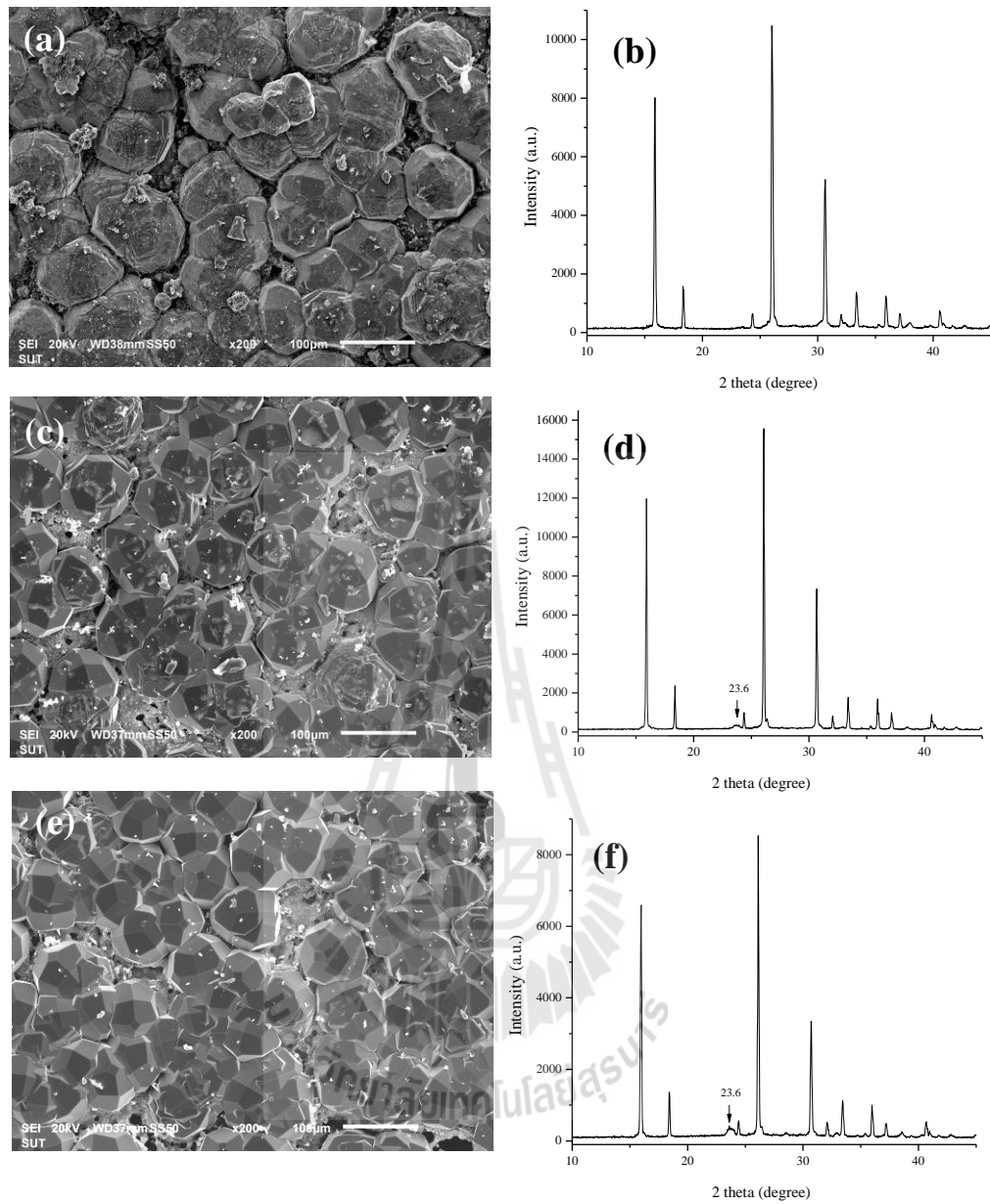


Figure A5 Surface SEM micrograph and XRD patterns of ANA membrane on 2.5A ((a) and (b)), 2.5Ca ((c) and (d)) and 2.5ACa ((e) and (f)).

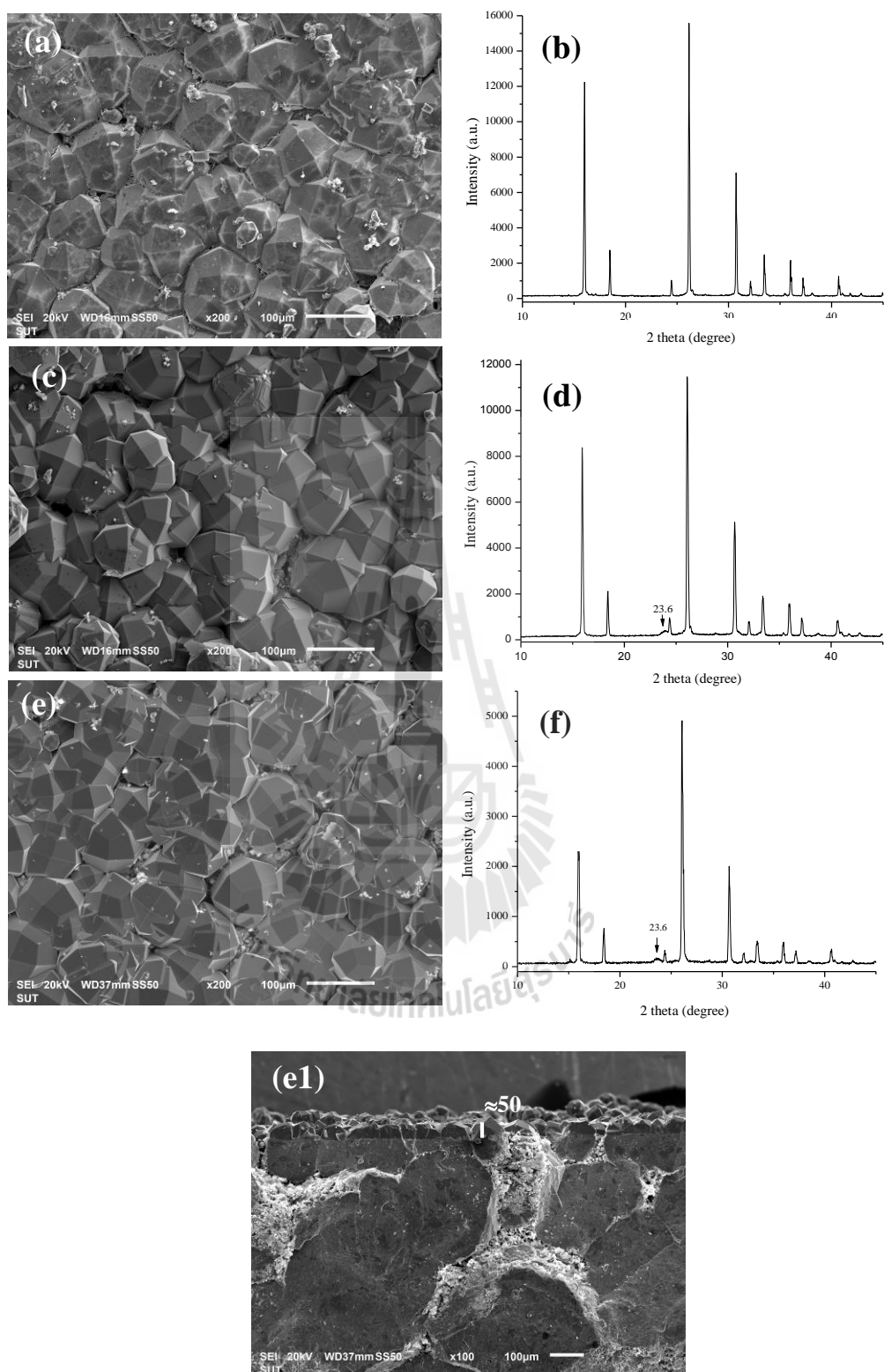


Figure A6 Surface SEM micrograph and XRD patterns of ANA membrane on 2.5A ((a) and (b)), 2.5Ca ((c) and (d)), 2.5ACa ((e) and (f)) and cross-section of ANA membrane on 2.5ACa (e1) with 10% w/v NaOH.

CURRICULUM VITAE

NAME: Miss Thapanee Khambudda

EDUCATIONAL BACKGROUND:

- 2004 Bachelor of Education (Chemistry)
Nakhon Ratchasima Rajabhat University, Nakhon Ratchasima,
Thailand
- 2008 Master of Science (Chemistry)
Suranaree University of Technology, Nakhon Ratchasima, Thailand

WORK EXPERIENCE:

- 2005-2006 Technician, Center of Scientific, Nakhon Ratchasima Rajabhat
University, Nakhon Ratchasima, Thailand
- 2006-2014 Teaching assistance, School of Chemistry, Institute of Science,
Suranaree University of Technology, Nakhon Ratchasima.

PUBLICATION:

- Thapanee Khumbudda , Aphiruk Chaisena, and Kunwadee Rangriwatananon. (2016).
Facile hydrothermal synthesis of zeolitic ANA membrane from raw kaolin.
Engineering Journal. 20(1): 197-210.

PRESENTATION:

- 2013 Poster presentation “Synthesis of pure phase cancrinite and sodalite
from modified kaolin” The Pure and Applied Chemistry International
Conference (PACCON). Burapha University, Chonburi, Thailand.